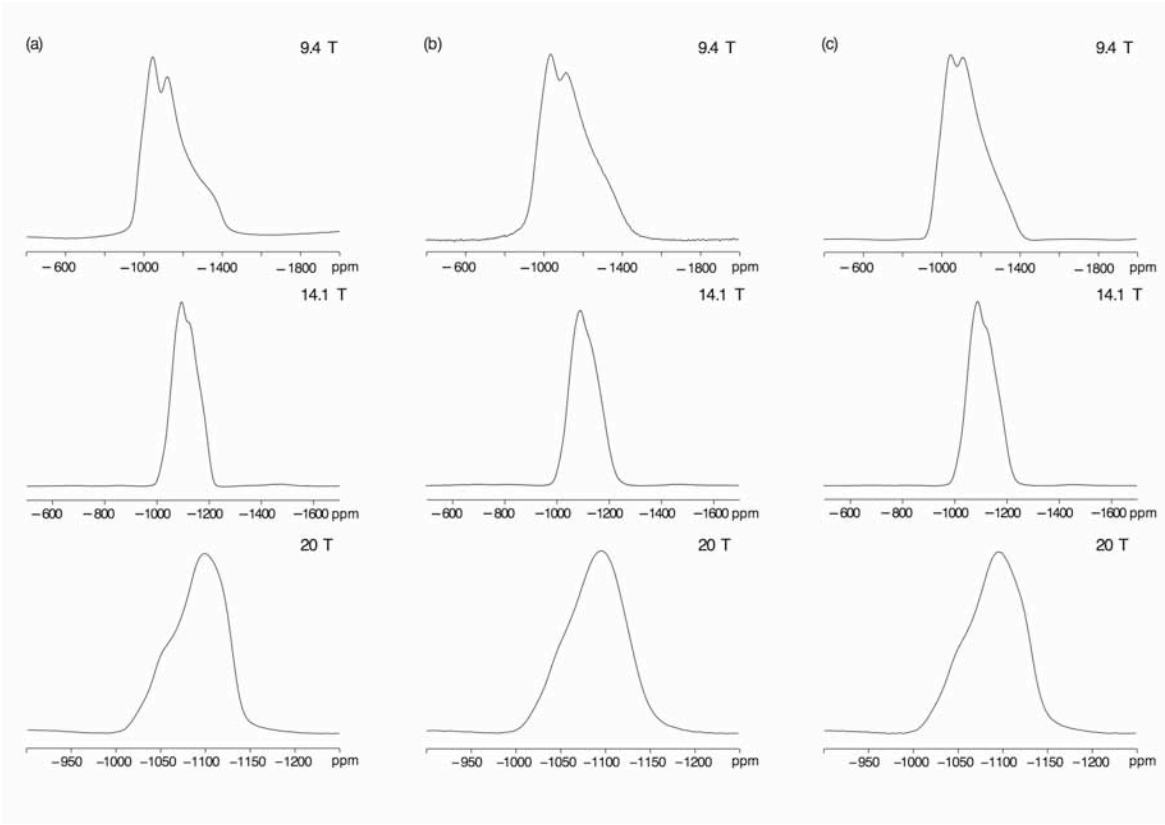

Figure 3.40: Static ^{93}Nb NMR spectra recorded for (a) commercial $NaNbO_3$ (Aldrich), (b) sol-gel $NaNbO_3$ and (c) Solid-State Sample A $NaNbO_3$ recorded at 9.4 T, 14.1 T and 20 T.

can then aid considerably in the understanding and interpretation of complex NMR spectra. Static spectra were therefore recorded for a phase pure sample of Pbcm $NaNbO_3$, Solid-State Sample A $NaNbO_3$ and the sol-gel $NaNbO_3$ sample at 9.4 T, 14.1 T and 20 T using a central-transition selective 90 - τ - 180 spin-echo pulse sequence.

All spectra recorded at 9.4 T were broad owing to the dominance of the quadrupolar interaction. However, unlike the lineshapes observed under MAS, there were distinct features present in each. This is highlighted in Figures 3.40(a), (b) and (c), where static ^{93}Nb NMR spectra for the Aldrich sample of $NaNbO_3$, the sol-gel sample of $NaNbO_3$ and Solid-State Sample A are compared. Interestingly, the commercially purchased sample of Pbcm $NaNbO_3$ and the sol-gel sample, believed to be composed of largely the $P2_1ma$ polymorph of $NaNbO_3$, produced very similar lineshapes, suggesting the Nb environments to be very similar in each. Solid-State Sample A is known to contain the Pbcm phase of

$NaNbO_3$ and a second very similar polymorph. The static ^{93}Nb NMR spectrum recorded for Solid-State Sample A (Figure 3.40(c)) appeared similar to both the phase pure sample of Pbcm $NaNbO_3$ and the sol-gel sample of $NaNbO_3$ with distinct features observed in the lineshape. Broad resonances were also observed for each sample using 14.1 T. However, it must be noted that the features previously identified in each lineshape began to diminish with increasing fieldstrength, also highlighted in Figure 3.40. This is most probably owing to the increasing dominance of the CSA. At 14.1 T each lineshape appeared very similar, with only slight differences observed. This therefore confirms that the two phases present in many of the samples of $NaNbO_3$ synthesised are extremely similar and also suggests that it may not be possible to accurately distinguish between the two using ^{93}Nb NMR. At 20 T the CSA is the more dominant interaction and, as a result, the lineshapes observed for both the phase pure Pbcm $NaNbO_3$ (Aldrich) and $P2_1ma$ $NaNbO_3$ were relatively broad, as shown in Figures 3.40(a) and (b). It must be noted that the quadrupolar features previously identified at lower fields were not present at 20 T owing to the dominance of the CSA.

The findings presented appear to suggest it is not possible to distinguish between different phases of $NaNbO_3$ using ^{93}Nb NMR. This therefore confirms earlier conclusions regarding the very similar nature of the different polymorphs present. Given the obvious similarities of the two phases it would be extremely challenging to obtain accurate ^{93}Nb NMR parameters for each phase. At present, it does not appear to be possible to determine the contribution of each phase to the observed lineshape. Recent work by Hanna *et al.*[251] suggests using DFT calculations, in conjunction with experiment, can aid in the understanding and interpretation of static ^{93}Nb NMR spectra. A detailed discussion regarding the possibility of ^{93}Nb DFT calculations within this particular investigation is given in section 3.4.

3.3.7 ^{17}O Enrichment of $NaNbO_3$

To complete a comprehensive structural investigation of $NaNbO_3$ several samples synthesised were post-synthetically enriched with $^{17}O_2$. This procedure is very costly (~$3,500 for 3 L 50% ^{17}O enriched O_2 gas). Successful enrichment is commonly achieved using either ^{17}O enriched water or gas and the method utilised is often sample dependent. To date, little work has been completed on the enrichment of dense perovskite-based materials using $^{17}O_2$. Work has, instead, concentrated on perovskites exhibiting conduction properties. This class of material has been shown to aid in the enrichment process. [253,254]

^{17}O enrichment is often highly informative and can aid considerably in the structural characterisation of complex materials. To date the experimental results presented have highlighted the structural confusion surrounding $NaNbO_3$. Both high-resolution powder diffraction and ^{23}Na MAS NMR confirm the presence of two very similar phases in many of the samples synthesised. Using ^{93}Nb NMR we have also shown that it is impossible to accurately distinguish between the two phases owing to virtually identical Nb environments in each. Both the nature and degree of tilting exhibited by the NbO_6 octahedra in each phase are key in the understanding of precisely how the two phases present differ. In addition, the position of the Na^+ cation in the $NaNbO_3$ structure is also affected by the tilt exhibited. Therefore, to understand the differences in tilting mechanism exhibited by each phase various samples of $NaNbO_3$ were enriched with ^{17}O. Using $^{17}O_2$ gas a molten salt sample of phase pure Pbcm $NaNbO_3$ (synthesised at 1000 °C for 24 hours) and Solid-State Sample D (synthesised using 450 °C for 24 hours and 850 °C for an additional 24 hours) were enriched.

The ^{17}O MAS NMR spectra recorded for both the phase pure sample of Pbcm $NaNbO_3$ and Solid-State Sample D appeared to display large CSA contributions, as shown in Figures 3.41(a) and (b). Therefore, to remove the effect of the CSA faster MAS were used and spectra were recorded using an MAS rate of 30 kHz. The ^{17}O MAS NMR spectrum recorded for phase pure Pbcm $NaNbO_3$ is shown in Figure 3.42(a). An

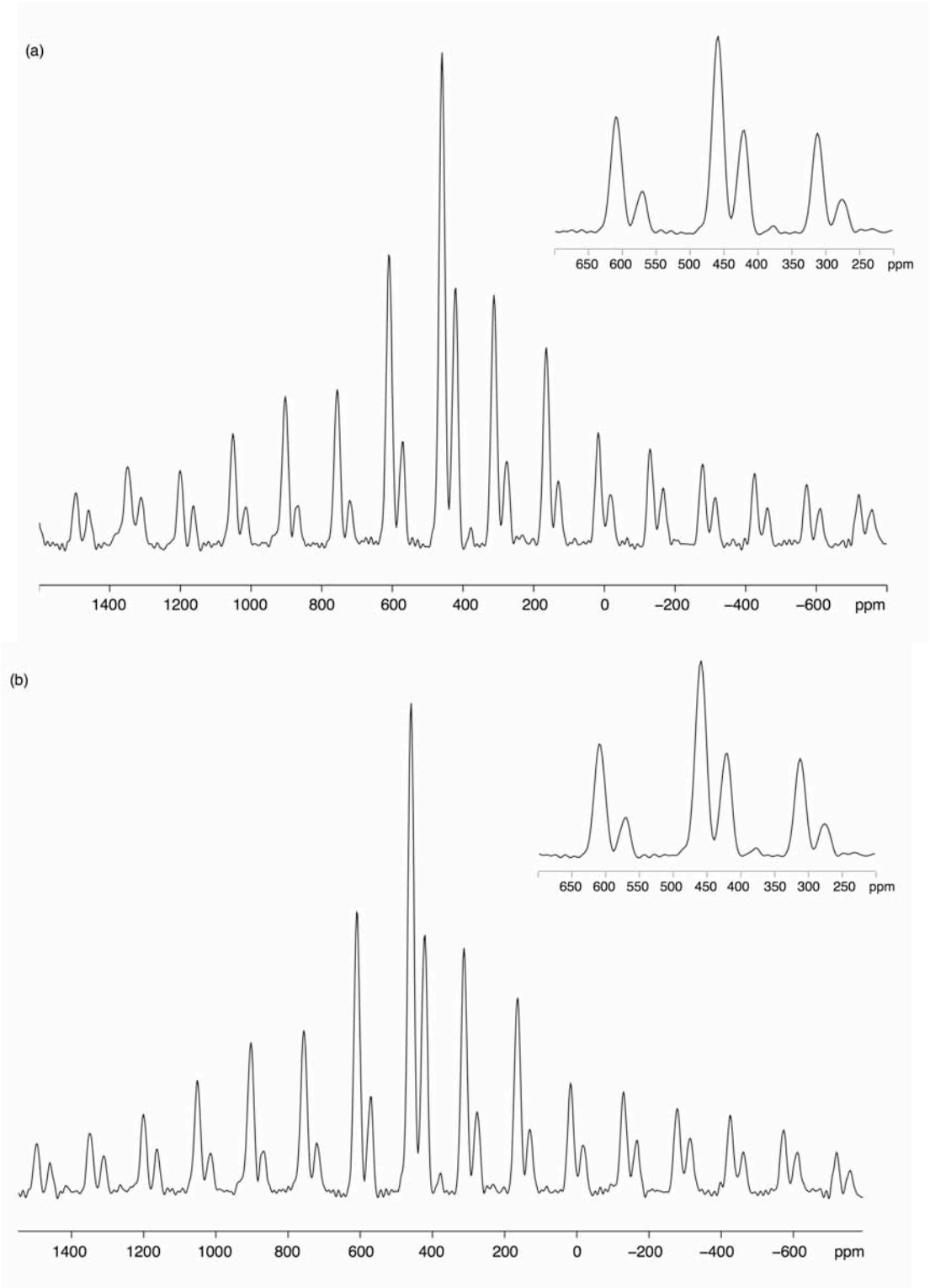

Figure 3.41: ^{17}O (14.1 T) MAS NMR spectra for (a) phase pure molten salt sample of Pbcm $NaNbO_3$ (synthesised using 1000 °C and 24 hours) and (b) Solid-State Sample D $NaNbO_3$ (synthesised using 450 °C for 24 hours and 850 °C for an additional 24 hours). Also shown in (a) and (b) are expansions of the central transition in each spectrum. The MAS rate was 14 kHz.

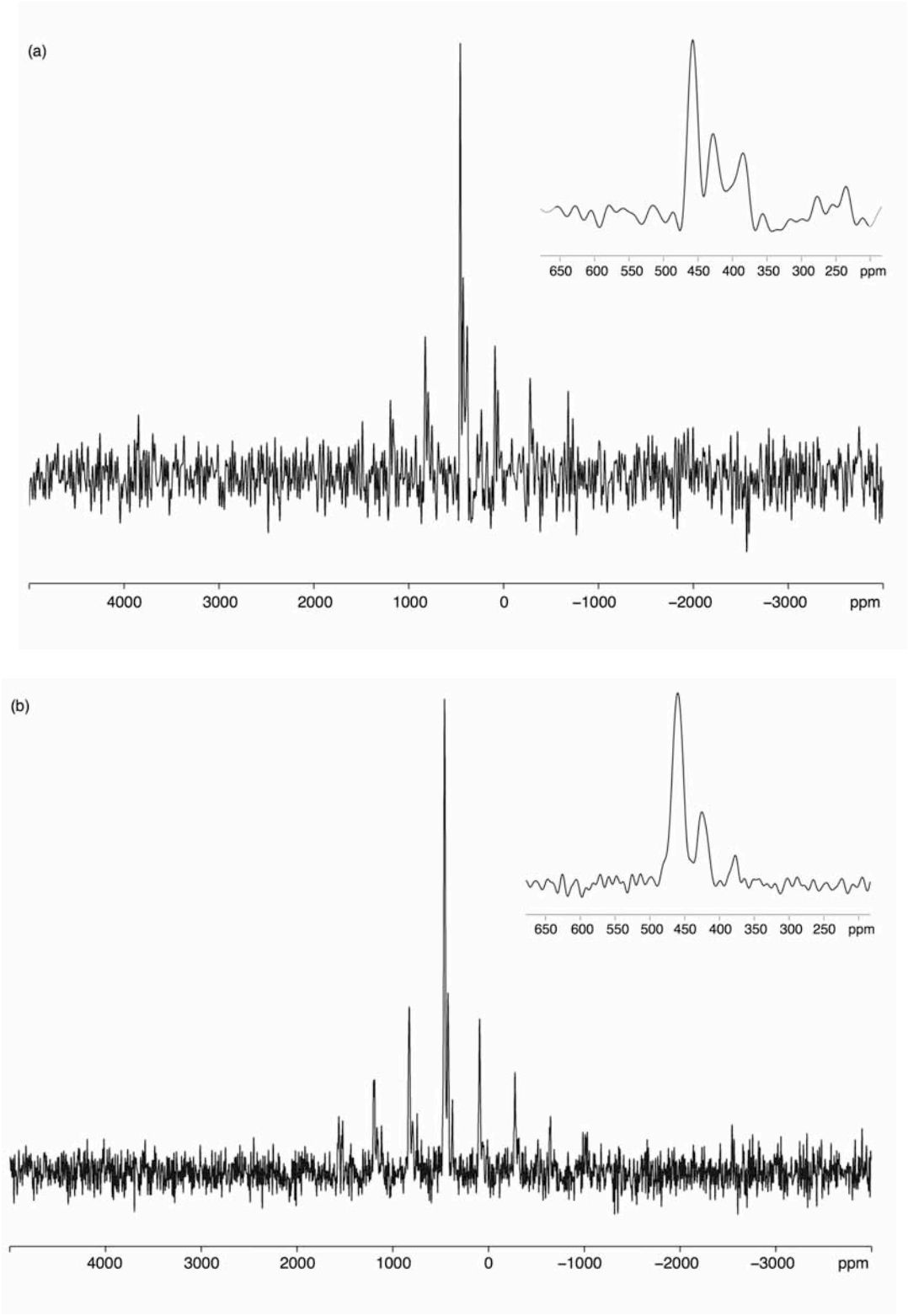

Figure 3.42: ^{17}O (14.1 T) MAS NMR spectra for (a) phase pure molten salt sample of Pbcm $NaNbO_3$ (synthesised using 1000 °C and 24 hours) and (b) Solid-State Sample D $NaNbO_3$ (synthesised using 450 °C for 24 hours and 850 °C for an additional 24 hours). Also shown in (a) and (b) are expansions of the central transition in each spectrum. The MAS rate was 30 kHz.

expansion of the central transition region of this spectrum is also shown as an inset in Figure 3.42(a). The ^{17}O MAS NMR spectrum displays three distinct oxygen resonances, with δ = 458.2 ppm, 428.5 ppm and 384.3 ppm. Published crystallographic data for Pbcm $NaNbO_3$ indicates the presence of four different oxygen environments. Hence there appeared to be a discrepancy between the NMR data presented and the known diffraction data. The resonance at δ = 384.3 ppm is believed to correspond to naturally occurring ^{17}O from ZrO_2 in the MAS rotor.[255] Therefore, only two peaks remained in the ^{17}O MAS NMR spectrum recorded for phase pure Pbcm $NaNbO_3$ and the four crystallographically distinct oxygen sites identified by diffraction must reside under the two observed resonances. The spectral overlap observed in the ^{17}O MAS NMR spectrum for phase pure Pbcm $NaNbO_3$ suggests that each of the four oxygen environments present in the structure are extremely similar and, as a result, it is very difficult to accurately assign each oxygen site. The ratio of the two resonances observed is 2:1, indicating there to be a greater number of oxygen sites under the resonance at δ = 458.2 ppm. The published crystallographic data for Pbcm $NaNbO_3$ indicates that there are eight O3 and O4 sites per unit cell and four O1 and O2 sites. This enabled us to assign the resonances at δ = 458.2 ppm and δ = 428.5 ppm to sites O3 and O4 and sites O1 and O2 respectively. However, owing to severe spectral overlap it was not possible to distinguish peaks belonging to each of the oxygen sites. The spectral overlap observed indicates just how similar each of the oxygen environments are in Pbcm $NaNbO_3$. In addition, each of the observed resonances appears to possess a relatively small quadrupolar interaction. The presence of such small quadrupolar interactions suggests that each of the oxygen environments in $NaNbO_3$ is highly symmetrical and relatively undistorted. To highlight how similar the four environments are in the Pbcm phase of $NaNbO_3$ each has been isolated and is shown in Figure 3.43(a-d). In addition, this provides a possible reason for the significant spectral overlap observed.

The ^{17}O MAS NMR spectrum recorded for Solid-State Sample D is shown in Figure 3.42 and, as for phase pure Pbcm $NaNbO_3$, it also displays three distinct resonances, δ = 460.3 ppm, 425.9 ppm and 379.0

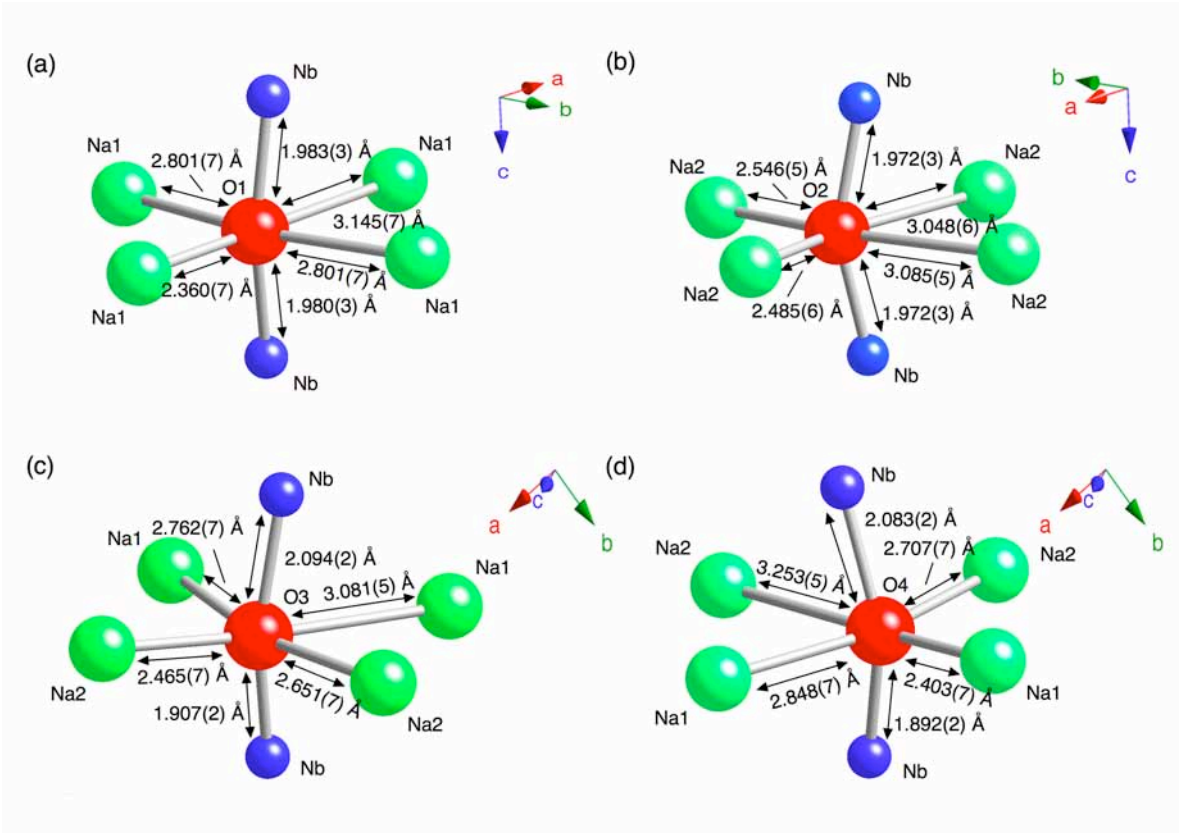

Figure 3.43: The coordination environments for sites (a) O1, (b) O2, (c) O3 and (d) O4 in Pbcm $NaNbO_3$, obtained from Rietveld refinement.

ppm. The resonance at δ = 379 ppm was assigned to ^{17}O signal from ZrO_2 in the MAS rotor. The two remaining sites are believed to correspond to the observed oxygen environments. Solid-State Sample D was synthesised using identical solid-state reaction conditions to Solid-State Sample A and using diffraction techniques the sample has been shown to contain the same two polymorphs as those present in Solid-State Sample A. Despite containing an additional polymorph the ^{17}O MAS NMR spectrum does not appear to contain any additional peaks. This therefore suggests that peaks belonging to both polymorphs reside under the two resonances observed in the MAS spectrum. Hence, this again highlights the very similar nature of the two polymorphs present in the sample and it appears to be virtually impossible to accurately distinguish peaks belonging to the respective phases using ^{17}O MAS NMR owing to their extreme similarities. The ratio of the resonances observed in the spectrum was the same as observed for phase pure Pbcm $NaNbO_3$, 2:1. Again, this indicated that a greater number of oxygen sites were under the resonance

at δ = 460.3 ppm. However, the exact nature of the second polymorph present in the sample was unknown, therefore it is difficult to identify the number of oxygen sites under this peak.

^{17}O enrichment of $NaNbO_3$ has therefore aided in confirming previous conclusions regarding the extreme similarities of the two phases of $NaNbO_3$ routinely synthesised in many samples. The ^{17}O MAS NMR spectrum recorded for phase pure Pbcm $NaNbO_3$ has shown that there is considerable spectral overlap of sites O1 and O2 and sites O3 and O4. When directly compared, as in Figure 3.43, it is clear to see why sites O1 and O2, and sites O3 and O4 are overlapped in the ^{17}O MAS NMR spectrum. Using crystallographic data obtained from diffraction it was possible to tentatively assign where each site lay in the spectrum. The ^{17}O MAS NMR spectrum recorded for Solid-State Sample D has shown that it is not possible to differentiate between the different polymorphs of $NaNbO_3$ present in many solid-state, molten salt and sol-gel samples of $NaNbO_3$ owing to considerable spectral overlap. The results presented therefore confirm that, experimentally, the easiest and most convenient way of distinguishing between the different polymorphs of $NaNbO_3$ is to use two-dimensional ^{23}Na MQMAS NMR techniques.

3.4 DFT Calculations

In conjunction with experiment, ^{23}Na, ^{93}Nb and ^{17}O density functional theory (DFT) calculations were completed to aid with spectral interpretation. Using the CASTEP[214] code it was possible to predict the NMR parameters δ_{iso}, C_Q and η_Q for any structural model and compare with the experimental values obtained. Initially, structures reported within the literature were calculated in order to establish the feasibility and accuracy of the calculations for $NaNbO_3$. Similar calculations were completed by Ashbrook *et al.*,[231] using both CASTEP and WIEN2k and our results were in good agreement.

^{23}Na NMR parameters were calculated for several $NaNbO_3$ phases suggested in the literature,[140] each of which was then compared with the experimental NMR parameters obtained. Two structures in particular,

Table 3.12: Calculated (using CASTEP) ^{23}Na NMR parameters, δ_{iso}, P_Q, C_Q and η_Q, post optimisation, for selected room temperature phases of $NaNbO_3$, obtained from both literature and Rietveld refinement.

Phase	Site	δ_{iso} (ppm)	P_Q / MHz	C_Q / MHz	η_Q
Literature					
Pbcm[217]	Na1	−4.8	2.23	2.22	0.17
	Na2	−9.0	0.96	0.87	0.79
$P2_1ma$[228]	Na1	−4.9	2.52	2.33	0.71
	Na2	−9.5	1.11	1.01	0.8
Pmma[226]	Na1	−9.4	−1.25	−1.25	0.07
	Na2	−9.4	−1.19	−1.19	0.06
Refinement					
Pbcm	Na1	−4.8	2.27	2.27	0.07
	Na2	−8.9	0.96	0.89	0.71
$P2_1ma$	Na1	−5.7	2.47	2.22	0.85
	Na2	−9.9	−0.89	−0.80	0.82
$Pnm2_1$	Na1	−8.4	1.61	1.61	0.13
	Na2	−7.3	−2.04	−1.88	0.74
Pnma	Na1	−7.7	1.60	1.28	0.86
$Pn2_1a$	Na1	−7.7	1.43	1.25	0.98

namely Pbcm and $P2_1ma$, displayed good correlation with experiment after geometry optimisation (allowing both the unit cell and atomic positions to vary), suggesting the structure was perhaps not an energy minimum initially. All ^{23}Na NMR parameters calculated for literature phases of $NaNbO_3$ (post optimisation) are listed in Table 3.12. Parameters were also calculated using structures obtained from Rietveld refinement of our NPD data, post optimisation values are also listed in Table 3.12. For completeness phases containing a single Na site, namely Pnma and $Pn2_1a$, were also calculated which aided further in eliminating them from our investigation as plausible secondary phases. All ^{23}Na parameters calculated for each phase prior to optimisation can be found in Table 3.13.

Table 3.13: Calculated (using CASTEP) ^{23}Na NMR parameters, δ_{iso}, P_Q, C_Q and η_Q, prior to optimisation, for selected room temperature phases of $NaNbO_3$, obtained from both literature and Rietveld refinement.

Phase	Site	δ_{iso} (ppm)	P_Q / MHz	C_Q / MHz	η_Q
Literature					
Pbcm[217]	Na1	−4.9	2.17	1.98	0.77
	Na2	−8.0	1.09	1.03	0.58
$P2_1ma$[228]	Na1	−3.9	2.42	2.20	0.80
	Na2	−7.5	1.22	1.13	0.72
Pmma[226]	Na1	−4.5	−2.50	−2.50	0.05
	Na2	−12.5	−0.20	−0.20	0.35
Refinement					
Pbcm	Na1	−3.7	2.22	2.22	0.02
	Na2	−6.6	1.19	1.16	0.38
$P2_1ma$	Na1	−2.8	2.50	2.39	0.54
	Na2	−7.9	0.72	0.69	0.48
$Pnm2_1$	Na1	−9.2	2.00	1.92	0.49
	Na2	−5.5	1.66	1.60	0.48
Pnma	Na1	−6.0	1.83	1.73	0.59
$Pn2_1a$	Na1	−5.7	2.13	1.88	0.92

^{23}Na DFT calculations were also completed using a fixed cell during the geometry optimisation of the structure and the calculated parameters can be found in Appendix II. Once optimised the atomic forces were closely examined and found to be considerably lower than those observed for the initial structure obtained from diffraction. This therefore indicated that the structure had been successfully optimised into a local energy minimum. Consistently the phases Pbcm and $P2_1ma$ provided the best agreement with experiment (both from the literature and Rietveld refinement), as they appeared to correlate with each of the phases identified. In particular the C_Q values obtained for ^{23}Na were in reasonable agreement, as highlighted by comparison of the solid-state

NMR (9.4 T) data in Table 3.2 and the calculated parameters for Pbcm and $P2_1ma$ (Table 3.12). Note that the sign of C_Q, although displayed for calculated values, is not determined by experiment. The asymmetry parameter, η_Q, displayed the greatest degree of discrepancy with experiment however this was a consistent finding with all structures calculated. This poor agreement has been observed previously, for example in the aluminophosphate framework AlPO-14.[195] It should be noted that C_Q depends upon one principal tensor component, V_{ZZ}, whereas η_Q depends upon all three. Similar differences were also found in the WIEN2k calculations completed by Ashbrook *at al*.[231]

Similarly, ^{93}Nb DFT calculations were completed for several of the $NaNbO_3$ phases suggested in the literature[140] and the calculated parameters were compared with the experimental results obtained. Using ^{93}Nb MAS NMR the lineshapes observed for the Pbcm and $P2_1ma$ phases of $NaNbO_3$ appeared very similar, suggesting it was not feasible to distinguish between different phases of $NaNbO_3$ using ^{93}Nb NMR. The calculated ^{93}Nb NMR parameters obtained, post optimisation of each phase of $NaNbO_3$ are shown in Table 3.14, where many of the phases calculated exhibit very similar values of C_Q and η_Q. Two of the phases, namely Pmma and Pnma, possessed considerably smaller values of C_Q (~3-4 MHz) that did not appear to correlate with any of the parameters observed experimentally, therefore suggesting that neither of these phases are present in any of the $NaNbO_3$ samples investigated. The calculated parameters obtained for the Pbcm and $P2_1ma$ phases of $NaNbO_3$ were extremely similar and both displayed the greatest degree of agreement with the observed experimental findings. This was true for structures obtained both directly from the literature and Rietveld refinement of the NPD data. The similarities observed in the calculated ^{93}Nb parameters for the Pbcm and $P2_1ma$ phases suggests that the Nb environment in each is extremely similar and it would therefore be virtually impossible to distinguish between the two using ^{93}Nb MAS NMR. These findings are again in good agreement with experiment. Recent work by Hanna *et al.*[251] suggests it is possible to distinguish between different phases of $NaNbO_3$ using ^{93}Nb DFT calculations. Their work concentrated on calculating the

Table 3.14: Calculated (using CASTEP) ^{93}Nb NMR parameters, δ_{iso}, P_Q, C_Q and η_Q, post optimisation, for selected room temperature phases of $NaNbO_3$, obtained from both literature and Rietveld refinement.

Phase	Site	δ_{iso} (ppm)	P_Q / MHz	C_Q / MHz	η_Q
Literature					
Pbcm[217]	Nb	−1057.0	29.28	25.61	0.96
$P2_1ma$[228]	Nb	−1055.1	−28.51	−25.24	0.91
Pmma[226]	Nb	−1069.5	2.76	2.45	0.90
Refinement					
Pbcm	Nb	−1057.9	31.10	27.00	0.99
$P2_1ma$	Nb	−1055.4	−29.99	−26.49	0.92
$Pnm2_1$	Nb	−1058.6	29.38	26.19	0.88
Pnma	Nb	−1060.6	−4.05	−3.80	0.64
$Pn2_1a$	Nb	−1053.8	−27.70	−26.69	0.48

Table 3.15: Calculated (using CASTEP) ^{93}Nb NMR parameters, δ_{iso}, P_Q, C_Q and η_Q, prior to optimisation, for selected room temperature phases of $NaNbO_3$, obtained from both literature and Rietveld refinement.

Phase	Site	δ_{iso} (ppm)	P_Q / MHz	C_Q / MHz	η_Q
Literature					
Pbcm[217]	Nb	−1098.8	−20.97	−20.80	0.22
$P2_1ma$[228]	Nb	−1077.4	−15.29	−15.11	0.27
Pmma[226]	Nb	−1076.0	−92.40	−88.50	0.52
Refinement					
Pbcm	Nb	−1089.0	−16.97	−14.84	0.96
$P2_1ma$	Nb	−1090.4	−20.14	−19.26	0.53
$Pnm2_1$	Nb	−1105.8	−33.84	−31.50	0.68
Pnma	Nb	−1084.5	−25.57	−25.17	0.31
$Pn2_1a$	Nb	−1072.1	25.49	23.77	0.67

NMR parameters for three of the most commonly reported phases of $NaNbO_3$; Pbcm, $P2_1ma$ and Pbma. Using powder X-ray diffraction their sample displayed good agreement with the Sakowski-Cowley[217] Pbcm model and of the three phases calculated the Pbcm phase displayed the greatest degree of agreement with their experimental ^{93}Nb (wideline) NMR spectra recorded. Within this particular investigation both the Pbcm and $P2_1ma$ structures obtained directly from the literature[140] were calculated and the NMR parameters obtained for each phase prior to optimisation were very different, as shown in Table 3.15. These appear to be in very good agreement with those reported by Hanna *et al*. Structures obtained directly from the crystal structure database or Rietveld refinement are, quite often, not in a local energy minimum and geometry optimisation is required. Within this investigation the Pbcm and $P2_1ma$ phases were geometry optimised and the calculated values obtained for each appeared to be very similar, as highlighted in Table 3.14. Therefore, the ^{93}Nb DFT calculations performed by Hanna *et al*. appear to be in very good agreement with our non-optimised values, suggesting that no structural optimisation had been performed and the structures calculated were either directly from the ICSD or refinement. We have shown that post optimisation the Pbcm and $P2_1ma$ phases produce virtually identical NMR parameters, making it difficult to distinguish between the two, as shown experimentally.

The ^{93}Nb DFT calculations completed within this investigation have aided in eliminating several phases as plausible secondary phases and appear to have confirmed initial experimental findings that it is not possible to distinguish between the different phases of $NaNbO_3$ using ^{93}Nb MAS NMR. We have also highlighted an important point regarding structural optimisation. For systems such as $NaNbO_3$ geometry optimisation is essential as often the initial structure is not in a local energy minimum. One possible reason for this is the presence of more than one polymorph in many samples. For $NaNbO_3$ better correlation with experiment was observed post geometry optimisation. All ^{93}Nb parameters calculated for each of the phases post optimisation using a fixed cell can be found in Appendix II.

^{17}O DFT calculations were also completed for the various phases of $NaNbO_3$ obtained from the literature and Rietveld refinement.[140] The ^{17}O NMR parameters obtained post optimisation of each structure are given in Table 3.16. All ^{17}O parameters calculated prior to optimisation and using a fixed unit cell are given in Appendix II. Experimentally, two oxygen resonances were observed in the ^{17}O MAS NMR spectra obtained for both phase pure Pbcm $NaNbO_3$ and Solid-State Sample D. Tentative assignments of the two peaks observed in each spectrum were initially made using published crystallographic data. However, it was hoped that the ^{17}O parameters calculated would provide additional assistance with spectral assignment. Each of the phases calculated predicted very small values of C_Q for each of the crystallographically distinct oxygen sites, as shown in Table 3.16. These values suggest that each oxygen is in a symmetrical local environment, in good agreement with the observed experimental findings. In addition, for several of the phases calculated the chemical shifts of sites O1 and O2, and O3 and O4 were very similar, suggesting the potential overlap of these sites experimentally. Consistently in each of the DFT calculations completed the Pbcm and $P2_1ma$ phases of $NaNbO_3$ displayed similar parameters. This was also true for the ^{17}O NMR parameters calculated for the two phases. The four oxygen environments in the $P2_1ma$ phase of $NaNbO_3$ have been isolated and are shown in Figure 3.44(a-d). As observed for the Pbcm phase the four sites appear very similar. In addition, when compared with Figure 3.43 it is clear to see how subtly different the two polymorphs of $NaNbO_3$ are. This therefore aids in confirming the similarities observed in the NMR parameters calculated. The calculated ^{17}O NMR parameters therefore provide a possible reason as to why it is so challenging to distinguish between the various different phases of $NaNbO_3$ experimentally using ^{17}O NMR. The combined effect of very similar chemical shifts and very small values of C_Q indicates that peaks corresponding to each site will lie almost directly on top of one another, making it impossible to distinguish between very similar phases. To confirm the number of sites under each resonance higher-resolution approaches such as DOR and MQMAS could be utilised. However, the

Table 3.16: Calculated (using CASTEP) ^{17}O NMR parameters, δ_{iso}, P_Q, C_Q and η_Q, post optimisation, for selected room temperature phases of $NaNbO_3$, obtained from both literature and Rietveld refinement.

Phase	Site	δ_{iso} (ppm)	P_Q / MHz	C_Q / MHz	η_Q
Literature					
Pbcm[217]	O1	445.1	−1.38	−1.38	0.08
	O2	458.2	−1.18	−1.12	0.55
	O3	489.4	−0.48	−0.46	0.47
	O4	495.3	0.90	0.78	0.99
$P2_1ma$[228]	O1	447.0	−1.22	−1.20	0.33
	O2	452.7	−1.28	−1.23	0.50
	O3	488.1	−0.44	−0.43	0.33
	O4	496.3	0.88	0.77	0.98
Pmma[226]	O1	493.7	−0.51	−0.48	0.60
	O2	493.9	−0.51	−0.48	0.58
	O3	490.3	−0.47	−0.47	0.23
	O4	490.3	−0.47	−0.47	0.23
Refinement					
Pbcm	O1	443.5	−1.38	−1.38	0.11
	O2	460.3	−1.14	−1.08	0.56
	O3	488.5	−0.50	−0.48	0.46
	O4	494.6	−0.89	−0.78	0.94
$P2_1ma$	O1	445.6	−1.27	−1.25	0.32
	O2	453.1	−1.33	−1.28	0.50
	O3	488.6	−0.46	−0.45	0.31
	O4	496.0	0.87	0.75	1.00
$Pnm2_1$	O1	446.7	−0.82	−0.80	0.37
	O2	457.2	−1.40	−1.36	0.43
	O3	487.1	−0.49	−0.48	0.33
	O4	493.8	−0.84	−0.75	0.85
Pnma	O1	492.4	−0.50	−0.48	0.52
	O2	490.6	−0.51	−0.49	0.54

$Pn2_1a$	O1	506.0	0.54	0.49	0.78
	O2	463.6	−0.96	−0.94	0.37
	O3	466.2	−1.18	−1.10	0.67

exact level of ^{17}O enrichment obtained for each sample of $NaNbO_3$ is unknown. It is anticipated that the level of enrichment will be relatively low, therefore an MQMAS experiement would take a considerable amount of time to obtain. In samples containing a mix of two phases it would be considerably more informative to determine which oxygen environments are connected to one another in the structure. To do this a two-dimensional NOESY-like correlation experiment is required that can detect the transfer of magnetization through dipolar couplings. This would enable us to obtain additional information regarding the composition of each sample and possible connectivity within the sample. The presence of cross peaks in the NOESY-type experiment would indicate magnetization had been transferred from one oxygen site to another, thereby indicating the nuclei are spatially in bonding proximity and able to transfer magnetization between one another.

3.5 Discussion

Overlaid two-dimensional ^{23}Na NMR spectra for Solid-State Sample A, molten salt and sol-gel samples are shown in Figure 3.45(a). Expansions of the upper and lower sets of ridges are also shown in Figures 3.45(b) and (c) respectively. All four distinct Na sites present in Solid-State Sample A correlate with those present in the sol-gel sample. In particular, the two Na sites with $\delta_1 = -7.1$ ppm and 13.5 ppm in the sol-gel sample align exactly with the second phase consistently found in all solid-state and molten salt samples, as illustrated in the overlaid isotropic projections in Figure 3.45(b). This, therefore, suggests that the major phase produced by sol-gel synthesis is consistently present in all samples, irrespective of synthesis route. The quantity of this phase produced, however, varies significantly depending upon synthesis method.

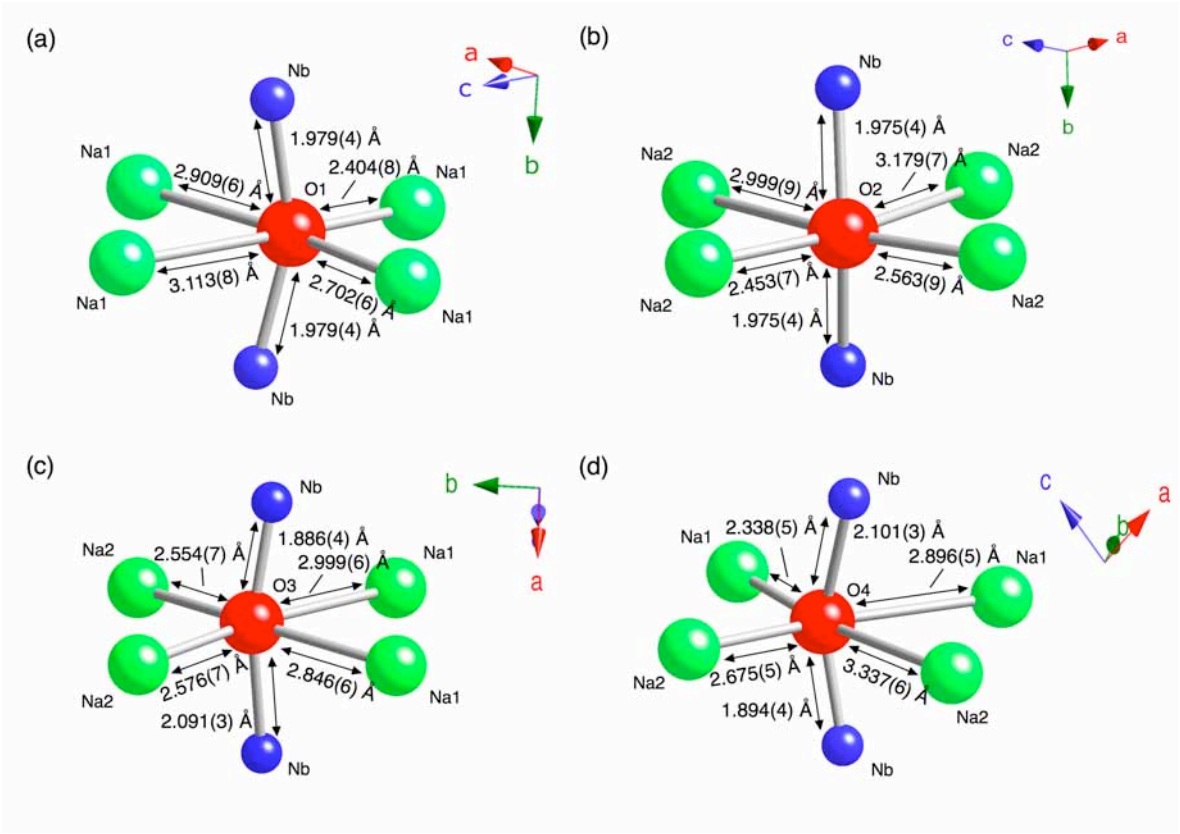

Figure 3.44: The coordination environments for sites (a) O1, (b) O2, (c) O3 and (d) O4 for the $P2_1ma$ polymorph of $NaNbO_3$ obtained from Rietveld refinement.

In a similar manner to solid-state reactions sol-gel methods can be difficult to control. It is often challenging to accurately monitor reaction temperatures during the reflux stage of the sol-gel synthesis owing to differences between internal and external vessel temperatures. In addition, for $NaNbO_3$ it is difficult to synthesise samples free from impurities using sol-gel reactions. For example, within our reactions the compound $Na_2Nb_4O_{11}$ was consistently formed.[256] There are, therefore, several contributing factors within the sol-gel reaction that aid in determining the exact polymorphs of $NaNbO_3$ produced.

Conclusions drawn from detailed comparison of the ^{23}Na NMR data aided considerably in the interpretation and structural refinement of both the s-PXRD and NPD data for Solid-State Sample A. Prior to such conclusions a variety of potential orthorhombic structures similar to Pbcm were tested using multiphase refinements, with little success. The potential identification of the $P2_1ma$ polymorph of $NaNbO_3$ by NMR in both the solid-state and molten salt samples provided a plausible structure

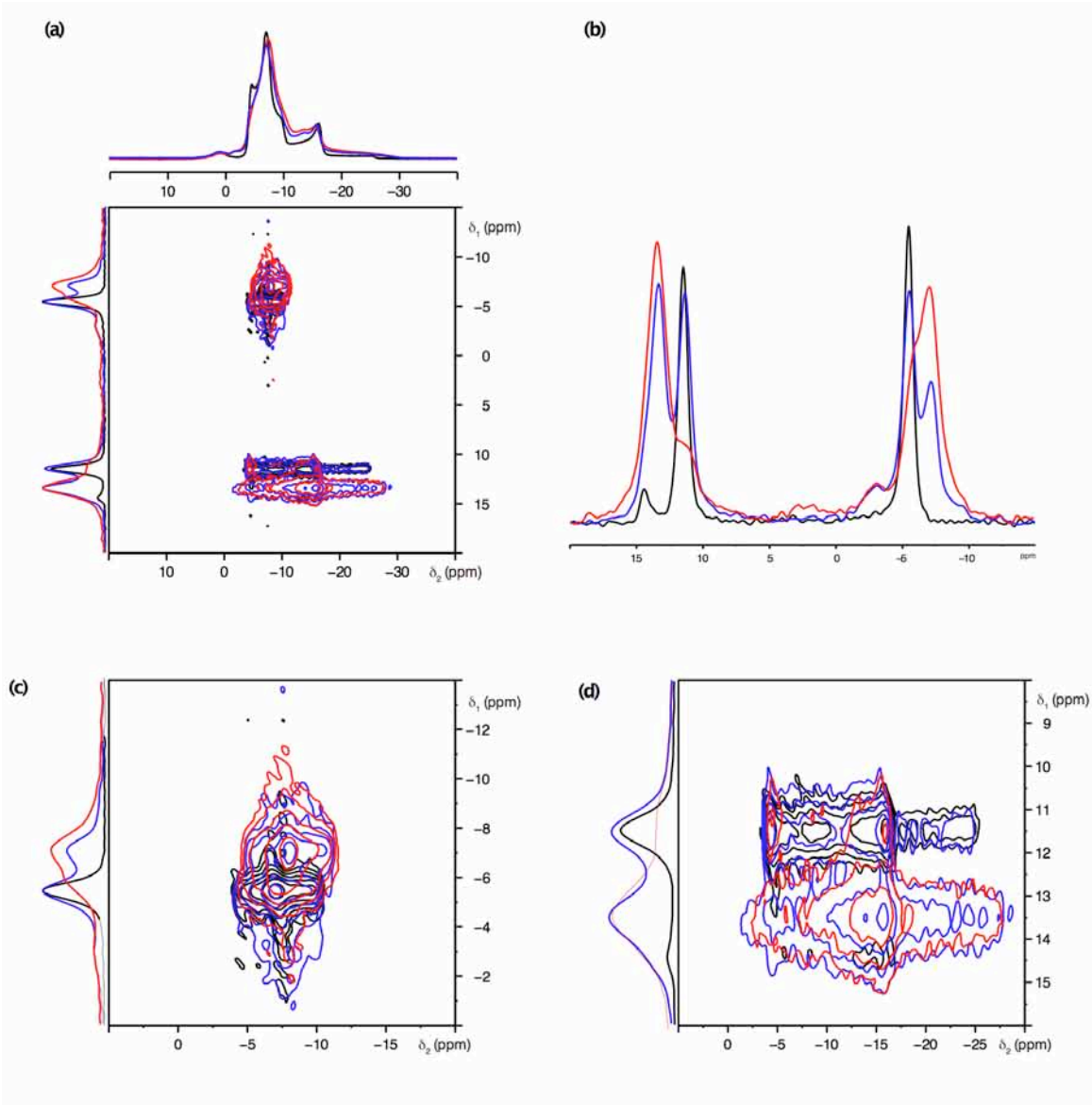

Figure 3.45: ^{23}Na (9.4 T) NMR of phase pure Pbcm $NaNbO_3$ (shown in black and synthesised using molten salt methods, 1000°C for 24 hours), Solid-State Sample A $NaNbO_3$ (shown in blue) and sol-gel $NaNbO_3$ (shown in red). (a) Conventional MAS and triple-quantum MAS NMR spectra, (b) corresponding isotropic projections and (c, d) expansions showing the upper (δ_{iso} = −5.08 ppm and δ_{iso} = −4.24 ppm) and lower (δ_{iso} = −0.51 ppm and δ_{iso} = 1.44 ppm) ridges.

to test by Rietveld refinement. Therefore, multiphase refinements were completed on both the s-PXRD and NPD data obtained for Solid-State Sample A using the previously obtained Pbcm and $P2_1ma$ models, and are shown in Figures 3.46 and 3.47, respectively. These models were fixed, with only lattice parameters and phase fractions being refined. Upon the

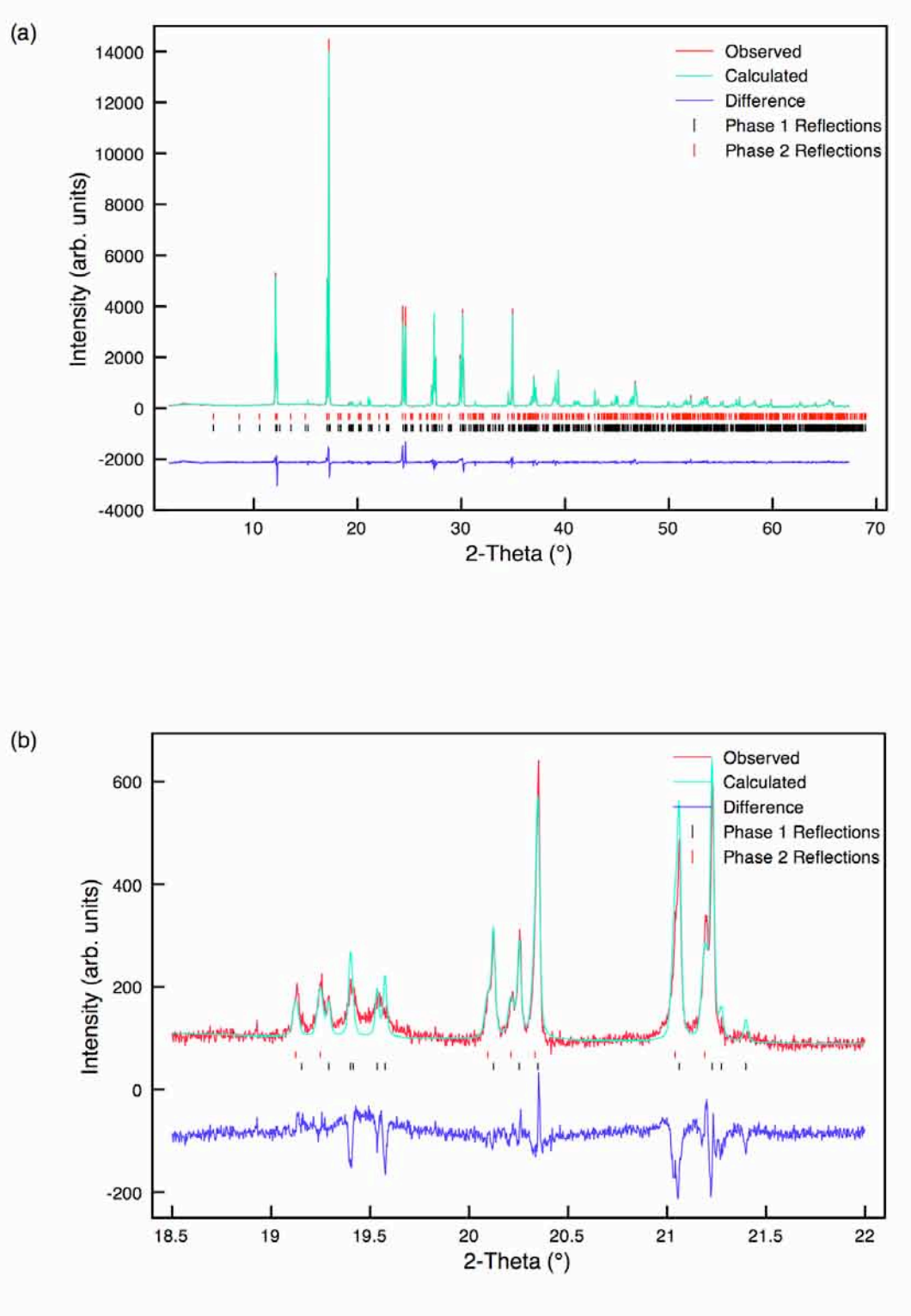

Figure 3.46: Multiphase Rietveld profiles for Solid-State Sample A $NaNbO_3$ using structural models Pbcm and $P2_1ma$ for s-PXRD data. Expansions of the corresponding superstructure peaks are shown in (b) 2θ = 18.5° - 22°.

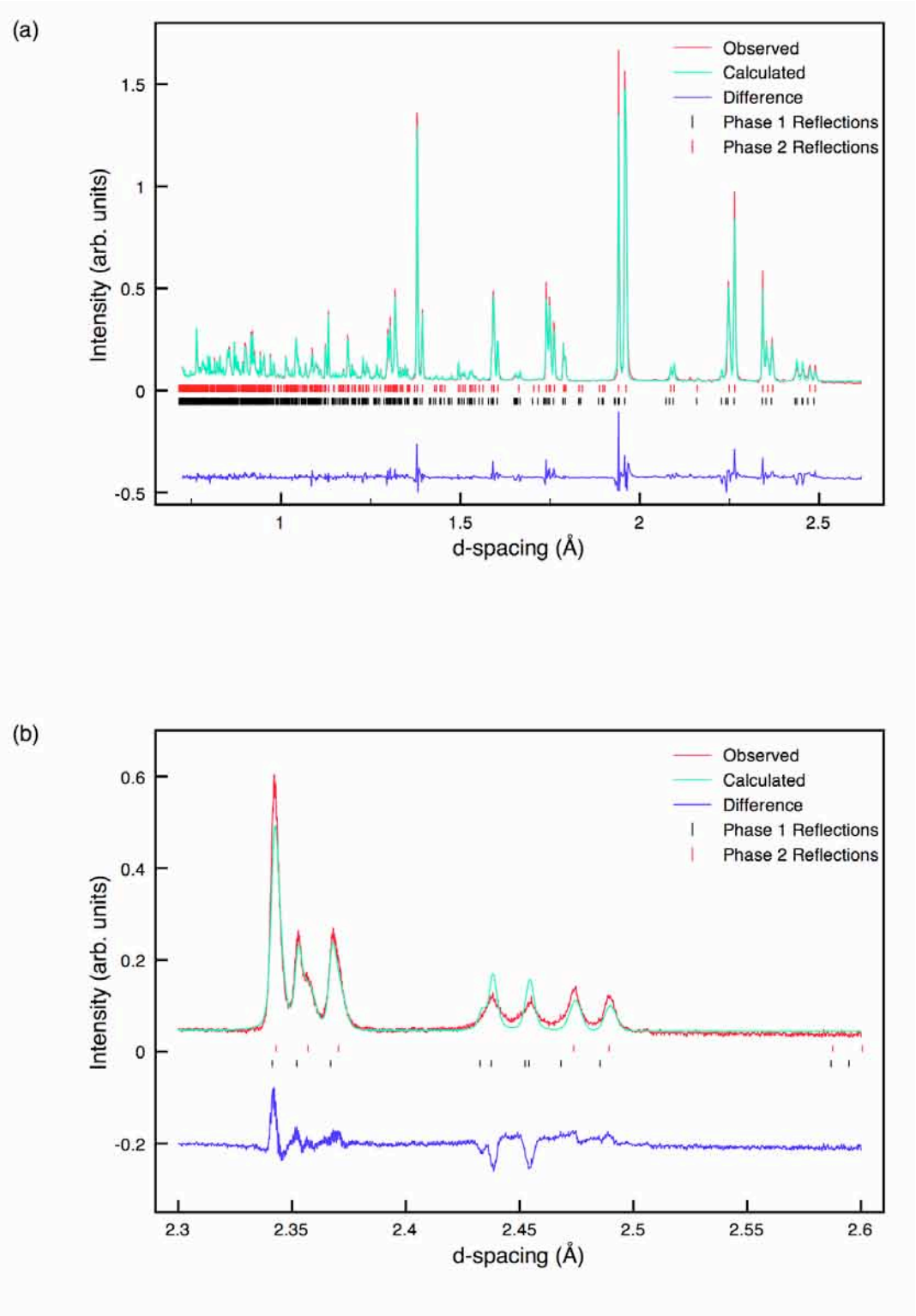

Figure 3.47: Multiphase Rietveld profiles for Solid-State Sample A $NaNbO_3$ using structural models Pbcm and $P2_1ma$ for NPD data. Expansions of the corresponding superstructure peaks are shown in (b) d = 2.3 Å – 2.6 Å.

Table 3.17: Monoclinic structural model used for refinement of NPD data for sol-gel $NaNbO_3$. Space group Pm, a = 5.57073(5) Å, b = 7.76625(6) Å, c = 5.51338(5) Å, β = 90.084(1)° and V = 238.529(3) Å^3. χ^2 = 4.2, wR_p = 6.2% and R_p = 5.7%.

Atom	Site	x	y	z	U(iso) × 100 / Å^2
Nb1(a)	2c	0.26246	0.25	0.2466	0.20
Nb1(b)	2c	0.76246	−0.25	−0.2466	0.20
Na1(a)	1a	0.2596	0	0.7481	0.50
Na1(b)	1a	0.7596	0	−0.7481	0.50
Na2(a)	1b	0.2915	0.5	0.7327	2.24
Na2(b)	1b	0.7915	−0.5	−0.7327	2.24
O1(a)	1a	0.2409	0	0.3124	0.53
O1(b)	1a	0.7409	0	−0.3124	0.53
O2(a)	1b	0.2257	0.5	0.1928	0.37
O2(b)	1b	0.7257	−0.5	−0.1928	0.37
O3(a)	2c	0.0131	0.279	0.5272	1.84
O3(b)	2c	0.5131	−0.279	−0.5272	1.84
O4(a)	2c	−0.049	0.2197	0.036	0.61
O4(b)	2c	0.451	−0.2197	−0.036	0.61

addition of the $P2_1ma$ phase the quality of refinement improved considerably for both datasets. Subtle peak splittings previously treated as single phase in the s-PXRD data were now accounted for and indexed which, in turn, assisted in the accurate modelling of both the profile parameters and peak intensities. An expansion of the superstructure region 18.5° – 22° is shown in Figure 3.46(b). Considerably better wR_p (14.2%) and χ^2 (7.6) values were obtained, with refined phase fractions of 60(2)% and 40(2)% for the Pbcm and $P2_1ma$ phases, respectively. A similar two-phase refinement of the NPD data considerably improved the quality of the fit at low d-spacing, in comparison to the single phase refinements previously discussed, leading to better wR_p (8.4%) and χ^2 (22.7) values, with refined phase fractions of 57(2)% and 43(2)% for the Pbcm and $P2_1ma$ phases, respectively. The phase fractions obtained from refinement are in

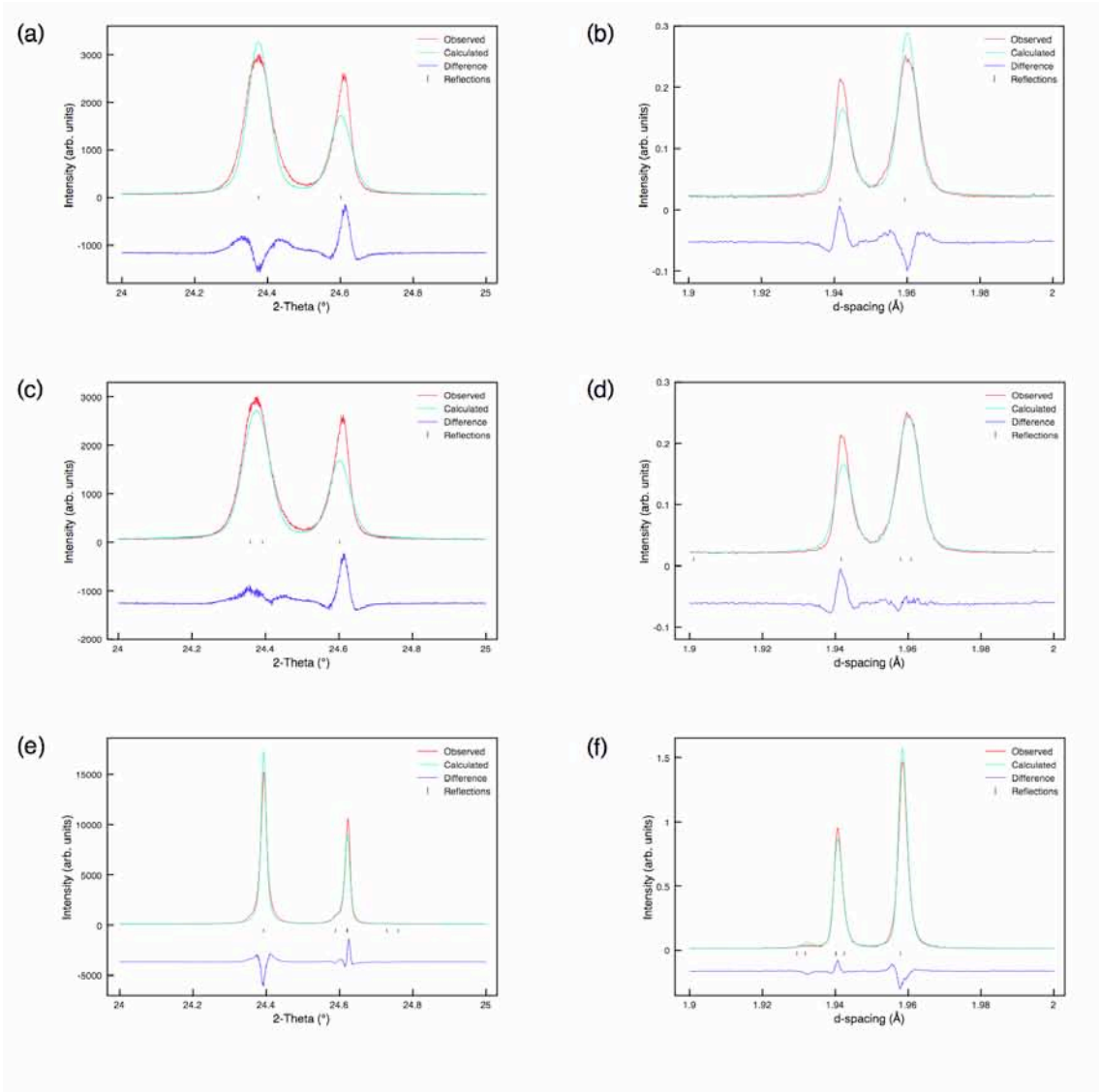

Figure 3.48: Rietveld profiles of (a, c) s-PXRD data (2θ = 24° - 25°) and (b, d) NPD data (d = 1.9 Å – 2 Å) for sol-gel $NaNbO_3$ using structural models (a, b) $P2_1ma$ and (c, d) Pm. Plots (e) and (f) show the corresponding regions for the refinement of commercial $NaNbO_3$ (Aldrich) using the Pbcm model, suggesting that this phase is truly orthorhombic, and does not have the monoclinic distortion previously suggested.

agreement with those from NMR (estimated to be ~60% and ~40%) from the MQMAS spectrum in Figure 3.6. In particular, the additional peaks previously highlighted in the single phase refinement at 2.47 Å and 2.49 Å were now adequately modelled, as shown in Figure 3.47(b).

On closer inspection of the refinements involving the suggested $P2_1ma$ phase it is apparent that subtle peak broadenings exist which are compatible with a symmetry-lowering to monoclinic ($\beta \neq 90°$). Such a

Table 3.18: Refined lattice parameters from multiphase refinement of Solid-State Sample A $NaNbO_3$ for the s-PXRD (χ^2 = 7.6, wR_p = 14.2% and R_p = 10.0%) and NPD data (χ^2 = 22.7, wR_p = 8.4% and R_p = 7.7%), using structural models Pbcm and $P2_1ma$.

		a (Å)	b (Å)	c (Å)	V (Å^3)
s-PXRD	Pbcm	5.50490(1)	5.56973(1)	15.51753(4)	475.780(2)
	"$P2_1ma$"	5.57667(3)	7.76157(4)	5.51774(3)	238.828(2)
NPD	Pbcm	5.50641(7)	5.57068(7)	15.52364(2)	476.179(14)
	"$P2_1ma$"	5.57734(8)	7.76281(16)	5.51986(9)	238.987(8)

symmetry-lowering has previously been observed in the KNN solid-solution at low potassium content.[257] Rietveld refinements were completed for both the s-PXRD and NPD data for the sol-gel $NaNbO_3$ sample using the monoclinic model Pm. Expansions of the regions 2θ = 24° - 25° in the s-PXRD data and d = 1.9 Å – 2 Å in the NPD data are shown in Figure 3.48. Also shown for comparison are the Rietveld refinements completed using the "$P2_1ma$" model. The quality of refinement for these particular regions in both datasets is improved using the structural model for a monoclinic cell, suggesting there may be a monoclinic distortion present in the sol-gel $NaNbO_3$ sample. The model used is given in Table 3.17. This model was derived from the $P2_1ma$ model by reducing the symmetry to monoclinic, Pm, but imposing strict "$P2_1ma$" constraints on all the structural parameters, and keeping these fixed. The only additionally refined structural parameter was therefore the β angle, which refines to 90.084(1)°. We stress that this refinement merely demonstrates that this phase may well be monoclinic and does not refine the true space group or the nature or driving force of the monoclinic distortion. The allowed non-centrosymmetric monoclinic subgroups of Pnma are Pm and $P2_1$, both of which are possibilities (also both are polar). Pm gives 4 Na sites whereas $P2_1$ gives only 2, which is perhaps more compatible with the NMR data. The precise nature of this monoclinic phase (and that of the analogous K-doped $NaNbO_3$[222]) has yet to be determined. The plots shown in Figures 3.48(e) and (f) show the

corresponding regions for the refinement of commercial $NaNbO_3$ (Aldrich) using the Pbcm model, suggesting that this phase is truly orthorhombic, and does not have the monoclinic distortion previously suggested.[222] The previous suggestion by Darlington and Knight[222] is now believed to be owing to the presence of the $P2_1ma$ phase which lay undetected in their sample. Therefore, we shall now refer to this phase as "$P2_1ma$", on the understanding that it appears very subtly monoclinic. Refined lattice parameters for multiphase refinement of Solid-State Sample A using both s-PXRD and NPD data are given in Table 3.18.

The space group $P2_1ma$ was a tentative suggestion by Ashbrook *et al.*,[231] for the nature of the unknown phase within their sample, made purely by a preliminary examination of the additional peaks in their l-PXRD pattern. Although high-resolution data is usually required to draw such conclusions, in this particular case their tentative suggestion appears to have been borne out. Their explanation as to why the "$P2_1ma$" polymorph is formed perhaps relates to their use of a low temperature synthetic route (hydrothermal methods using 200 °C) as opposed to conventional solid-state methods using temperatures in excess of 1000 °C. We have shown, using a variety of techniques, that this "$P2_1ma$" polymorph is consistently formed, regardless of specific experimental conditions. Their suggestion as to why is also consistent with our findings; temperature plays a prominent role in the phases of $NaNbO_3$ synthesised and their relative quantities.

The two polymorphic phases of $NaNbO_3$, Pbcm and "$P2_1ma$", routinely coexist in many samples irrespective of synthesis route and are seen, from both diffraction and solid-state NMR, to be structurally similar. However, crystallographic examination shows that the two adopt subtly different octahedral tilt systems. This cooperates with local Na^+ cation displacements to produce both a centrosymmetric and a polar phase of similar stability. In the Pbcm phase the Na displacements are out-of-phase with one another leading to the longer periodicity of the c-axis ($4a_p$ or about 15.5 Å), as shown in Figure 3.1(a). The mechanism of octahedral tilting within the Pbcm structure is effectively a 'twinning' operation when compared with $P2_1ma$ (or, more strictly the parent Pnma). Hence

the standard $a^-a^-b^+$ system in $P2_1ma$ becomes [$a^-a^-b^+$ / $a^-a^-b^-$ / $a^-a^-b^+$] *via* an inversion about the central block (equivalent to an additional out-of-phase tilt between blocks 2 and 3 along the c-axis). It is perhaps therefore little surprise that two polymorphs based on these very similar tilt systems can compete, depending on synthetic variables, and also no surprise that their diffraction patterns are so similar. In fact, a further manifestation of the similarity of the two structures can be seen in the NPD data (Figure 3.47), where the additional superlattice peaks due to the $4a_p$ supercell in the Pbcm phase (i.e., the l-odd reflections) are noticeably broader than the subcell peaks, suggesting that long-range registry of the additional out-of-phase tilt is weak.

The subtle effects that drive the appearance of both polymorphs are currently unknown, but the influence of the 'ferroelectrically–active' Nb^{5+} cation on the B-site must be considered. In the case of $NaNbO_3$ diffraction indicates that in the Pbcm phase Nb 'on average' lies approximately centrosymmetrically within the octahedra. However, the local environment probe, solid-state NMR, suggests it may be disordered in some manner. The ^{93}Nb MQMAS NMR spectrum recorded for the commercially purchased sample (Figure 3.35) displays a degree of additional broadening, suggesting Nb may exhibit some positional disorder. In the "$P2_1ma$" polymorph the Nb^{5+} cation lies significantly off-centre (towards an edge of the octahedron). All bond lengths obtained from the Rietveld refinement are given in Appendix II.

Ultimately, the use of several complementary techniques within this investigation has led to the accurate structural identification of two polymorphic room temperature phases of $NaNbO_3$ present in a variety of samples synthesised by various synthetic routes. Previous studies have often concentrated solely on one particular characterisation technique. However, as presented within this particular study, it can be extremely challenging, and dangerous, to rely on such an approach. Using diffraction alone for example, it can be difficult to identify and correctly model weak superlattice peaks and peak splittings or broadenings. In such cases it is vital to utilise a number of different techniques in order to ensure an accurate and robust structural characterisation.

3.6 Prediction of Perovskites using *Ab Initio* Random Structure Searching (AIRSS)

3.6.1 Introduction to AIRSS

The theoretical prediction of crystal structures is highly desirable. However, in reality it is extremely complex and challenging. In recent years computational codes capable of finding new phases and structures have been successfully developed. One such method is *ab initio* random structure searching (AIRSS), a first-principles DFT approach.[244-247] This particular method of structure searching works by relaxing many random structures to their enthalpy minimum at fixed pressures. It is important to note that this method does not rely on any previous theoretical or experimental results. To date, AIRSS has successfully predicted high-pressure phases of materials such as silane,[244] aluminium hydride[246] and ammonia.[247] This particular method of structure searching has also been used for pure elements such as hydrogen,[245] nitrogen,[258] lithium[259] and iron.[260] More recently AIRSS has been successfully used to investigate defect complexes in silica[261,262] and, at present, there is considerable interest in determining whether AIRSS may be extended to other structurally complex materials, for example perovskites. AIRSS is a DFT approach, and an important limitation of this method is the number of atoms per unit cell. As a result, it is often challenging to implement structure searching methods on systems with a large number of atoms per unit cell. In many cases, however, this can be overcome by the application of sensible constraints to a system, such as cell volume, bond distances, number of symmetry operations or coordination number.

As stated previously, perovskites are currently one of the most widely studied areas of solid-state chemistry, with numerous applications to a variety of materials and devices. Hence, a technique capable of predicting complex perovskite structures would be extremely useful to many solid-state chemists. Within this particular investigation structure searching techniques have been used in conjunction with experimental methods and initial DFT calculations. Structure prediction has been

attempted for $NaNbO_3$ to determine whether any alternative phases of $NaNbO_3$ exist which differ from those found experimentally.

3.6.2 AIRSS Computational Details

The following procedure was used for the prediction of perovskite structures using AIRSS. Perovskites are composed of ABO_3 units, commonly referred to as formula units (f.u.). A specific number of f.u., usually 2, 4, 6 or 8, are randomly placed into a unit cell where the starting structure is a simple cubic perovskite. The lattice parameters are then redefined to produce a new structure corresponding to the number of $NaNbO_3$ units placed into the cell. Structures are then generated by randomising the positions of the atoms to within 0.5 Å about their initial position. Each of these configurations is then relaxed to a minimum in enthalpy. This search is then continued until the lowest enthalpy structures are consistently found. In this particular investigation it was possible to search for different phases of $NaNbO_3$ with up to 40 atoms per unit cell. This was possible owing to the application of carefully selected constraints.

3.6.3 Structure Searching $NaNbO_3$

Structure searching for $NaNbO_3$ was completed using 2, 4, 6 and 8 formula units (f.u.) as the initial configurations. During each search the known low temperature phase of $NaNbO_3$, R3c, was consistently found as the lowest energy structure. The R3c phase was therefore identified as the most thermodynamically stable polymorph of $NaNbO_3$. All DFT calculations were completed at 0 K and therefore it is of little surprise a low temperature phase was identified as the most stable. During each search many other phases were also found, the results of which will be discussed in the following section.

Initial searches for $NaNbO_3$ were completed using 2 $NaNbO_3$ formula units. This search produced 219 structures, the most stable of which was the orthorhombic $Pmc2_1$ phase (alternative setting $P2_1ma$),

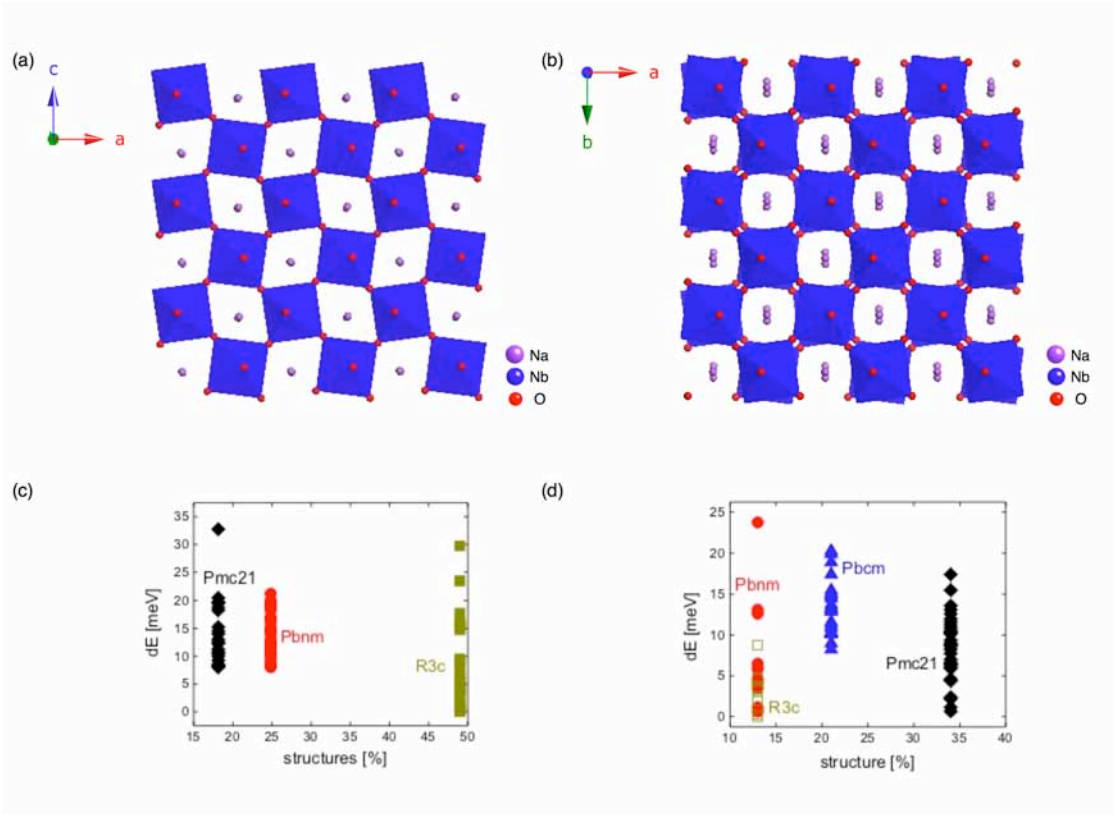

Figure 3.49: The (a) $Pmc2_1$ and (b) Pbcm structure of $NaNbO_3$ found using AIRSS. (c, d) Plots showing the relative energies of the phases found during the 4 f.u. and 8 f.u. searches, respectively.

shown in Figure 3.49(a). Searches completed using 4 f.u. produced 149 structures. The low temperature R3c phase of $NaNbO_3$ was again identified as the most stable, with 49% of all structures found being this phase. After the R3c phase, the most frequently found structures with the lowest energies were the Pbnm (24.8%) and $Pmc2_1$ (18.1%) phases. All of the phases discovered during the 4 f.u. search and their relative percentages are shown in Figure 3.49(c). Redefining the lattice parameters in the 4 f.u. search in an alternative manner produced a 2 × 2 × 1 4 f.u. perovskite. This search produced 141 structures and, as previously observed in the 2 f.u. searches, the $Pmc2_1$ phase was found to be the most stable. Of the lowest energy structures obtained 69.5% were this phase, as shown in Figure 3.49(c). Interestingly, a different structure type belonging to space group Amm2 was also found in this search. As previously stated, the $KNbO_3$ structure is widely accepted as an orthorhombic structure in space group Amm2. The identification of this particular phase of $NaNbO_3$

suggests it is possible for $NaNbO_3$ to adopt a structure-type similar to $KNbO_3$. However, despite being discovered in 29.8% of cases the high energy of this phase indicates that, experimentally, it is unlikely to be observed as there are phases with considerably lower energies that can be more feasibly observed.

Using 6 f.u. 102 structures were found and, as in the 4 f.u. search, consistently the lowest energy structure was the $Pmc2_1$ phase (68.6%). Searches completed using 8 f.u. produced 100 structures, 13% of which were the lowest energy R3c phase. In this search 13% of the structures found were a Pbnm phase, however, these were at relatively high energies. Therefore, in the 8 f.u. search the most energetically stable structures of $NaNbO_3$ were the $Pmc2_1$ (34%) and Pbcm (shown in Figure 3.49(b)) (21%) phases respectively. A plot of the relative percentages of each phase found for all 8 f.u. searches is shown in Figure 3.49(d). When symmetry checks were completed for each of the structures found using 8 f.u. the most stable $Pmc2_1$ phases were discovered to transform into 4 f.u. $Pmc2_1$ structures, whilst the higher energy $Pmc2_1$ phases yielded 8 formula units per unit cell. It must be noted that when the $Pmc2_1$ and Pbcm phases of $NaNbO_3$ found using AIRSS were compared with those found experimentally there were subtle differences in the position of the Na. It is possible that slight differences in the Na positions within each phase could be responsible for the phases observed experimentally. Very subtle changes of this type to the position of the Na is not likely to be observed using diffraction techniques as diffraction will only observe the average position of the Na.

Shown in Figure 3.50 is an energy plot displaying the phases of $NaNbO_3$ found using structure searching methods and their relative energies. Consistently the most thermodynamically stable phases of $NaNbO_3$ identified were the low temperature R3c phase, followed by both the $Pmc2_1$ and Pbcm phases. However, Figure 3.50(a) highlights an important point regarding the energy difference observed between the very similar $Pmc2_1$ and Pbcm phases. The difference observed between the two is extremely small. This therefore suggests that, experimentally, it would be very difficult to distinguish between the two phases owing to

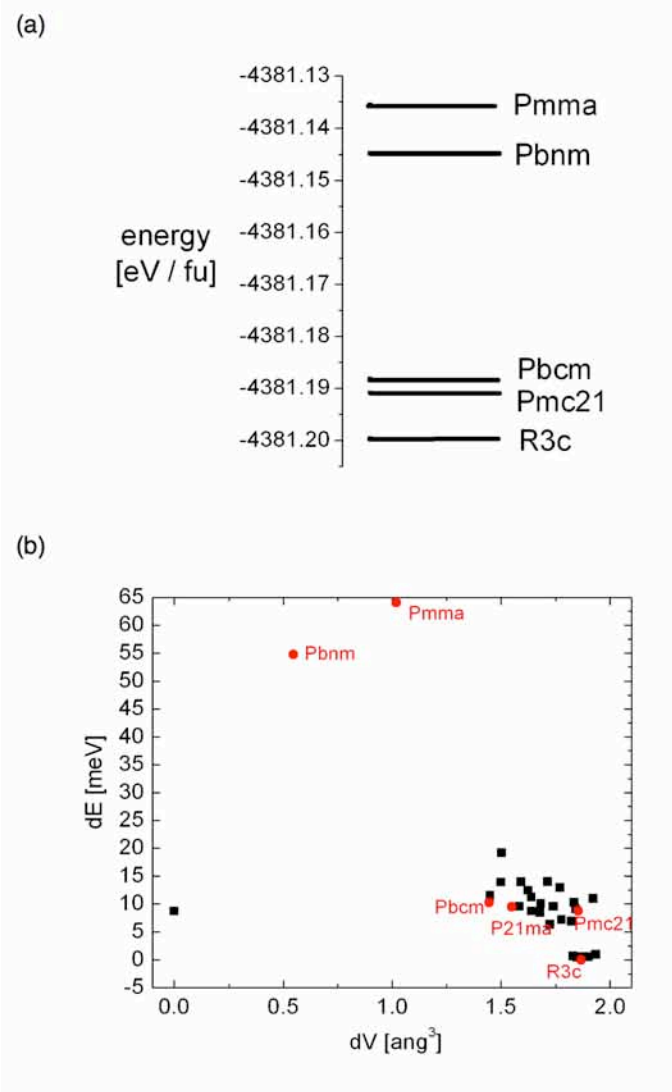

Figure 3.50: (a) Plot showing the relative energies of all phases of $NaNbO_3$ found during the structure search using AIRSS. (b) Plot displaying the experimental (red) and predicted (black) phases of $NaNbO_3$ and their relative energies as a function of cell volume.

their very similar energies. This, to some extent, confirms many of the experimental findings presented within this work. Experimentally, samples of $NaNbO_3$ are composed of two structurally very similar phases, Pbcm and $P2_1ma$, the quantities of which have been shown to vary depending on the precise reaction conditions used. It is therefore extremely challenging to routinely synthesise samples of $NaNbO_3$ with identical ratios of the two phases. The results obtained using structure prediction methods highlight a possible reason for such behaviour. The energies of the two phases have been shown to be extremely similar,

suggesting factors such as annealing temperature and/or time may affect the phases that form experimentally. For example, marginally higher or lower reaction temperatures could potentially cause one phase to preferentially form over the other. In addition, the particle size, stress and strain exhibited by the structure may also play a vital role in determining the phases observed experimentally. Also shown in Figure 3.50(b) is a plot displaying each of the phases found experimentally, denoted in red, and the optimised structures obtained using AIRSS, denoted in black. Using this plot it is clear to see that the phases found using structure searching correlate with the major phases of $NaNbO_3$ obtained experimentally within this investigation.

The major phases of $NaNbO_3$ predicted using AIRSS were the Pbcm and $P2_1ma$ phases, and this is in good agreement with those observed experimentally. The low temperature R3c phase of $NaNbO_3$ was also consistently found using AIRSS owing to the calculations being completed at 0 K. It must be noted that several of the additional phases of $NaNbO_3$ found using AIRSS, namely Pbnm and Pmma, exhibit no real agreement with those observed experimentally. For example, the Pbnm phase possesses only a single Na site and therefore bears no correlation with the high-resolution ^{23}Na MQMAS data obtained. The Pmma phase was relatively high in energy when compared with all other phases of $NaNbO_3$ found. Therefore, experimentally, it is highly unlikely this high energy phase would form under ambient temperature and pressure conditions.

The identification of the Pbcm and $Pmc2_1$ polymorphs of $NaNbO_3$ by structure searching is both an interesting and surprising result. Starting from a random arrangement of $NaNbO_3$ units in a unit cell it was possible to match experimental findings. $NaNbO_3$ is an extremely complex perovskite and for many years there has been considerable dispute regarding the phases of $NaNbO_3$ formed. Therefore, the identification of the same two phases consistently observed experimentally using computational methods is extremely encouraging. This, in turn, suggests that structure searching using AIRSS could be successfully applied to many other perovskite-based compounds. It is therefore hoped that these methods will be extended to other complex

solid-state systems in the future and that structure predicting techniques could aid many solid-state chemists.

3.7 A Third Polymorph?

The ^{23}Na MQMAS spectra presented in this chapter have shown almost all samples of $NaNbO_3$ to comprise of two very similar phases, now known to be the Pbcm and $P2_1ma$ polymorphs. However, consistently in each two-dimensional ^{23}Na MAS NMR spectrum recorded, including that of the commercially purchased sample of $NaNbO_3$, an additional resonance was observed that did not appear to correlate with either the Pbcm or $P2_1ma$ phases of $NaNbO_3$. Initially signal corresponding to this extra site was attributed to 'noise' in the MQMAS spectrum. However, upon closer inspection and calculation of the isotropic projections onto the δ_1 axis it became apparent that this signal produced a corresponding peak in the isotropic spectrum. This, therefore, suggested the presence of a third phase. The peak was consistently present in spectra recorded at both 9.4 T and 14.1 T and, as with the Pbcm and $P2_1ma$ polymorphs of $NaNbO_3$, the quantity of this phase present in each spectrum appeared to vary depending on the precise reaction conditions used. In addition, there did not appear to be any direct correlation between the synthesis method used and the quantity of this phase produced. Consistently, only very small percentages of this phase were present in each sample, i.e., ~1-2%. Therefore, it was very difficult to detect its presence by MAS NMR. The ^{23}Na MQMAS (14.1 T) NMR spectrum shown in Figure 3.51 contains the greatest quantities of this third phase and it is clear to see how small the quantity of this phase is. In addition, the position of this resonance, δ_1 = 5.47 ppm, is very close to the overlapped Na1 sites of the Pbcm and $P2_1ma$ polymorphs in spectra recorded at 14.1 T. To highlight how the quantity of this phase varies from sample to sample and depends on the synthesis method, several isotropic projections obtained from MQMAS spectra are shown in Figure 3.52.

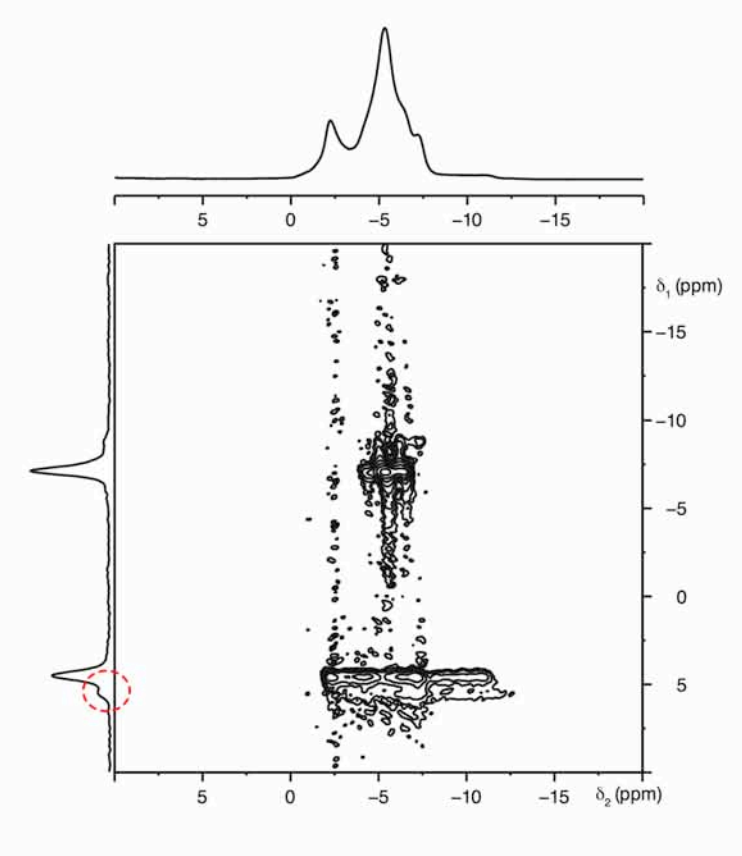

Figure 3.51: Conventional ^{23}Na (14.1 T) MAS NMR spectrum, triple-quantum MAS NMR spectrum, and corresponding projection for a molten salt sample of $NaNbO_3$ synthesised using 1000 °C for 12 hours. The region highlighted indicates the possible presence of a third polymorph of $NaNbO_3$. The MAS rate was 14 kHz.

At present, it is only possible to identify the presence of this phase using ^{23}Na MQMAS techniques. The high-resolution diffraction patterns obtained for each of the samples investigated do not appear to possess any additional peaks. Given the exceptionally small quantities of this phase present in each sample it is likely that peaks belonging to this phase lie in the background of any diffraction pattern. This will therefore make it very difficult to accurately identify and structurally characterise this phase. If this phase is a different polymorph of $NaNbO_3$ it is highly likely that the most intense peaks in the diffraction pattern will reside under those belonging to the Pbcm and/or $P2_1ma$ polymorphs already present in the sample. This would, in turn, make it impractical to identify peaks belonging to this phase and structurally characterise the phase. We are confident that this resonance is not related to either the Pbcm or $P2_1ma$

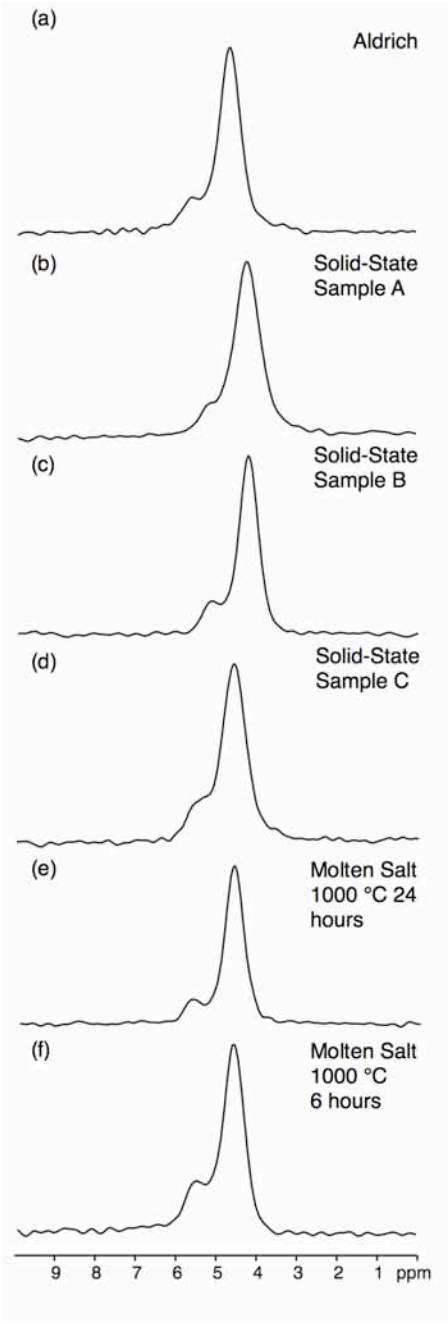

Figure 3.52: Isotropic projections obtained from triple-quantum ^{23}Na (14.1 T) MAS NMR spectra of (a) Solid-State Sample A, (b) Solid-State Sample B, (c) Solid-State Sample C and (d, e) molten salt samples of $NaNbO_3$ synthesised at 1000 °C for 24 hours and 6 hours, respectively.

polymorphs of $NaNbO_3$. Therefore, we believe that this phase is either a different polymorph of $NaNbO_3$ or an unrelated Na-bearing phase. At present there is no evidence to suggest that the quantity of this phase correlates with the ratio of the Pbcm/$P2_1ma$ phases present in each sample, i.e., it does not increase or decrease with the changing ratios of the

Pbcm and $P2_1ma$ phases. It must be noted that there may be other additional sites relating to this unknown phase present in the MQMAS spectrum. However, given the relative quantities of this phase it is likely that signal corresponding to these sites is heavily masked by noise and/or the other Na sites belonging to the Pbcm and $P2_1ma$ polymorphs. The only feasible way of characterising this phase is to synthesise a sample with much greater quantities, as peaks corresponding to this phase would then appear in the diffraction pattern. However, at present the precise reaction conditions required to synthesise a sample containing greater quantities of this particular phase are unknown. Therefore, in order to establish the necessary conditions a systematic study of synthetic method is needed. A considerable amount of work is therefore required before any accurate conclusions may be drawn regarding the exact nature of this third phase.

3.8 Conclusions

In summary, we have confirmed it is possible to synthesise a polar phase (probably monoclinic, but of symmetry very close to orthorhombic, space group $P2_1ma$) of $NaNbO_3$ using sol-gel techniques. We have also shown, by means of a systematic study, that synthetic method affects the polymorphic forms of $NaNbO_3$ produced in any one reaction. It is possible to isolate a pure sample of the Pbcm polymorph, and high-resolution powder diffraction studies confirm that this is indeed a correct space group assignment for this phase: previous confusion regarding the possibility of a symmetry-lowering to monoclinic might be explained by the occurrence of a significant "$P2_1ma$" phase impurity in the sample studied by Darlington and Knight.[222] Routinely the phases Pbcm and "$P2_1ma$" coexist as the two major room temperature polymorphs of $NaNbO_3$. The thermodynamic stabilities of the two phases are believed to be extremely similar, therefore slight variations in the reaction conditions force one to preferentially form over the other. Consistently, the Pbcm polymorph forms more readily, suggesting it to be the more thermodynamically stable of the two. The identification of the Pbcm and

$P2_1ma$ phases is also consistent with initial DFT calculations and preliminary structure searching results. Using AIRSS the R3c, $Pmc2_1$ and Pbcm phases were routinely found to be the most thermodynamically stable phases of $NaNbO_3$. Very little difference in energy was identified between the $Pmc2_1$ and Pbcm phases, highlighting once again how similar the two phases are. The possible occurrence of a third polymorph of $NaNbO_3$ was also suggested using ^{23}Na MQMAS NMR techniques. The quantities of this phase were extremely low (~1-2%) which made it impossible to successfully identify and/or characterise the phase. Further work is therefore needed to determine whether this corresponds to a different polymorphic form of $NaNbO_3$. It is therefore important to emphasise that it is essential to be aware of this subtle polymorphism in $NaNbO_3$, its occurrence as a function of preparative method, and how to identify it from both diffraction and NMR data; much of the earlier work regarding $NaNbO_3$ and its phase diagram should be treated with some degree of caution in light of our findings. Furthermore, these findings have implications for the present and future study of the KNN solid-solution and its piezoelectric behaviour.

Chapter 4

Synthesis and Characterisation of $NaNbO_3$-based Solid-Solutions

4.1 Introduction

Sodium niobate, $NaNbO_3$, is an extremely complex perovskite that has been studied extensively for many years.[222,223,263-266] The comprehensive structural study completed in the previous chapter employed a variety of complementary techniques to characterise room temperature $NaNbO_3$ and samples were found to routinely comprise of two structurally very similar orthorhombic phases; the centrosymmetric Pbcm and polar $P2_1ma$ polymorphs. The quantities of the two phases present are now known to vary considerably depending on the precise synthesis method used.

Lead zirconium titanate, $Pb(Zr_xTi_{1-x})O_3$ (PZT), is currently the most widely used piezoelectric material, with numerous applications to a variety of materials and devices. There is, however, considerable motivation to establish lead-free alternatives capable of achieving responses equal to or superior to PZT. Several recent high profile publications within the literature suggest $NaNbO_3$-based ceramics are capable of achieving such responses.[25,26] In particular the solid-solution $K_xNa_{1-x}NbO_3$ (KNN) has been shown to produce exceptional piezoelectric responses at compositions close to $x = 0.5$.[25,26] This has, in turn, accelerated the alkaline niobates to the forefront of the search for suitable lead-free piezoelectric ceramics. The room temperature phase diagram of KNN, initially published by Athee and Glazer,[267] suggests the presence of three phase boundaries; $x = 0.17$, $x = 0.3$ and $x = 0.5$. Whilst there is confusion regarding the Na-rich region of the phase diagram the crystal structure of the other end-member $KNbO_3$ is widely known as being orthorhombic, in space group Amm2.[220] To date, several structural studies have been completed for many compositions in the KNN series.[268,269] This particular series is widely known to exhibit the highest dielectric and piezoelectric responses at $x = 0.5$, near to the suggested morphotropic phase boundary

(MPB) at x = 0.45.[270,272] Hence, many investigations have concentrated in this region.[273-276] It must be noted that, at present, despite considerable research in this field no effective alternative to PZT has yet been found. The KNN series is therefore still the focus of many important structural investigations throughout the world.

The $NaNbO_3$ literature is extensive and largely dominated by KNN, and in particular x = 0.5. Detailed investigations are currently being undertaken for polycrystalline, nanocrystalline and submicron powders to determine whether enhanced piezoelectric responses are also observed in samples with varying particle size distributions. To date, however, relatively little work has been completed on the other predicted phase boundaries in the KNN phase diagram, namely x = 0.17 and x = 0.3. It is possible such areas may also exhibit MPBs and, in turn, may be potential 'green' replacements for PZT. Comprehensive studies have recently been completed by Baker *et al*.[277] and Zhang *et al*.[257] for compositions close to x = 0.3. The first of these concluded that samples with composition x = 0.3 refined well to the monoclinic space group Pm at room temperature and the tetragonal space group P4mm at 523 K. This work also highlighted a region of phase coexistence between the monoclinic and tetragonal phases, consistent with a first-order phase boundary. Zhang and co-workers conducted a similar structural study at low temperatures for compositions x = 0.05 and x = 0.3, both of which were found to be rhombohedral, in space group R3c. In a similar manner to the work by Baker *et al*., a region of phase coexistence was found close to room temperature between the rhombohedral and monoclinic phases, indicating the presence of a phase boundary. This was in good agreement with earlier suggestions by Ahtee and Glazer.[267] Interestingly, both publications suggested a lowering in symmetry to a monoclinic phase was observed when 30% K was doped into the $NaNbO_3$ structure at room temperature. As discussed in the previous chapter, many of our $NaNbO_3$ samples exhibited two phases, the orthorhombic structure Pbcm and a polar phase labelled '$P2_1ma$'. This, to date, is the most appropriate space group allocation for the polar phase, as it provides the greatest agreement with the experimental data presented. However, it must be noted that a

lowering of symmetry to monoclinic space group Pm for the '$P2_1ma$' phase cannot be ruled out. During the room temperature structural characterisation of $NaNbO_3$ the sol-gel sample, composed of principally the $P2_1ma$ phase, was also refined using the monoclinic space group Pm and the deviation observed in the monoclinic angle was extremely subtle, 90.084(1)°. Similarly, the monoclinic angle suggested by Baker *et al.* was extremely small, $\beta = 89.914°$. Such distortions are commonly proposed owing to subtle peak splittings and/or broadenings identified in high-resolution diffraction data. The broadenings observed can, however, be the result of many different effects, for example crystallite size and shape, strain and grain boundaries. Therefore, the contribution from all such effects needs to be considered when establishing whether a real monoclinic distortion is observed.

The structural challenges faced in the KNN series appear to be mirrored in other related $NaNbO_3$ solid-solutions, for example the $Li_xNa_{1-x}NbO_3$ (LNN) and $Na_{1-x}Sr_{x/2}\square_{x/2}NbO_3$ (SNN) series, where □ denotes a vacancy. Although the LNN series has been investigated numerous times, the phase diagram is still a subject of considerable confusion.[278-282] The Na-rich region of the phase diagram is believed to contain classic perovskite-type structures with corner-linked NbO_6 octahedra. Li-rich compositions, however, are believed to exhibit structures composed of face sharing ocatahedra along the threefold axis. To date, literature regarding low level Li doping ($x < 0.15$) is considered controversial, with several contradictory reports of observed phase transitions occurring at various different Li compositions. Yuzyuk *et al.*,[283] investigated very low percentage Li doping, $0 \leq x \leq 0.145$ using high-resolution powder diffraction and Raman spectroscopy. Their findings confirmed previous reports of a phase transition from the orthorhombic Pbma structure to a polar orthorhombic phase, in space group $P2_1ma$. This transition was observed at extremely low doping levels ($0.02 \leq x \leq 0.03$). Furthermore, the polar $P2_1ma$ phase was found to be stable up to $x = 0.145$. Interestingly, samples with composition $x = 0.12$ were found to exhibit a two phase region of coexistence between a rhombohedral phase, R3c, and the previously recognised polar $P2_1ma$ phase.

The $NaNbO_3$-$Sr_{0.5}NbO_3$ system was first studied by Mori *et al.*,[284] who established the formation of two solid-solutions $Na_{1-x}Sr_{x/2}\square_{x/2}NbO_3$ (SNN) in the compositional ranges $0 \leq x \leq 0.03$ and $0.14 \leq x \leq 0.5$. Interestingly, in the intermediate range a region of coexistence was observed between the two. The first of these solid-solutions, in the range $0 \leq x \leq 0.03$, produced antiferroelectric compounds, whereas the second produced ferroelectric materials. However, no specific role was assigned by Mori *et al.* for the A site vacancies or their influence on the dielectric properties exhibited. It was not until much later that the room temperature ferroelectric behaviour exhibited in the SNN system was found to exist through the introduction of the cation vacancies.[285] Changing the chemical composition caused a structural change which, in turn, modified the dielectric behaviour of the system. Using room temperature X-ray diffraction, samples with compositions $x = 0.1$ and 0.2 were found to be isostructural with the $P2_1ma$ phase of $NaNbO_3$. The identification of this phase suggests the introduction of Sr into the structure favours a polar, ferroelectric phase. However, using transmission electron microscopy (TEM) a region of phase coexistence was found for the $x = 0.1$ composition, with intergrowths from two orthorhombic perovskite phases; $P2_1ma$ and $Pbma$. Previous studies also observed similar regions of phase coexistence, however, they were reported as being restricted to the compositional range $0.022 \leq x \leq 0.05$. No two phase regions were identified in samples with $x = 0.2$ and electrical measurements completed by Torres-Pardo *et al.*,[285] suggest a pure ferroelectric material at this composition.

Evidence obtained from recent literature studies suggests doping the $NaNbO_3$ structure with cations such as Li or Sr results in the formation of the same polar $P2_1ma$ phase of $NaNbO_3$ identified earlier in this work. Hence, within this chapter a variety of $NaNbO_3$-based solid-solutions will be investigated, in particular $K_xNa_{1-x}NbO_3$ ($0.01 \leq x \leq 0.05$), $Li_xNa_{1-x}NbO_3$ ($0.01 \leq x \leq 0.1$) and $Na_{1-x}Sr_{x/2}\square_{x/2}NbO_3$ ($0.1 \leq x \leq 0.4$), to determine whether the $P2_1ma$ phase is formed. Both high-resolution powder diffraction and solid-state NMR data is presented and discussed.

4.2 Experimental

4.2.1 Synthesis

All samples in the $K_xNa_{1-x}NbO_3$ (KNN), $Li_xNa_{1-x}NbO_3$ (LNN) and $Na_{1-x}Sr_{x/2}\square_{x/2}NbO_3$ series were synthesised using conventional solid-state methods. Stoichiometric amounts of Na_2CO_3 (Fisher Scientific, 99.5%), K_2CO_3 (Fisher Scientific, 99%), Li_2CO_3 (Sigma-Aldrich, 99%), $SrCO_3$ (Sigma-Aldrich, 99.9%) and Nb_2O_5 (Sigma-Aldrich, 99.99%) were mixed and ground in an agate mortar and pestle. Samples were pressed into 1 cm pellets, using a pressure of 10 tons cm^{-2}. All samples in the KNN and LNN series were prepared using an annealing temperature of 850 °C. For compositions $0.03 \leq x \leq 0.05$ in the KNN series an annealing time of 48 hours was utilised, with an intermediate regrind occurring after 24 hours of heating. All samples in the LNN series, in addition to $x = 0.01$ and 0.02 in the KNN series, utilised an annealing time of 10 hours, with an intermediate regrind.[282] All $Na_{1-x}Sr_{x/2}\square_{x/2}NbO_3$ samples were synthesised using an annealing temperature of 1300 °C for 24 hours.[285]

4.2.2 X-ray and Neutron Powder Diffraction

Using Beamline Ill at the Diamond Light Source Synchrotron (λ = 0.827267 Å) high-resolution room temperature PXRD experiments were conducted for all samples in the KNN, LNN and $Na_{1-x}Sr_{x/2}\square_{x/2}NbO_3$ series.[122,123] Room temperature time-of-flight neutron powder diffraction experiments were completed for the KNN and LNN series using HRPD[134,135] at the ISIS neutron spallation source, Rutherford-Appleton Laboratories. All diffraction data were analysed using the GSAS software package.[125]

4.2.3 NMR Spectroscopy

Solid-state NMR spectra were acquired using a Bruker 600 Avance III spectrometer, equipped with a wide-bore 14.1 T magnet using a Larmor frequency of 158.75 MHz. The finely powdered samples were tightly

packed into conventional 4-mm ZrO_2 rotors and a MAS rate of 14 kHz was employed. Chemical shifts were reference to 1 M NaCl (aq), using NaCl (s) as a secondary reference at 7.8 ppm.

Conventional ^{23}Na MAS NMR spectra were obtained using single pulse experiments with a typical pulse length of 1.1 μs. The optimised recycle interval for ^{23}Na was 3 s and a typical radiofrequency field strength of between 100 and 170 kHz was employed. Two-dimensional MAS NMR experiments were recorded using a phase-modulated rotor-synchronised split-t_1 shifted-echo pulse sequence.[181] Spectra result from the averaging of 96 transients with a recycle interval of 3 s for each of the 128 t_1 increments. Additional experimental information can be found in the relevant figure captions.

4.3 Results and Discussion

4.3.1 Low Percentage K doping

4.3.1.1 $K_{0.01}Na_{0.99}NbO_3$

Initial investigations concentrated on low percentage doping of K into the $NaNbO_3$ structure. Samples in the range $0.01 \leq x \leq 0.05$ were synthesised with structure and phase purity examined using l-PXRD. To gain accurate structural information high-resolution NPD and s-PXRD experiments were also conducted for each sample. Rietveld refinement of the $x = 0.01$ sample using the NPD data was initially completed using the Pbcm structural model.[248] However, the level of fit obtained was relatively poor, with $wR_p = 13.7\%$ and $\chi^2 = 19.3$, as shown in Figure 4.1(a). Several additional peaks were present in the diffraction pattern that were not indexed by the Pbcm model. This, in turn, suggested the possible presence of a different phase of $NaNbO_3$. An expansion of the superstructure peaks, 2.3 Å – 2.55 Å, is shown in Figure 4.1(b) and highlights the four major peaks in the pattern not fitted by the Pbcm model. Interestingly, the two peaks at ~2.47 Å and ~2.49 Å appeared to correlate with those previously identified in the $P2_1ma$ phase of $NaNbO_3$ discussed in the previous chapter. The identification of these peaks suggested the $P2_1ma$ polymorph of $NaNbO_3$ to also be present in the

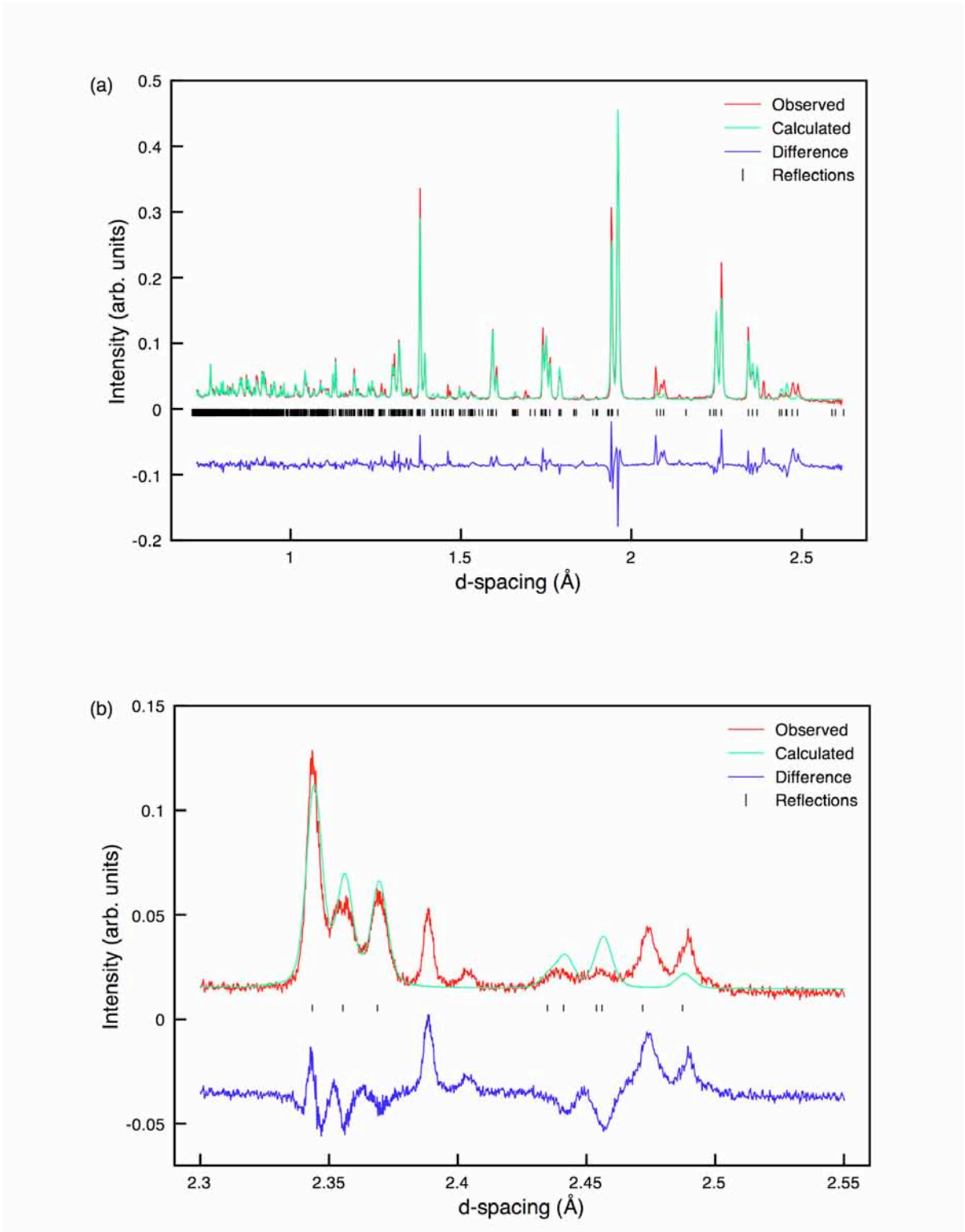

Figure 4.1: (a) Single phase Rietveld refinement of the NPD for $K_{0.01}Na_{0.99}NbO_3$ using the Pbcm structural model and (b) an expansion of the superstructure region of the refinement, 2.3 Å – 2.55 Å, highlighting the poor level of fit.

Table 4.1: Structural parameters for $K_{0.01}Na_{0.99}NbO_3$ from NPD data, using isotropic thermal factors. Space group Pbcm, a = 5.51575(15) Å, b = 5.57350(15) Å, c = 15.5328(4) Å and V = 477.51(3) Å^3. χ^2 = 19.3, wR_p = 13.7% and R_p = 12.6%.

Atom	Site	x	y	z	U(iso) × 100 / Å^2
Na1*	4c	0.2569(15)	0.25	0	1.9(2)
Na2	4d	0.2554(12)	0.2288(13)	0.25	0.36(17)
Nb1	8e	0.2659(14)	0.7483(6)	0.1227(2)	1.13(3)
O1	4c	0.6901(9)	0.25	0	1.04(3)
O2	4d	0.1784(9)	0.7653(10)	0.25	1.04(3)
O3	8e	0.4699(6)	0.4444(4)	0.1403(3)	1.04(3)
O4	8e	0.0102(8)	0.0035(8)	0.1094(2)	1.04(3)
*Na 0.99, K 0.01					

sample. Therefore, a multiphase Rietveld refinement was completed using both the $P2_1ma$[228] and Pbcm[248] polymorphs of $NaNbO_3$ as shown in Figure 4.2(a). The quality of refinement improved upon the addition of the two models (wR_p = 8.9% and χ^2 = 8.1%) and the refined phase fractions obtained suggested an almost 50% mix of the two phases in the sample, with 52.8(2)% and 47.2(2)% of the Pbcm and $P2_1ma$ phases, respectively. The four superstructure peaks initially identified in the region 2.3 Å – 2.55 Å were now accurately modelled using the two phases, as shown in Figure 4.2(b). It must be noted that several other additional peaks were also present in the NPD data for the x = 0.01 sample which could not be correctly modelled by either the Pbcm or $P2_1ma$ phases. These additional peaks indicated the presence of an unknown third phase, believed to be either unreacted metal oxides and/or carbonates or a non-stoichiometric mix of reagents. This phase was not considered to be a different polymorphic form of $NaNbO_3$ as peaks belonging to this phase did not appear to correlate with any of the known polymorphs of $NaNbO_3$. Similarly, these peaks were not considered as being related to the other end-member in the KNN series, $KNbO_3$. Full refinement details obtained

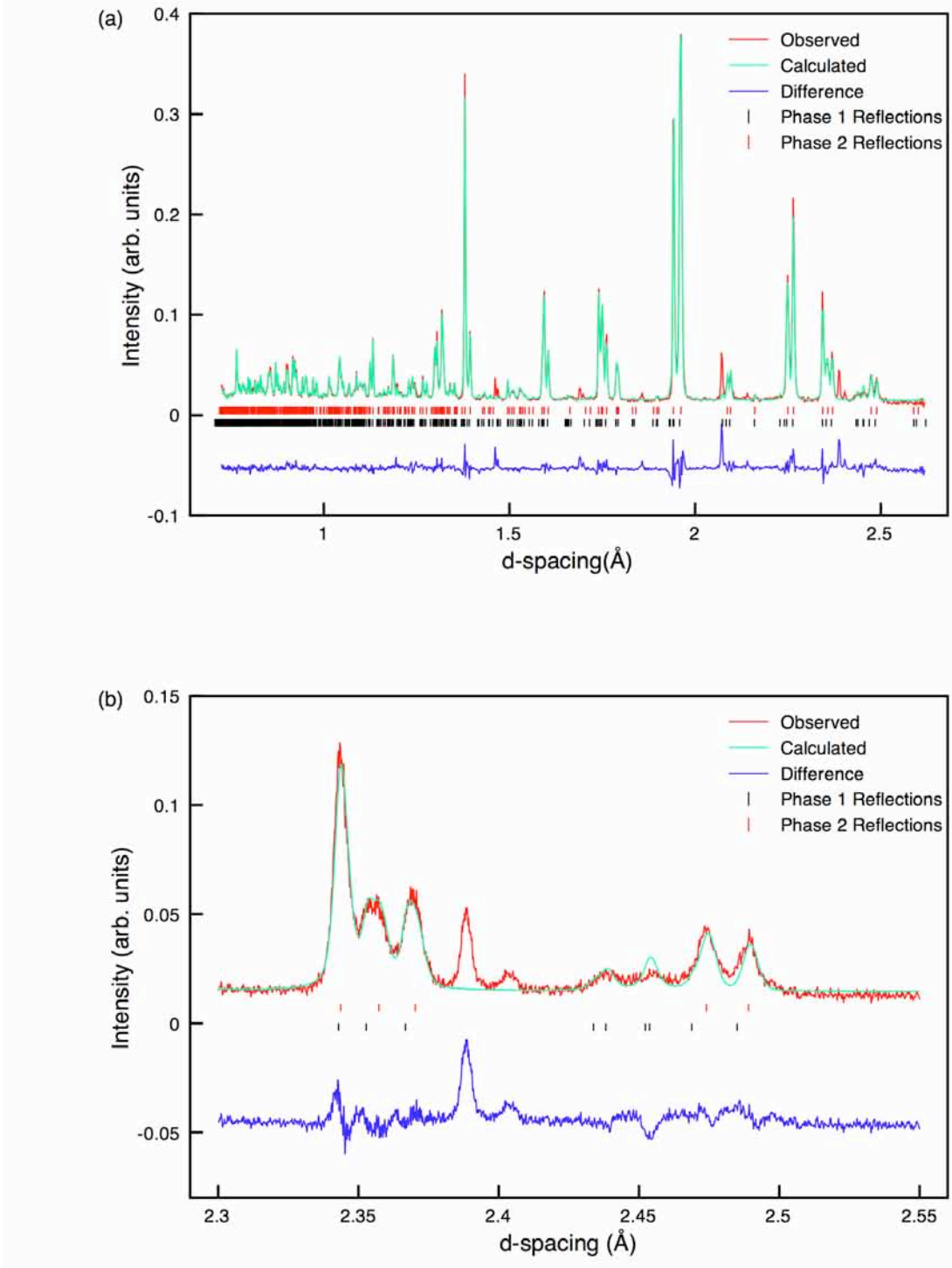

Figure 4.2: (a) Multiphase Rietveld refinement of the NPD data for $K_{0.01}Na_{0.99}NbO_3$ using structural models Pbcm and $P2_1ma$, (b) an expansion of the superstructure region of the refinement, 2.3 Å – 2.55 Å, highlighting the better quality of fit obtained using two structural models.

Table 4.2: Structural parameters for $K_{0.01}Na_{0.99}NbO_3$ from NPD data, using isotropic thermal factors. Space group Pbcm, a = 5.50818(11) Å, b = 5.56847(10) Å, c = 15.5321(5) Å and V = 476.403(15) Å^3. Space group $P2_1ma$, a = 5.57652(8) Å, b = 7.76508(17) Å, c = 5.52056(9) Å and V = 239.052(6) Å^3. χ^2 = 8.10, wR_p = 8.9% and R_p = 7.8%.

Phase	Atom	Site	x	y	z	U(iso) × 100 / Å^2
Pbcm	Na1*	4c	0.250(3)	0.25	0	1.70(4)
	Na2	4d	0.248(3)	0.220(3)	0.25	2.90(5)
	Nb1	8e	0.2420(11)	0.7513(8)	0.1250(7)	1.43(9)
	O1	4c	0.688(2)	0.25	0	3.3(3)
	O2	4d	0.1818(18)	0.7613(3)	0.25	1.02(19)
	O3	8e	0.4707(9)	0.4549(10)	0.1409(5)	1.99(12)
	O4	8e	0.0174(12)	0.0113(13)	0.1062(5)	3.3(2)
	*Na 0.99, K 0.01					
$P2_1ma$	Na1	2a	0.2478(16)	0	0.743(2)	2.00(4)
	Na2	2b	0.2719(17)	0.5	0.7326(16)	1.2(3)
	Nb1	4c	0.2647(6)	0.2497(7)	0.2463(6)	0.11(5)
	O1	2a	0.2351(7)	0	0.3108(15)	0.32(19)
	O2	2b	0.2179(8)	0.5	0.2013(15)	0.34(19)
	O3	4c	0.0197(8)	0.2749(9)	0.5349(9)	1.09(10)
	O4	4c	−0.0527(7)	0.2211(7)	0.0413(8)	0.09(8)

from the NPD data for both the single phase and multiphase refinements of the x = 0.01 sample can be found in Tables 4.1 and 4.2, respectively. All associated bond lengths are given in Appendix III.

As a direct result of the initial findings obtained from the NPD data a multiphase Rietveld refinement was also completed for the s-PXRD data and, in a similar manner, a two phase coexistence was observed between the Pbcm and $P2_1ma$ phases. The multiphase Rietveld refinement of the s-PXRD data is shown in Figure 4.3(a) with an expansion of the superstructure peaks, 18.5° - 22°, also shown in Figure 4.3(b). The refined

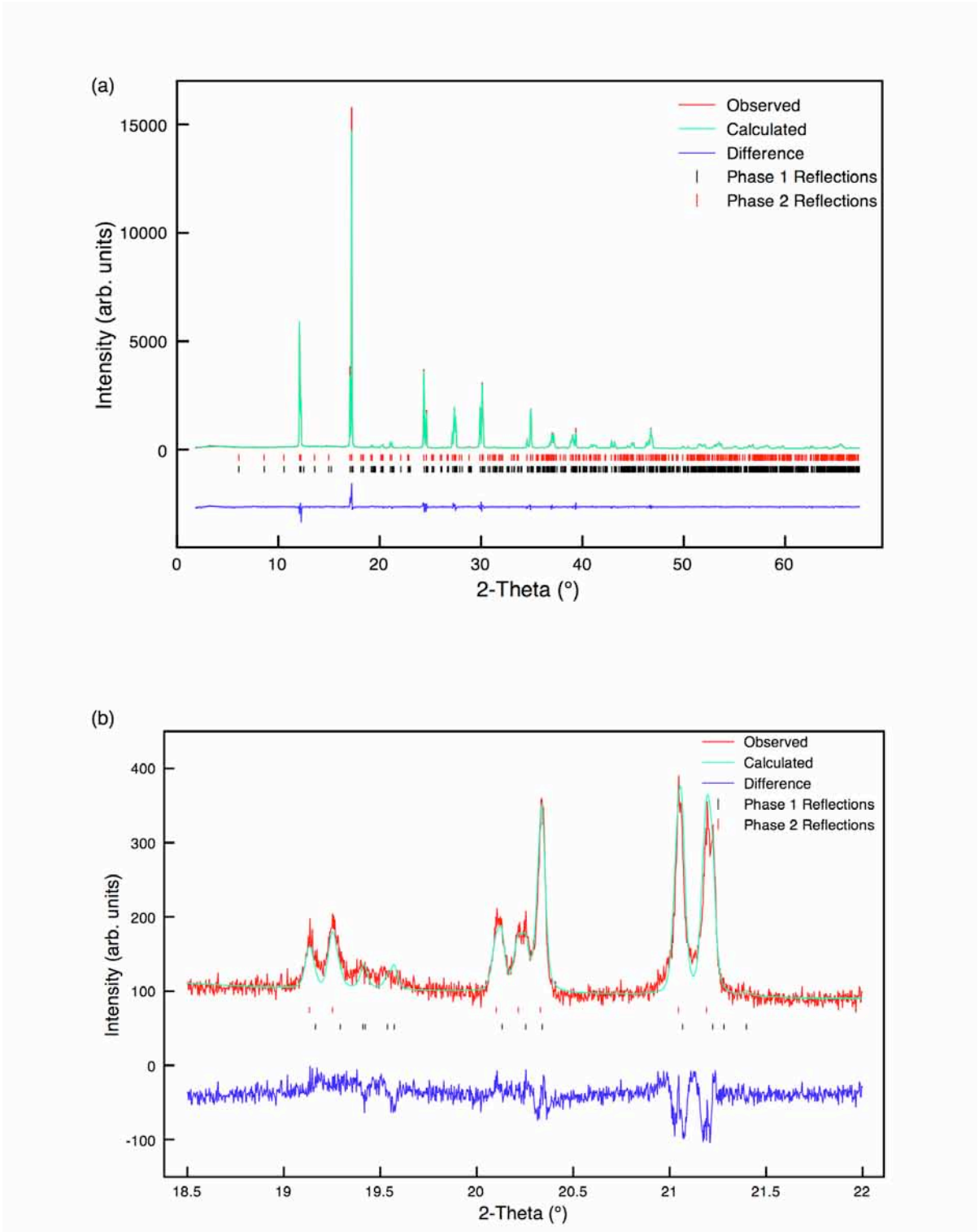

Figure 4.3: (a) Multiphase Rietveld refinement of the s-PXRD data for $K_{0.01}Na_{0.99}NbO_3$ using structural models Pbcm and $P2_1ma$, (b) an expansion of the superstructure region of the refinement, 18.5° – 22°, indicating a good level of fit using the two orthorhombic models.

Table 4.3: Structural parameters for $K_{0.01}Na_{0.99}NbO_3$ from s-PXRD data, using isotropic thermal factors. Space group Pbcm, a = 5.50593(3) Å, b = 5.66902(3) Å, c = 15.52649(8) Å and V = 475.902(3) Å^3. Space group $P2_1ma$, a = 5.57519(2) Å, b = 7.76397(3) Å, c = 5.51813(2) Å and V = 238.855(1) Å^3. χ^2 = 2.1, wR_p = 10.7% and R_p = 7.9%.

Phase	Atom	Site	x	y	z	U(iso) × 100 / Å^2
Pbcm	Na1*	4c	0.2280(12)	0.25	0	0.9(2)
	Na2	4d	0.2315(13)	0.2163(9)	0.25	0.9(2)
	Nb1	8e	0.2530(3)	0.7387(2)		0.76(1)
	O1	4c	0.683(3)	0.25	0	0.86(8)
	O2	4d	0.204(3)	0.7366(18)	0.25	0.86(8)
	O3	8e	0.4752(12)	0.4363(13)	0.1427(7)	0.86(8)
	O4	8e	0.0137(15)	−0.027(2)	0.1062(6)	0.86(8)
	*Na 0.99, K 0.01					
$P2_1ma$	Na1	2a	0.266(2)	0	0.7403(10)	1.20(4)
	Na2	2b	0.2736(13)	0.5	0.7418(10)	1.10(4)
	Nb1	4c	0.2532(5)	0.2499(7)	0.2446(1)	0.85(1)
	O1	2a	0.237(2)	0	0.3086(16)	0.40(5)
	O2	2b	0.2168(16)	0.5	0.192(2)	2.17(5)
	O3	4c	0.032(2)	0.2787(17)	0.5332(16)	0.76(5)
	O4	4c	−0.038(2)	0.222(2)	0.0322(19)	2.26(5)

phase fractions obtained from the multiphase refinement of the s-PXRD data suggested the $P2_1ma$ phase to be slightly more abundant, with 62.8(2)% and 37.2(2)% of the $P2_1ma$ and Pbcm phases, respectively. This was in contrast to the phase fractions obtained from the NPD data, which suggested there to be very similar quantities of the two phases present in the x = 0.01 sample. There are many possible reasons for this discrepancy. It is possible such a difference could be owing to disorder in the sample. The addition of small quantities of K into the $NaNbO_3$ structure is most

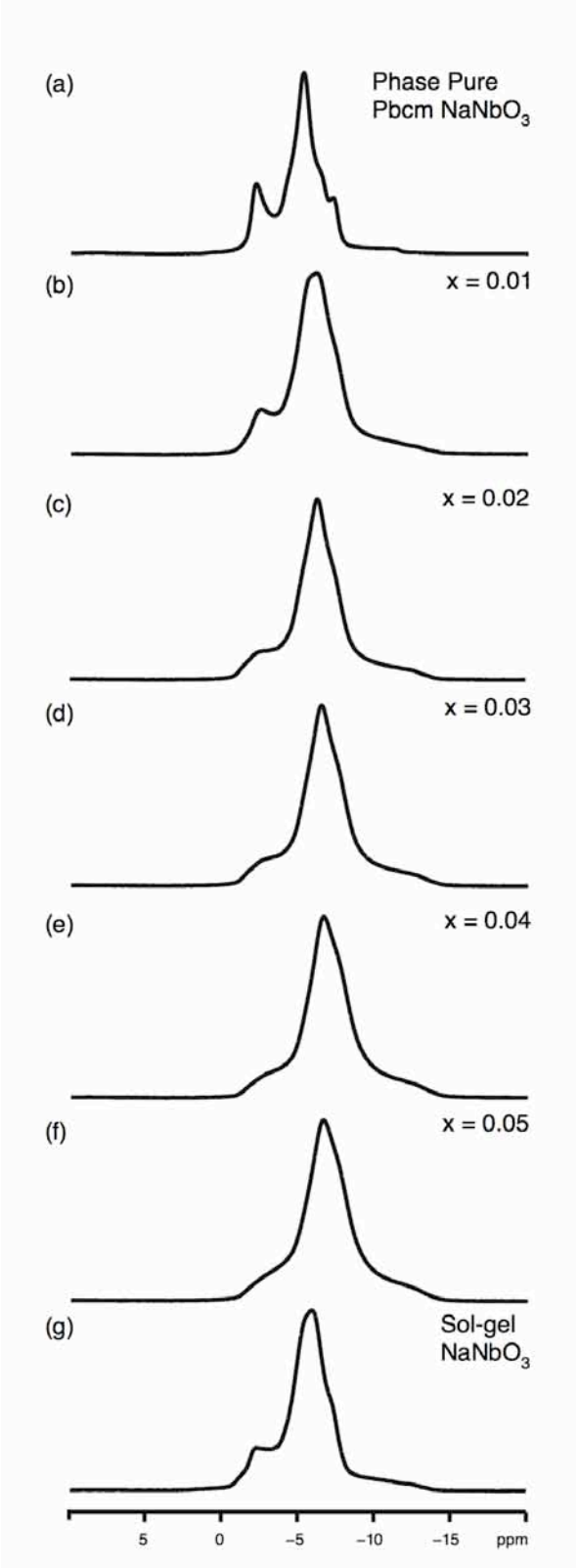

Figure 4.4: Comparison of ^{23}Na (14.1 T) MAS NMR spectra obtained for the $K_xNa_{1-x}NbO_3$ series. Also shown in (a) and (g) for comparison are phase pure Pbcm $NaNbO_3$ (synthesised using molten salt techniques) and the sol-gel sample of $NaNbO_3$ composed of ~90% of the $P2_1ma$ and ~10% of the Pbcm polymorphs of $NaNbO_3$.

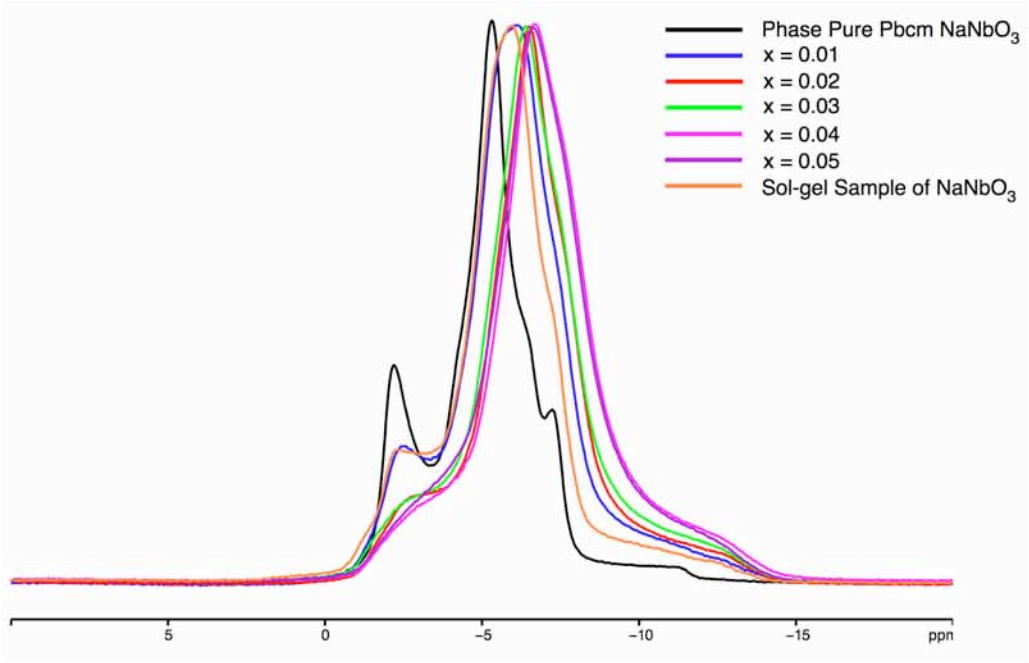

Figure 4.5: Overlay of all ^{23}Na (14.1 T) MAS NMR spectra obtained for the $K_xNa_{1-x}NbO_3$ series. Also shown for comparison are phase pure Pbcm $NaNbO_3$ (synthesised using molten salt techniques) and the sol-gel sample of $NaNbO_3$ composed of ~90% of the $P2_1ma$ and ~10% of the Pbcm polymorphs of $NaNbO_3$.

likely to occur in a disordered manner. As a result this can often lead to broadening of the peaks in the diffraction patterns obtained. It was shown earlier in Chapter 3 that in all X-ray diffraction patterns peaks belonging to the $P2_1ma$ and Pbcm phases were severely overlapped and the only observable discrepancies occurred in the superstructure peaks. Therefore, given the obvious difficulties in distinguishing between the two phases it is possible that with additional peak broadening it is much harder to accurately determine the quantities of each phase present in each diffraction pattern. This is, however, only one of the possible reasons for the discrepancy observed in the phase fractions obtained in the NPD and s-PXRD data for the x = 0.01 sample. Full refinement details obtained from the multiphase Rietveld refinement of the s-PXRD data can be found in Table 4.3 and all associated bond lengths are given in Appendix III.

The ^{23}Na MAS NMR spectrum recorded for $K_{0.01}Na_{0.99}NbO_3$ appeared broadened and subtly different when compared with single phase Pbcm $NaNbO_3$. This is highlighted in Figures 4.4(a) and (b) where

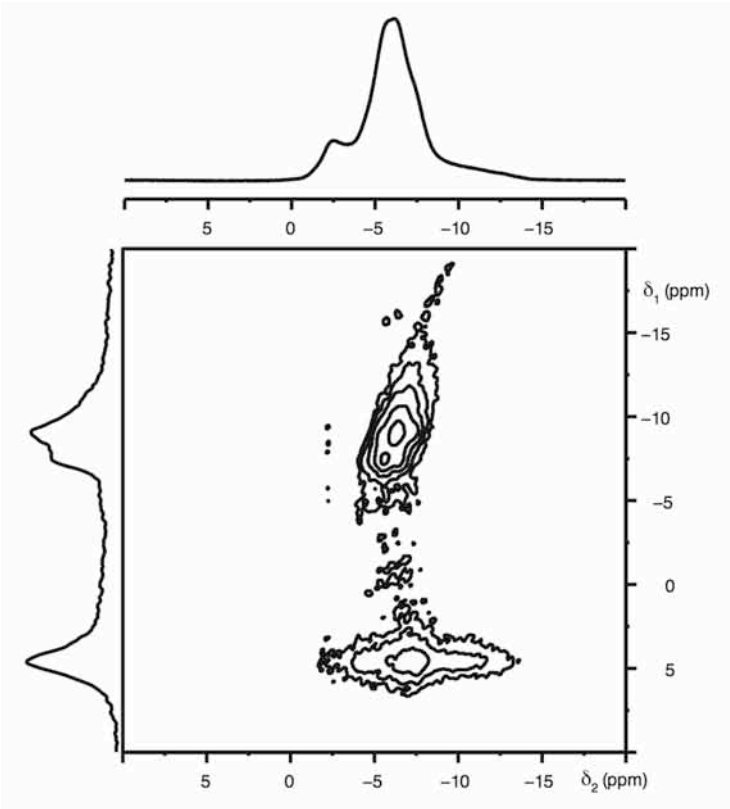

Figure 4.6: The conventional ^{23}Na (14.1 T) MAS NMR spectrum, triple-quantum MAS NMR spectrum, and corresponding isotropic projections for the $K_{0.01}Na_{0.99}NbO_3$ sample. The MAS rate was 14 kHz.

the two lineshapes are compared. Most notably, the lineshape obtained for the x = 0.01 sample appeared to have lost several of the distinct features previously identified in phase pure Pbcm $NaNbO_3$. Also shown for comparison in Figure 4.4(g) is the ^{23}Na MAS NMR spectrum recorded for the sol-gel sample of $NaNbO_3$, composed of ~90% of the $P2_1ma$ polymorph of $NaNbO_3$. When Figures 4.4(b) and (g) are compared they appear very similar, thereby confirming the possible presence of the $P2_1ma$ polymorph in the x = 0.01 sample. This is perhaps clearer to observe in Figure 4.5 where the two are directly overlaid. Many of the lineshape features appear considerably broadened owing, most probably, to the presence of two different phases and different crystallite sizes. It is not possible to accurately determine precisely which phases are present and in which quantities by solely inspection of the MAS spectrum, therefore two-dimensional techniques are required. In general, solid-

Table 4.4: ^{23}Na (14.1 T) MAS NMR parameters obtained for the series $K_{1-x}Na_xNbO_3$, where $0.01 \leq x \leq 0.05$. All parameters were obtained from the position of the centre of gravity (δ_1, δ_2) of the resonance.

x	$\langle\delta_1\rangle$ (ppm)	$\langle\delta_{iso}\rangle$ (ppm)	$\langle P_Q\rangle$ / MHz
0.01	−9.0	−5.1(5)	1.2(2)
	−7.4	−4.4(5)	1.2(2)
	4.7	−1.3(5)	2.3(2)
0.02	−9.0	−5.1(5)	1.2(2)
	4.6	−1.3(5)	2.4(2)
0.03	−10.2	−5.6(5)	1.2(2)
	4.5	−1.4(5)	2.4(2)
0.04	−11.7	−6.2(5)	1.1(2)
	4.3	−1.5(5)	2.4(2)
0.05	−11.4	−6.1(5)	1.1(2)
	3.9	−1.5(5)	2.4(2)

solutions exhibit some degree of disorder owing to the substitution of cations onto the A and/or B sites in a 'random' or disordered manner. However, it is often difficult to determine the precise nature and full extent of the disorder exhibited using diffraction techniques alone. Therefore, in an attempt to establish the extent of disorder exhibited in the $K_{0.01}Na_{0.99}NbO_3$ system MQMAS techniques were also used. The triple-quantum ^{23}Na MQMAS spectrum, shown in Figure 4.6, displayed three distinct Na resonances. The upper of the three ridges, with $\langle\delta_1\rangle$ = −9.0 ppm and $\langle P_Q\rangle$ = 1.2 MHz was in good agreement with that observed for the $P2_1ma$ phase of $NaNbO_3$ accurately assigned earlier in this work (Chapter 3, section 3.3.4). The ridge below, with $\langle\delta_1\rangle$ = −7.4 ppm and $\langle P_Q\rangle$ = 1.2 MHz was also in good agreement with Na2 in the Pbcm phase of $NaNbO_3$. The third ridge, with $\langle\delta_1\rangle$ = 4.7 ppm, possessed a considerably

larger quadrupolar contribution, $\langle P_Q \rangle$ = 2.5 MHz. It was shown earlier that spectra recorded using 14.1 T for samples comprising a mix of the Pbcm and $P2_1ma$ phases possessed two overlapped resonances at $\langle \delta_1 \rangle$ = 4.3 ppm and in order to accurately distinguish the two, multi-field two-dimensional ^{23}Na NMR techniques were required. The three sites identified in the x = 0.01 sample suggested it contained the same two polymorphs previously identified in samples of $NaNbO_3$ synthesised using solid-state, molten salt and sol-gel methods. Hence, it is suggested that two extremely similar resonances reside under the site at $\langle \delta_1 \rangle$ = 4.7 ppm. The presence of disorder results in broader lineshapes and a distribution of parameters. Therefore, in such cases it is only possible to extract average values for the isotropic chemical shift, $\langle \delta_{iso} \rangle$, and the quadrupolar product, $\langle P_Q \rangle$. The NMR parameters obtained from the MQMAS spectrum shown in Figure 4.6 and can be found in Table 4.4. The site at $\langle \delta_1 \rangle$ = −9.0 ppm appears to be aligned along a gradient of +2.125, suggesting there to be a distribution of chemical shifts. Interestingly, the site at $\langle \delta_1 \rangle$ = 4.7 ppm does not appear to exhibit the same alignment along +2.125. This suggests that this particular Na site is less affected by the distribution of chemical shifts. The ^{23}Na MQMAS spectrum for the x = 0.01 sample therefore appears to be dominated largely by a distribution of chemical shifts. In contrast, the contribution from a distribution of quadrupoles is thought to be relatively small in this particular sample. The relative ratios of the two peaks in the isotropic projection for the x = 0.01 sample perhaps suggest the $P2_1ma$ polymorph to be the more abundant of the two, however, no quantitative measurement of the phase fractions could be obtained owing to the extent of peak broadening exhibited in the isotropic projection.

Using high-resolution powder diffraction and ^{23}Na MQMAS techniques, the $K_{0.01}Na_{0.99}NbO_3$ sample was found to comprise of a mix of two phases, believed to be the antiferroelectric Pbcm and polar $P2_1ma$ polymorphs. An additional phase, believed to be a mixed metal oxide and/or carbonate phase was also identified using diffraction methods. However, the exact composition and quantity of this phase are, at present, unknown. No traces of this third phase were present in the ^{23}Na MQMAS

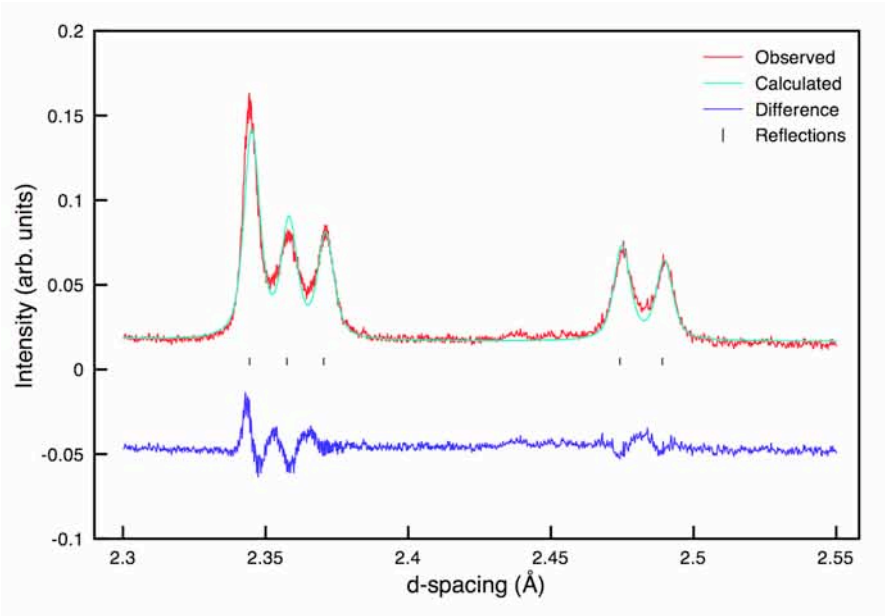

Figure 4.7: An expansion of the superstructure region, 2.3 Å – 2.55 Å, of the Rietveld refinement completed using the NPD data for the $K_{0.02}Na_{0.98}NbO_3$ sample. The refinement was completed using the $P2_1ma$ structural model and, as shown, a good level of fit was obtained.

spectrum, suggesting this additional phase is either below the level of detection or not Na-based.

4.3.1.2 Higher Percentage Doping ($0.02 \leq x \leq 0.05$)

Structure and phase purity of all remaining samples synthesised in the $K_xNa_{1-x}NbO_3$ series (x = 0.02, 0.03, 0.04 and 0.05) were also verified using high-resolution NPD and s-PXRD. Rietveld refinement of each sample suggested the presence of a single phase perovskite and consistently, all samples refined well to the polar orthorhombic $P2_1ma$ structure, suggesting the complete removal of the Pbcm phase from each sample. An expansion of the superstructure peaks, 2.3 Å – 2.55 Å, in the NPD data for the x = 0.02 sample is shown in Figure 4.7. The peaks previously identified in the x = 0.01 sample as belonging to the Pbcm polymorph of $NaNbO_3$ (~2.44 Å and ~2.46 Å) appeared to have been removed completely, confirming the presence of a single phase perovskite in space group $P2_1ma$. All Rietveld refinements completed using the NPD

data in the range $0.02 \leq x \leq 0.05$ are shown in Figures 4.8 and 4.9. Corresponding χ^2 values obtained for x = 0.02, 0.03, 0.04 and 0.05 were 6.9, 7.5, 6.2 and 5.4, respectively. The quality of refinement appeared to improve as greater quantities of K were introduced to the system. This therefore suggested that the introduction of K to the structure favours the formation of the $P2_1ma$ phase and perhaps stabilises this particular polymorph. All structural parameters obtained from each refinement can be found in Tables 4.5 - 4.8. All corresponding bond lengths obtained from each refinement are given in Appendix III. In a similar manner, Rietveld refinement of the s-PXRD data also suggested the presence of a single phase perovskite and each sample in this series refined well to the polar orthorhombic $P2_1ma$ phase. All Rietveld refinements completed using the s-PXRD data are shown in Figures 4.10 and 4.11. Corresponding χ^2 values obtained for x = 0.02, 0.03, 0.04 and 0.05 were 9.5, 3.8, 1.7 and 1.6 respectively. In a similar manner to the NPD data, the quality of the refinement appeared to improve with increasing x. All associated structural parameters obtained from each refinement using the s-PXRD data, including corresponding bond lengths, can be found in Appendix III.

The substitution of K into the $NaNbO_3$ structure produced a corresponding change in both the lattice parameters and unit cell volume. As x was increased a gradual increase in the unit cell parameters and cell volume was observed for both the NPD and s-PXRD data. The variation of each parameter with increasing K content is shown in Figures 4.12, 4.13, 4.14 and 4.15, respectively. Potassium possesses a larger ionic radius (1.51 Å)[4] than Na (1.02 Å),[4] and so, as K is introduced into the structure it will result in an expansion of the unit cell. This hypothesis is in good agreement with the findings presented. A near linear correlation was observed with increasing x for each parameter.

As observed for the x = 0.01 sample, the ^{23}Na MAS NMR spectra recorded for each composition appeared subtly different. All ^{23}Na MAS NMR spectra recorded in this series are compared in Figure 4.4 and overlaid in Figure 4.5. Consistently, each lineshape appeared broadened relative to phase pure Pbcm $NaNbO_3$ and as x was increased many of the

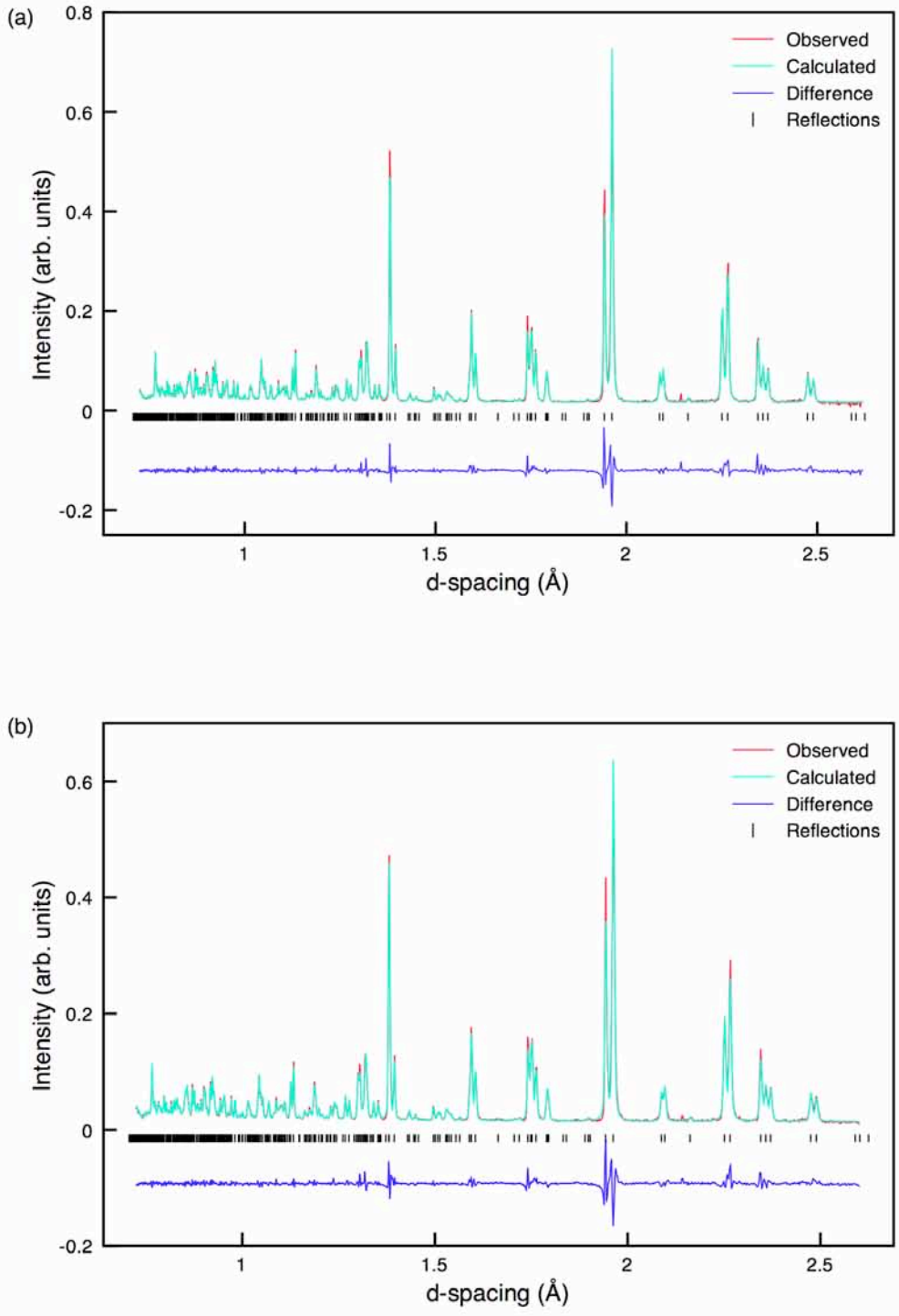

Figure 4.8: Single phase Rietveld refinements of the NPD for (a) $K_{0.02}Na_{0.98}NbO_3$ and (b) $K_{0.03}Na_{0.97}NbO_3$ using the $P2_1ma$ structural model. Both refinements indicate a good level of fit.

Table 4.5: Structural parameters for $K_{0.02}Na_{0.98}NbO_3$ from NPD data, using isotropic thermal factors. Space group $P2_1ma$, a = 5.57687(6) Å, b = 7.76821(8) Å, c = 5.52147(6) Å and V = 239.203(7) Å^3. $\chi^2 = 6.9$, $wR_p = 7.1\%$ and $R_p = 6.8\%$.

Atom	Site	x	y	z	U(iso) × 100 / Å^2
Na1*	2a	0.2648(9)	0	0.7410(7)	1.77(13)
Na2	2b	0.2817(9)	0.5	0.7369(7)	1.65(12)
Nb1	4c	0.2696	0.2494(3)	0.2454(3)	0.35(3)
O1	2a	0.2411(3)	0	0.3099(9)	0.94(10)
O2	2b	0.2264(3)	0.5	0.1966(9)	0.70(8)
O3	4c	0.0224(4)	0.2787(4)	0.5332(4)	1.42(5)
O4	4c	−0.0450(4)	0.2210(4)	0.0375(4)	0.95(5)
*Na 0.98, K 0.02					

Table 4.6: Structural parameters for $K_{0.03}Na_{0.97}NbO_3$ from NPD data, using isotropic thermal factors. Space group $P2_1ma$, a = 5.57761(4) Å, b = 7.77092(5) Å, c = 5.52332(4) Å and V = 239.398(2) Å^3. $\chi^2 = 7.5$, $wR_p = 7.5\%$ and $R_p = 7.1\%$.

Atom	Site	x	y	z	U(iso) × 100 / Å^2
Na1*	2a	0.2660(10)	0	0.7408(8)	1.78(14)
Na2	2b	0.2791(10)	0.5	0.7368(7)	1.41(12)
Nb1	4c	0.2694	0.2494(3)	0.2453(3)	0.25(2)
O1	2a	0.2404(4)	0	0.3085(10)	0.79(10)
O2	2b	0.2263(3)	0.5	0.1971(10)	0.69(9)
O3	4c	0.0217(4)	0.2786(4)	0.5332(4)	1.22(5)
O4	4c	−0.0454(4)	0.2219(4)	0.0376(4)	0.84(4)
*Na 0.97, K 0.03					

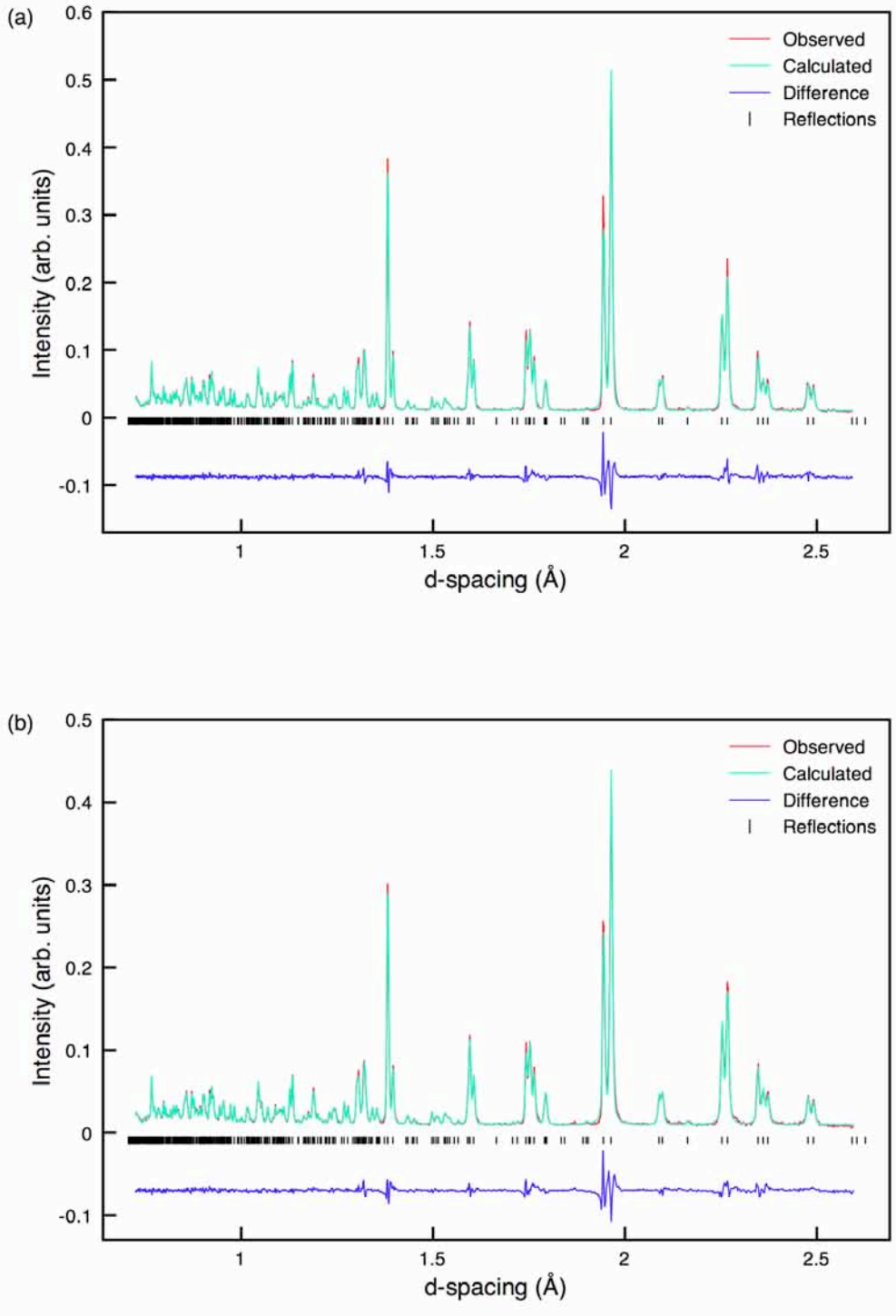

Figure 4.9: Single phase Rietveld refinements of the NPD for (a) $K_{0.04}Na_{0.96}NbO_3$ and (b) $K_{0.05}Na_{0.95}NbO_3$ using the $P2_1ma$ structural model. Both refinements indicate a good level of fit.

Table 4.7: Structural parameters for $K_{0.04}Na_{0.96}NbO_3$ from NPD data, using isotropic thermal factors. Space group $P2_1ma$, a = 5.58003(8) Å, b = 7.77488(10) Å, c = 5.52736(8) Å and V = 239.799(9) Å^3. $\chi^2 = 6.2$, $wR_p = 7.7\%$ and $R_p = 7.1\%$.

Atom	Site	x	y	z	U(iso) × 100 / Å^2
Na1*	2a	0.2657(10)	0	0.7404(8)	1.72(14)
Na2	2b	0.2749(10)	0.5	0.7374(7)	1.58(13)
Nb1	4c	0.2688	0.2494(3)	0.2458(3)	0.39(3)
O1	2a	0.2386(4)	0.	0.3083(8)	0.85(10)
O2	2b	0.2250(4)	0.5	0.2003(8)	0.88(10)
O3	4c	0.0218(4)	0.2777(4)	0.5333(4)	1.21(5)
O4	4c	−0.0453(4)	0.2225(4)	0.0386(4)	1.00(5)

*Na 0.96, K 0.04

Table 4.8: Structural parameters for $K_{0.05}Na_{0.95}NbO_3$ from NPD data, using isotropic thermal factors. Space group $P2_1ma$, a = 5.58067(8) Å, b = 7.77549(11) Å, c = 5.52787(8) Å and V = 239.868(9) Å^3. $\chi^2 = 5.4$, $wR_p = 7.7\%$ and $R_p = 7.2\%$.

Atom	Site	x	y	z	U(iso) × 100 / Å^2
Na1*	2a	0.2670(11)	0	0.7411(8)	1.77(16)
Na2	2b	0.2756(11)	0.5	0.7354(8)	1.66(15)
Nb1	4c	0.2688	0.2495(3)	0.2462(3)	0.43(3)
O1	2a	0.2394(4)	0	0.3086(10)	0.92(11)
O2	2b	0.2259(4)	0.5	0.1987(10)	0.82(10)
O3	4c	0.0216(4)	0.2786(4)	0.5331(4)	1.24(5)
O4	4c	−0.0442(4)	0.2232(4)	0.0375(4)	1.07(5)

*Na 0.95, K 0.05

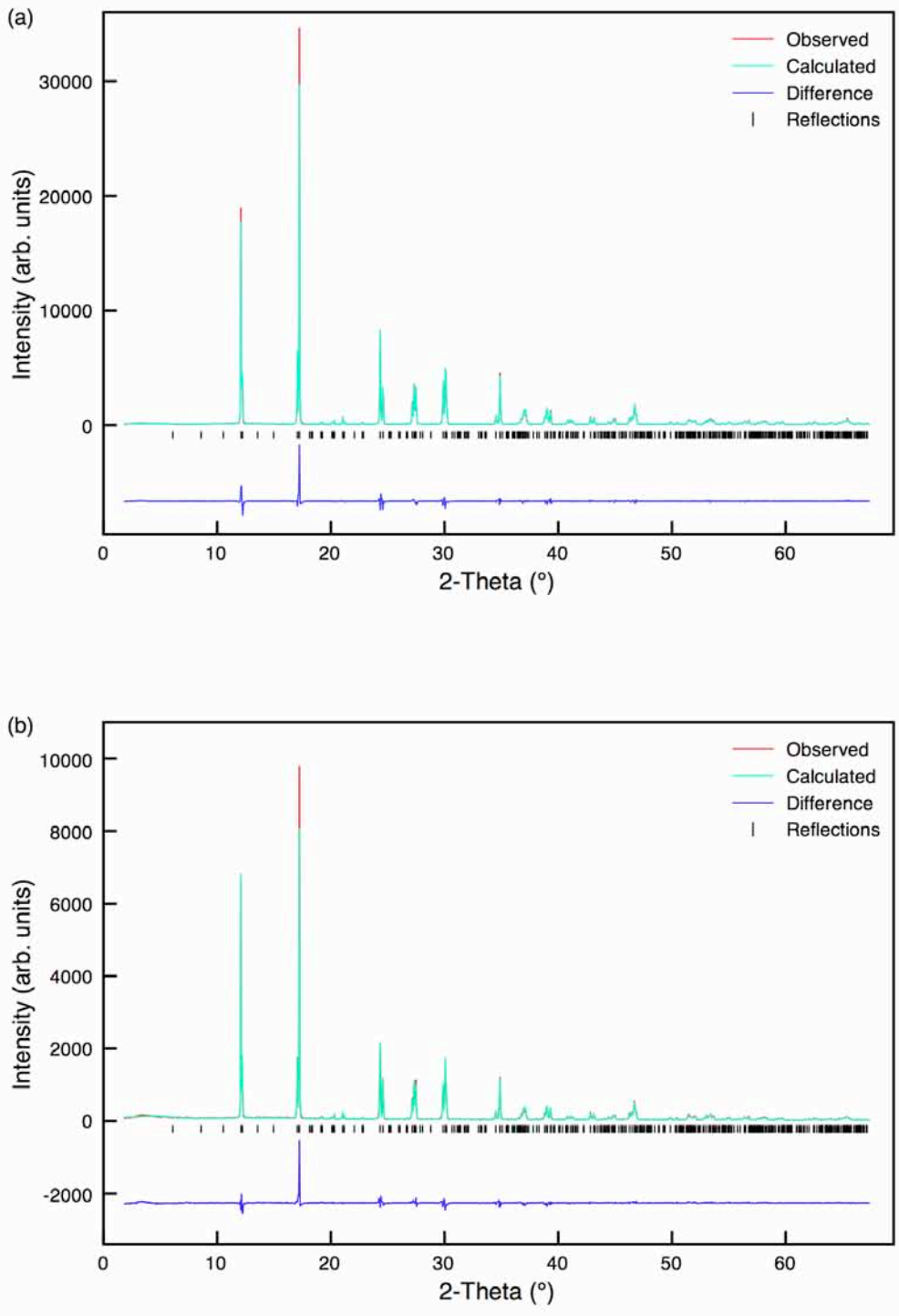

Figure 4.10: Single phase Rietveld refinements of the s-PXRD data for (a) $K_{0.02}Na_{0.98}NbO_3$ and (b) $K_{0.03}Na_{0.97}NbO_3$ using the $P2_1ma$ structural model. Both refinements indicate a good level of fit.

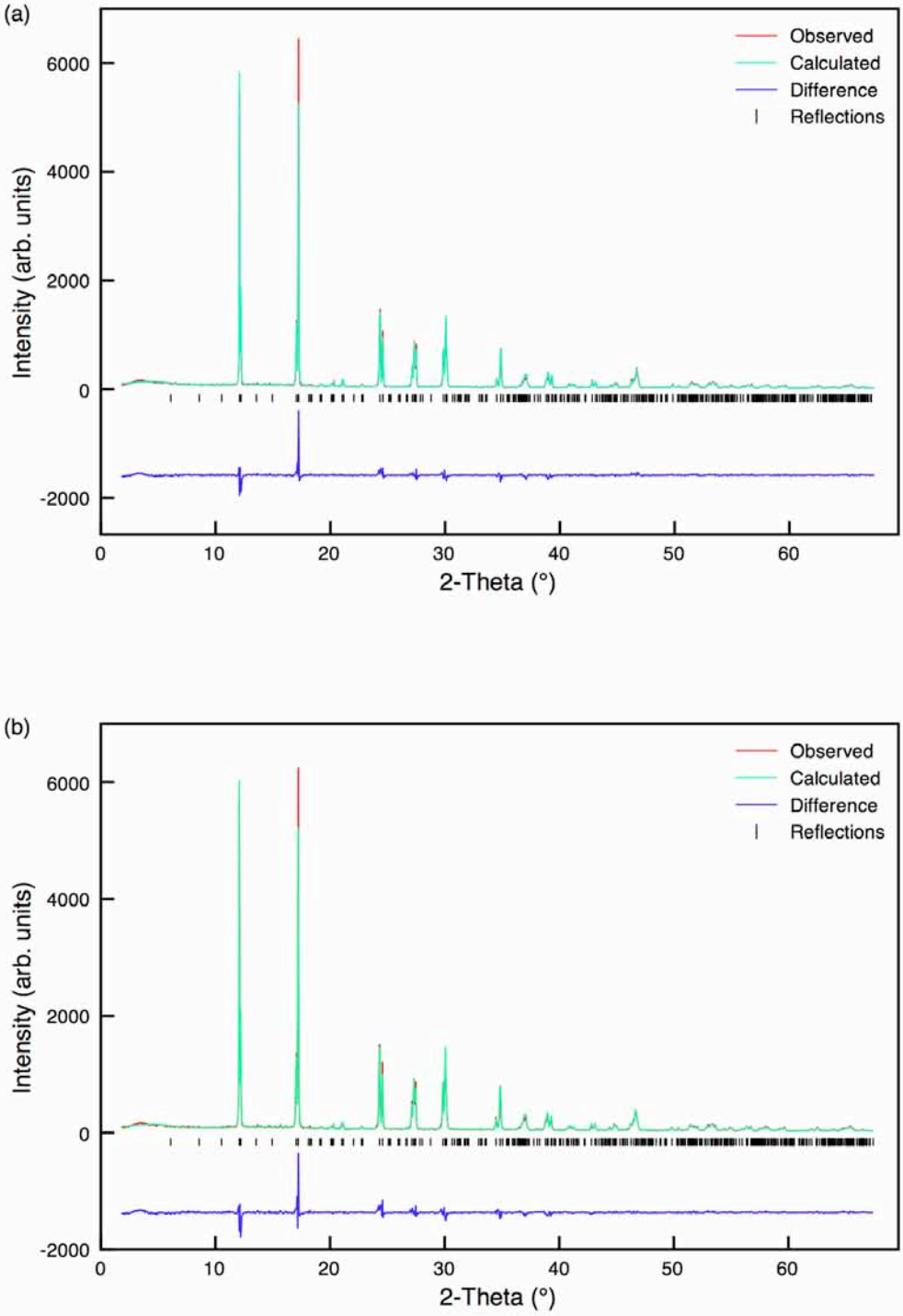

Figure 4.11: Single phase Rietveld refinements of the s-PXRD data for (a) $K_{0.04}Na_{0.96}NbO_3$ and (b) $K_{0.05}Na_{0.95}NbO_3$ using the $P2_1ma$ structural model. Both refinements indicate a good level of fit.

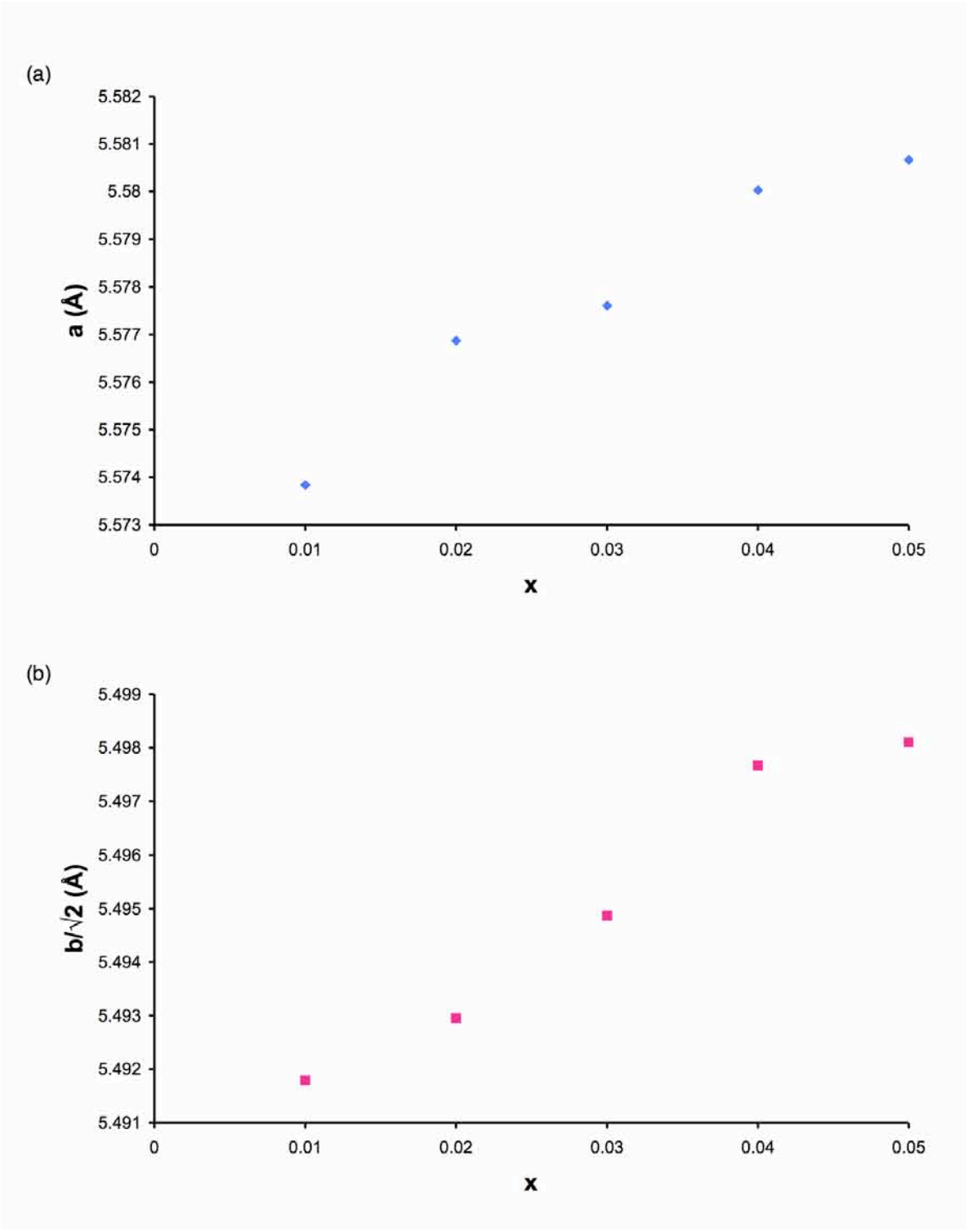

Figure 4.12: Variation observed in the unit cell parameters (a) a and (b) b with increasing x in the solid-solution $K_xNa_{1-x}NbO_3$ using the NPD data. Note that for ease of comparison with unit cell parameters a and c, the b parameter has been divided by √2. The estimated error bars are smaller than the symbols used and are therefore not shown.

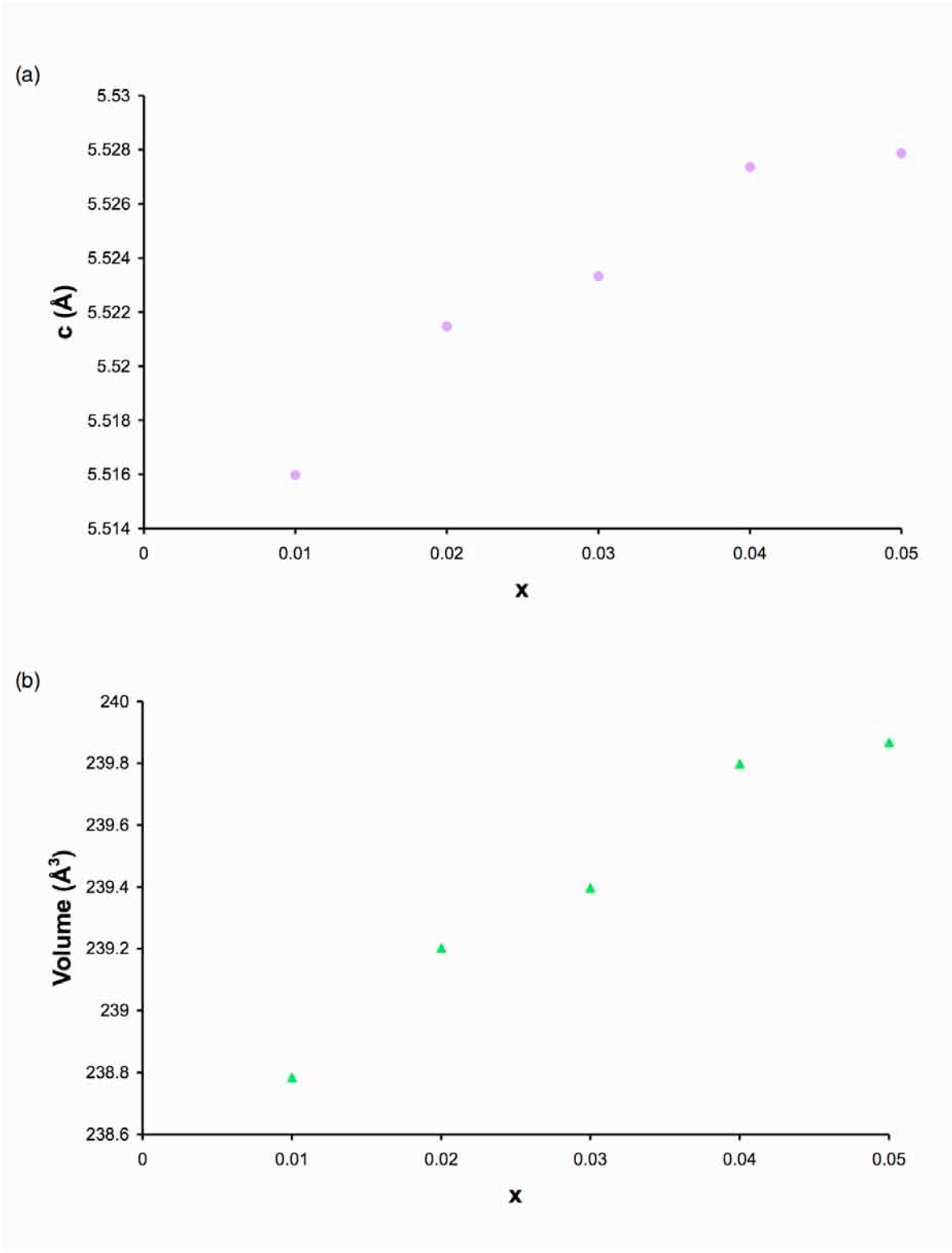

Figure 4.13: Variation observed in (a) the unit cell parameter c and (b) the unit cell volume with increasing x for $K_xNa_{1-x}NbO_3$ using the NPD data. The estimated error bars are smaller than the symbols used and are therefore not shown.

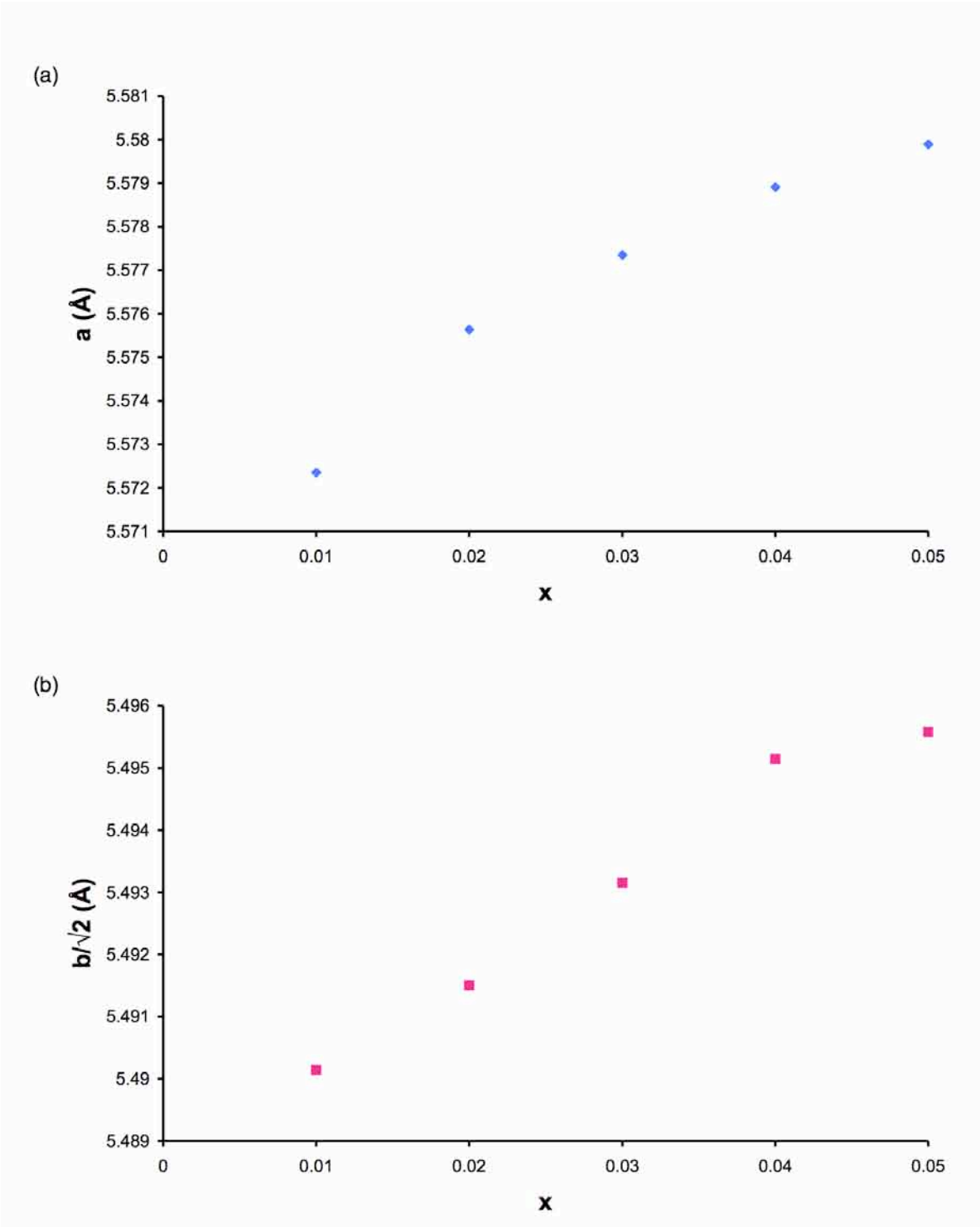

Figure 4.14: Variation observed in the unit cell parameters (a) a and (b) b with increasing x in the solid-solution $K_xNa_{1-x}NbO_3$ using the s-PXRD data. Note that for ease of comparison with unit cell parameters a and c, the b parameter has been divided by √2. The estimated error bars are smaller than the symbols used and are therefore not shown.

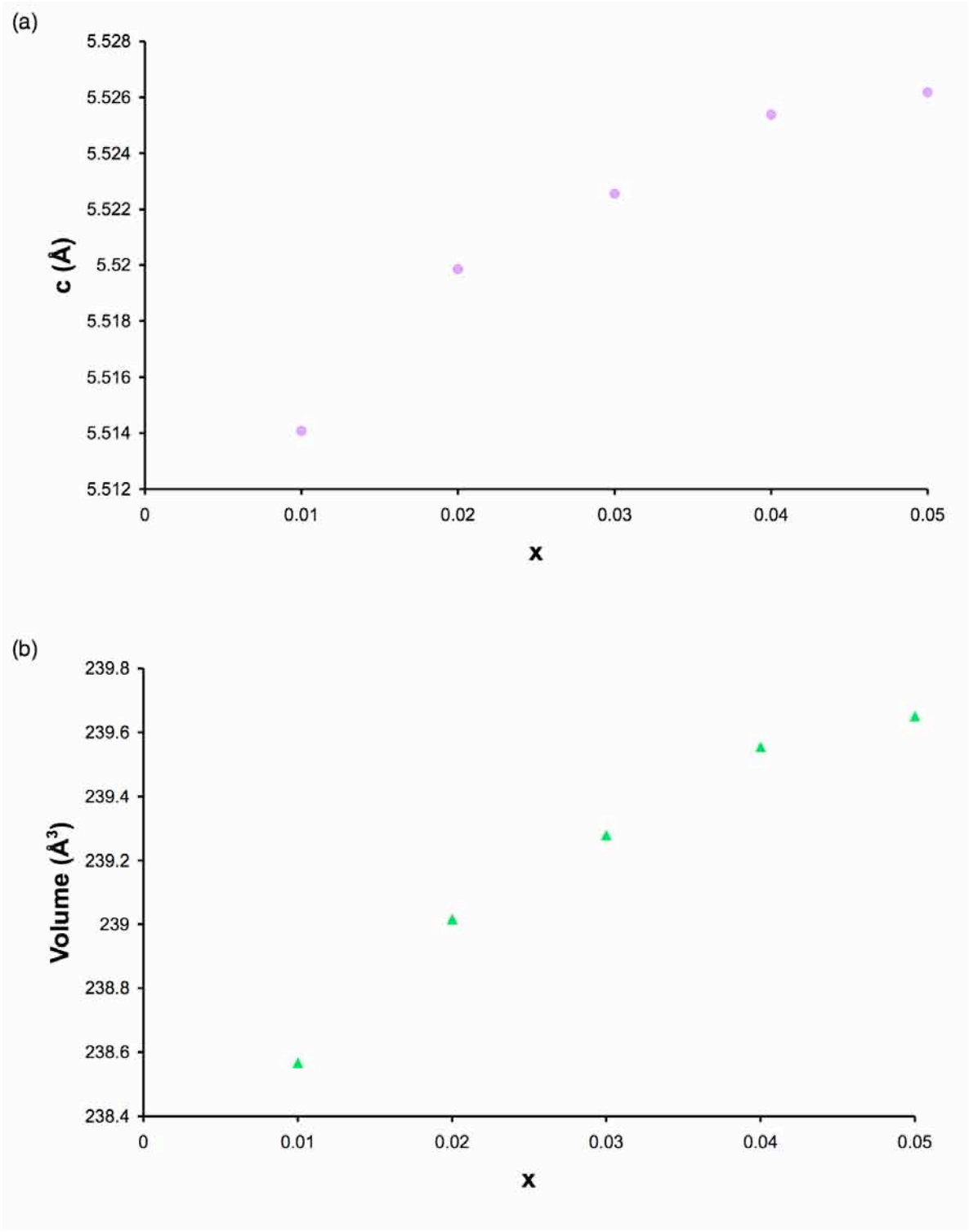

Figure 4.15: Variation observed in (a) the unit cell parameter c and (b) the unit cell volume with increasing x for $K_xNa_{1-x}NbO_3$ using the s-PXRD data. The estimated error bars are smaller than the symbols used and are therefore not shown.

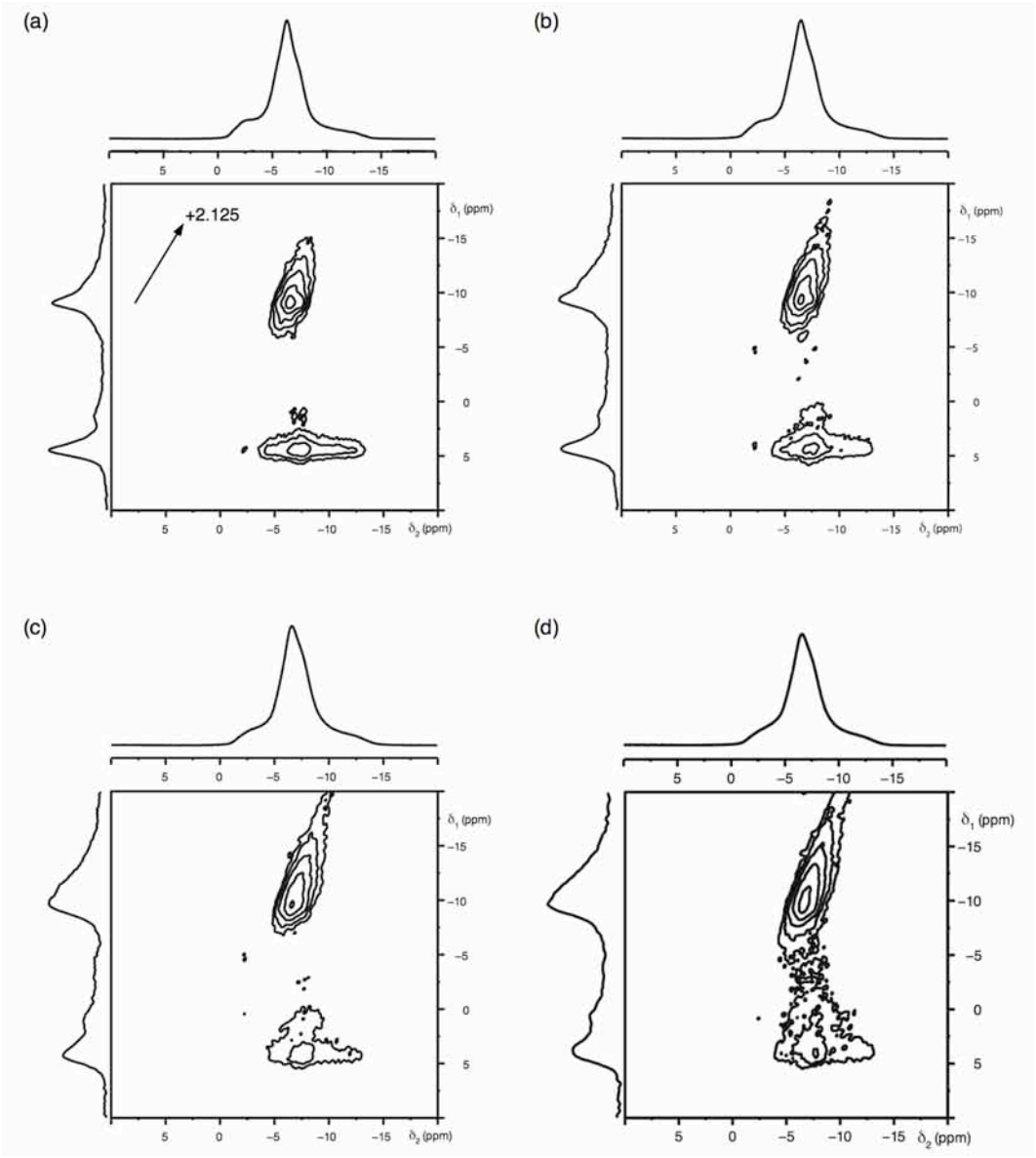

Figure 4.16: ^{23}Na MAS NMR spectra, triple-quantum MAS NMR spectra, and corresponding isotropic projections for (a) $K_{0.02}Na_{0.98}NbO_3$, (b) $K_{0.03}Na_{0.97}NbO_3$, (c) $K_{0.04}Na_{0.96}NbO_3$ and (d) $K_{0.05}Na_{0.95}NbO_3$. The spectral broadening observed increases with increasing x, indicating the presence of disorder. Also shown is an axis along +2.125 denoting the direction along which a distribution of chemical shifts would lie.

distinct features previously observed were gradually lost as the extent of broadening exhibited in each increased. Each lineshape therefore bore more resemblance to the $P2_1ma$ polymorph of $NaNbO_3$ and, as a result, appeared in good agreement with the diffraction data presented. Broadening of the MAS spectrum, in this particular case, is presumably

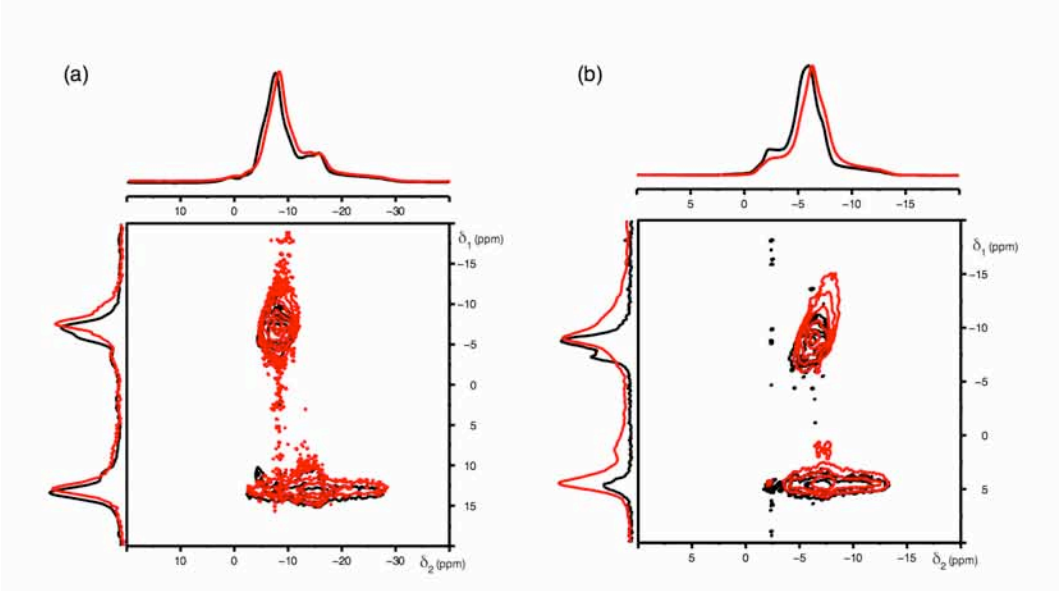

Figure 4.17: An overlay of the ^{23}Na MAS NMR spectra, triple-quantum MAS NMR spectra, and corresponding isotropic projections for sol-gel $NaNbO_3$ (shown in black) and $K_{0.02}Na_{0.98}NbO_3$ (shown in red) at (a) 9.4 T and (b) 14.1 T.

owing to both the inefficient removal of the quadrupolar interaction and disorder. Hence, to accurately determine the number of crystallographically distinct Na sites present in each sample MQMAS techniques were also used. The ^{23}Na MQMAS NMR spectra recorded for each composition are shown in Figures 4.16(a-d). Each spectrum displays two broadened Na sites. The extent of broadening observed in each does, however, make it difficult to detect the presence of very small amounts of the Pbcm phase. The δ_1 position of each site was the same as the $P2_1ma$ polymorph, and at a lower shift than that expected for Pbcm. The spectra (9.4 T and 14. 1 T) for sol-gel $NaNbO_3$ (~90% $P2_1ma$ and ~10% Pbcm phases) and $K_{0.02}Na_{0.98}NbO_3$ have been overlaid and are shown in Figures 4.17(a) and (b), respectively. The two sites in each spectrum appear to align, indicating good agreement between the two, confirming the presence of the $P2_1ma$ polymorph. Note that the extent of broadening exhibited in each spectrum in the KNN series is consistent with the presence of disorder and this is most probably owing to disorder across the A site. The spectral broadening exhibited increases with increasing x and, as observed for the x = 0.01 sample, each spectrum appears to be

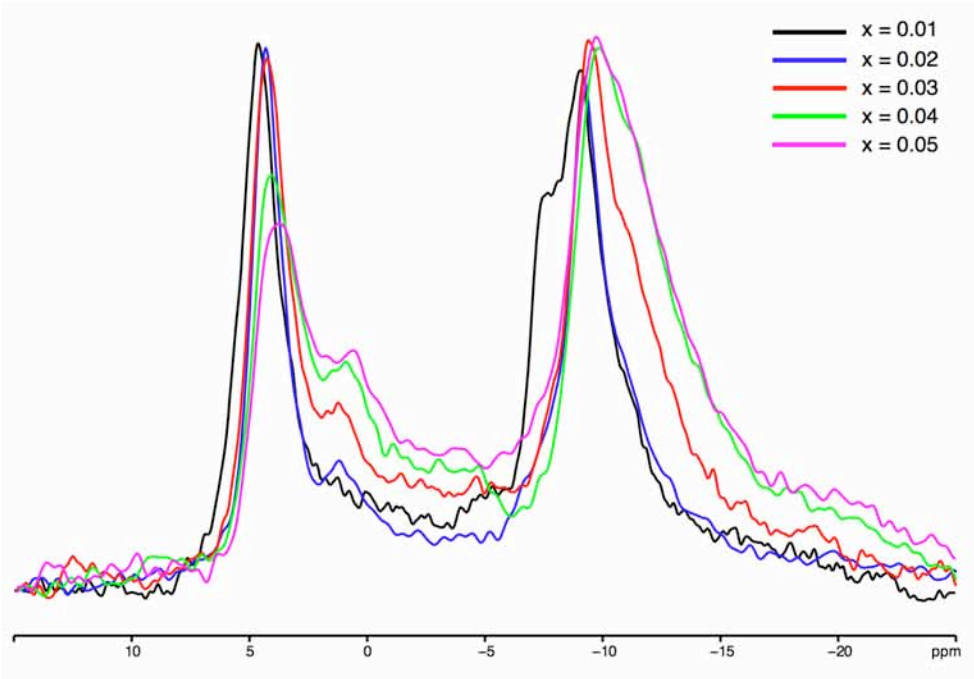

Figure 4.18: An overlay of the isotropic projections obtained from all two-dimensional ^{23}Na MQMAS NMR spectra recorded in the KNN series.

dominated by a distribution of chemical shifts. Again the contribution from a distribution of quadrupoles is thought to be relatively small in each sample. To highlight the extent of broadening exhibited in each spectrum the isotropic projections obtained from each have been overlaid and compared, as shown in Figure 4.18. In addition, the variation in linewidth, i.e., the full width half maximum ($\Delta\upsilon_{1/2}$) of each projection with increasing x has been plotted and is shown in Figure 4.19(a) and (b). The trend observed suggests that the line broadening increases in a non-linear manner with increasing x. Owing to the presence of disorder and hence a distribution of parameters, $\langle\delta_{iso}\rangle$ and $\langle P_Q\rangle$ values were extracted from each spectrum and are given in Table 4.4.

The results obtained for the compositional range, $0.01 \leq x \leq 0.05$, in the KNN series suggest low percentage doping of K into the $NaNbO_3$ structure produces the polar orthorhombic $P2_1ma$ polymorph. In a similar manner, Schuvaeva *et al.*[228] suggested samples with composition $K_{0.025}Na_{0.975}NbO_3$ possessed a structure type similar to that of the field induced ferroelectric $P2_1ma$ phase identified in their work. The only major difference observed between the two phases was a more

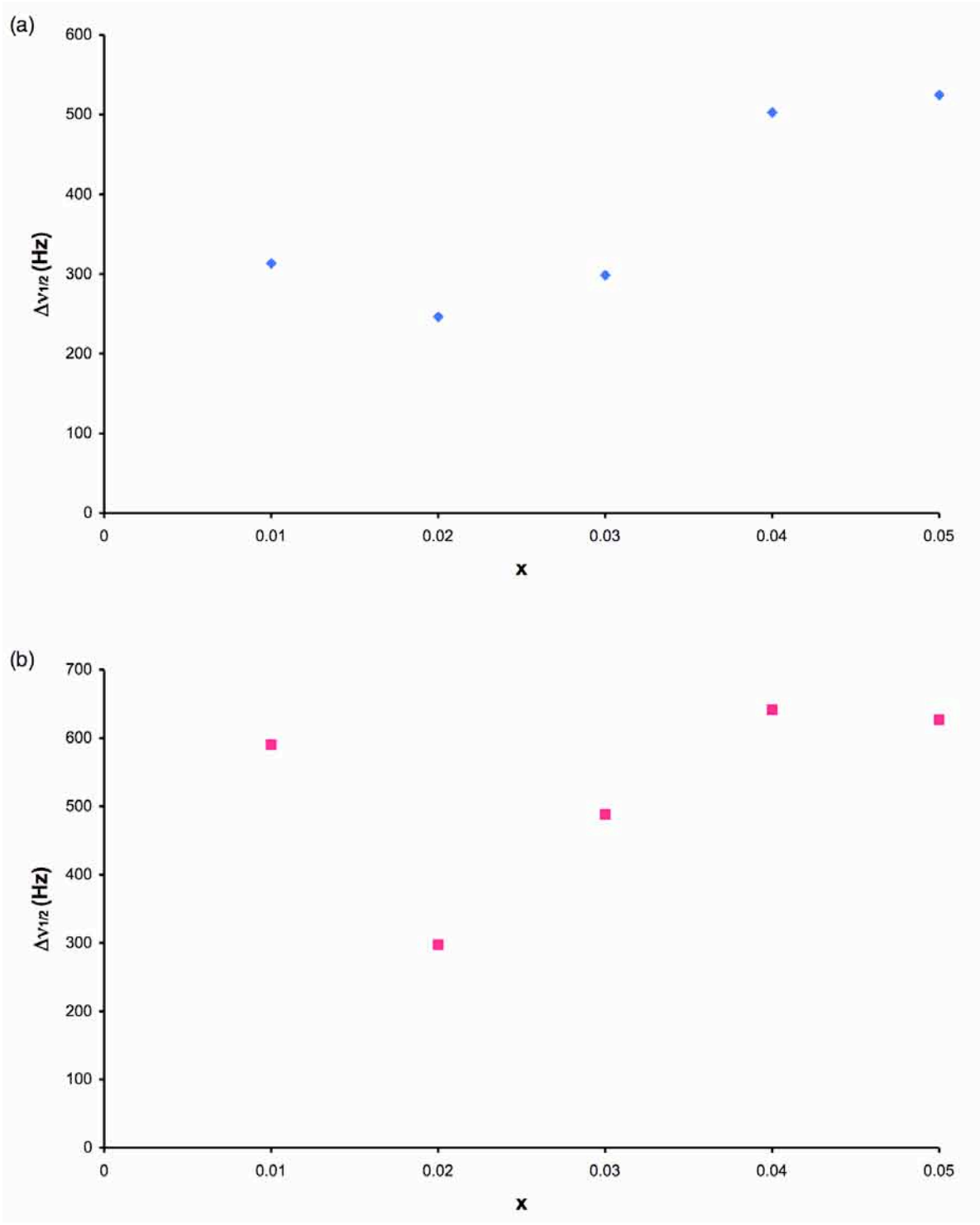

Figure 4.19: Variation in δ_1 linewidth of the resonances corresponding to the two Na sites (a) $\langle\delta_1\rangle \approx 4.7$ ppm and (b) $\langle\delta_1\rangle \approx -9.0$ ppm extracted from the spectra of $K_xNa_{1-x}NbO_3$ with increasing x in Figure 4.16.

pronounced tilting of the NbO_6 octahedra around the [010] axis in the electric field induced phase. The presence of the $P2_1ma$ phase in their work is in good agreement with the findings presented in this investigation. One possible reason for the formation of the $P2_1ma$ polymorph is a 'stabilisation' effect, i.e., the introduction of K into the $NaNbO_3$ structure stabilises this particular polymorph. There are many possible reasons for such an effect, including cation size, structural stress and strain. Athee and Hewat[268] found that compositions x = 0.01 and x = 0.02 in the KNN series could be refined using monoclinic symmetry. However, they also discovered the differences exhibited between monoclinic and orthorhombic structures was extremely small and often difficult to detect. Within this investigation we have shown that compositions x = 0.02, 0.03, 0.04 and 0.05 refine well to the polar orthorhombic $P2_1ma$ structure previously identified in the room temperature structural characterisation of $NaNbO_3$. However, it must be noted that a lowering of symmetry to monoclinic cannot be ruled out. At present it is, therefore, believed that in the case of both $NaNbO_3$ and the KNN series the structural differences exhibited between the orthorhombic and monoclinic structures are too subtle to be accurately characterised, using even the highest resolution diffraction data available.

Using high-resolution powder diffraction and ^{23}Na solid-state NMR we have therefore confirmed that the polar, and potentially ferroelectric, $P2_1ma$ phase of $NaNbO_3$ can be produced with relative ease by doping small quantities of K into the $NaNbO_3$ structure. We believe that the formation of this phase is owing to a stabilisation effect, most probably due to factors such as cation size and structural stress/strain. No additional phase transitions were observed for any of the compositions investigated in this particular study. As x was increased the ^{23}Na MQMAS spectra were severely broadened owing to the presence of disorder in the system, thereby preventing any more detailed structural information being gained.

The findings presented in Chapter 3 indicated that phase pure samples of Pbcm $NaNbO_3$ could be synthesised using molten salt methods. This particular synthesis method was also attempted for

$KNbO_3$. However, this proved unsuccessful as each sample contained a mix of the initial starting reagents, K_2CO_3 and Nb_2O_5. Several different reaction conditions were attempted varying annealing temperature and time. However, it appeared that $KNbO_3$ could not be synthesised using this method. Therefore, molten salt techniques were not used to synthesise samples in the KNN series. Similarly, sol-gel methods were not used to synthesise any samples in the KNN series. Each of these methods are, however, possible areas for future investigation. A systematic study of synthesis method for the KNN series could be completed to determine whether any additional polymorphs of $NaNbO_3$ can be produced. The findings presented concentrated solely on characterising the Na environment of each sample in the KNN series. There are, however, two other NMR active nuclei in each sample, ^{39}K (I = 3/2) and ^{17}O (I = 5/2). It would be interesting to investigate the K environment of each sample in the KNN series as it is hoped that this will provide additional detail regarding how K is substituted onto the A site in the $NaNbO_3$ structure. Similarly, it would also be of interest to probe the oxygen environment in each sample. However, to do so post-synthetic enrichment of each sample in the KNN series would be required using ^{17}O enriched O_2 gas. Once completed this would enable the oxygen environments to be investigated in detail and provide information regarding the tilting mechanisms observed in each structure. Therefore, several additional areas of investigation still remain.

4.3.2 Low Percentage Li Doping ($Li_xNa_{1-x}NbO_3$)

In a similar manner to the KNN series, this investigation concentrated on low percentage doping of Li into the $NaNbO_3$ structure. Structure and phase purity were initially verified using l-PXRD, which suggested the presence of a single phase perovskite. All samples were subsequently analysed using high-resolution NPD and s-PXRD. A Rietveld refinement of the x = 0.01 sample using the NPD data was initially completed using the Pbcm structural model[248] for $NaNbO_3$ and is shown in Figure 4.20(a). The quality of fit obtained was relatively poor,

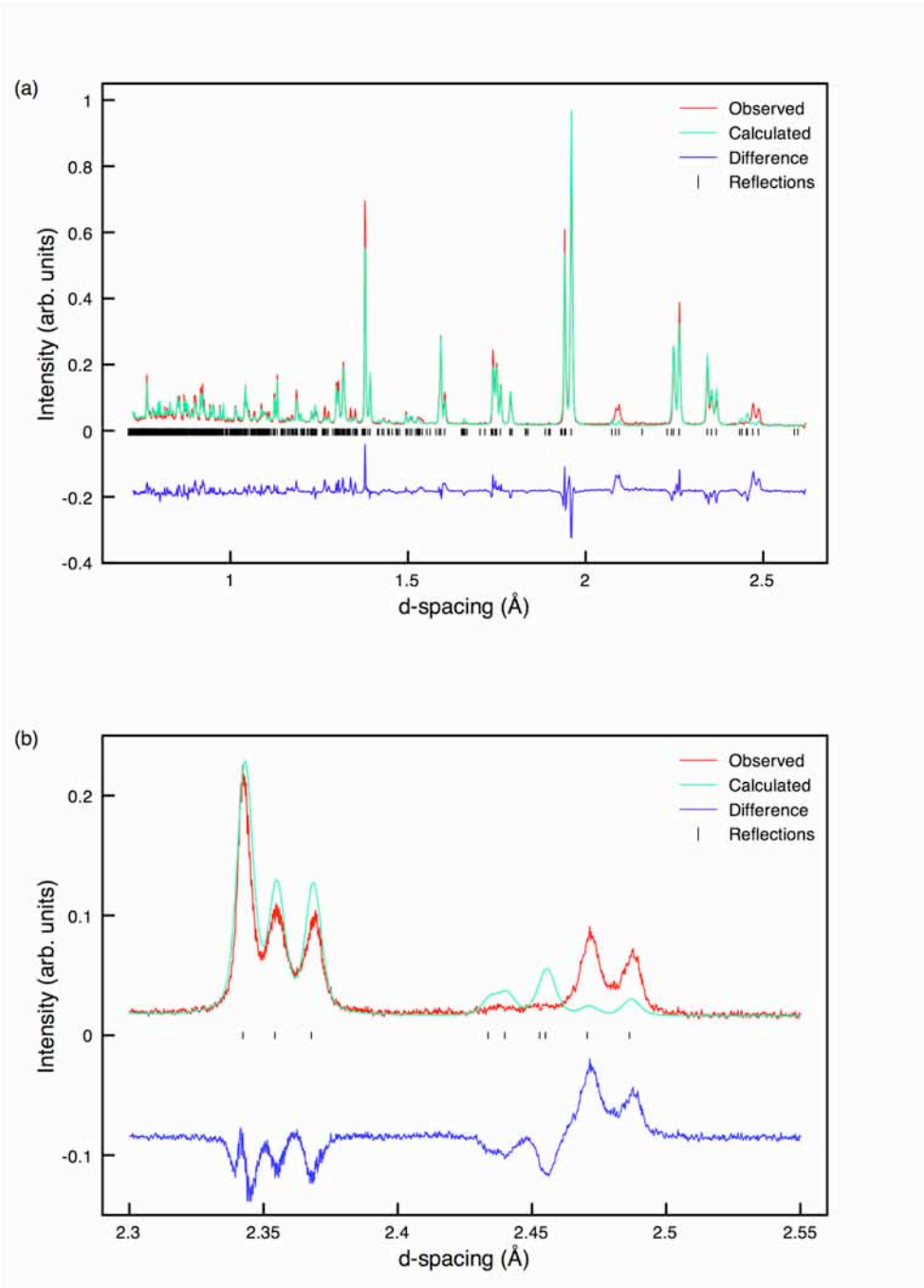

Figure 4.20: (a) Single phase Rietveld refinement of the NPD for $Li_{0.01}Na_{0.99}NbO_3$ using the Pbcm structural model and (b) an expansion of the superstructure region of the refinement, 2.3 Å – 2.55 Å, highlighting the poor level of fit obtained.

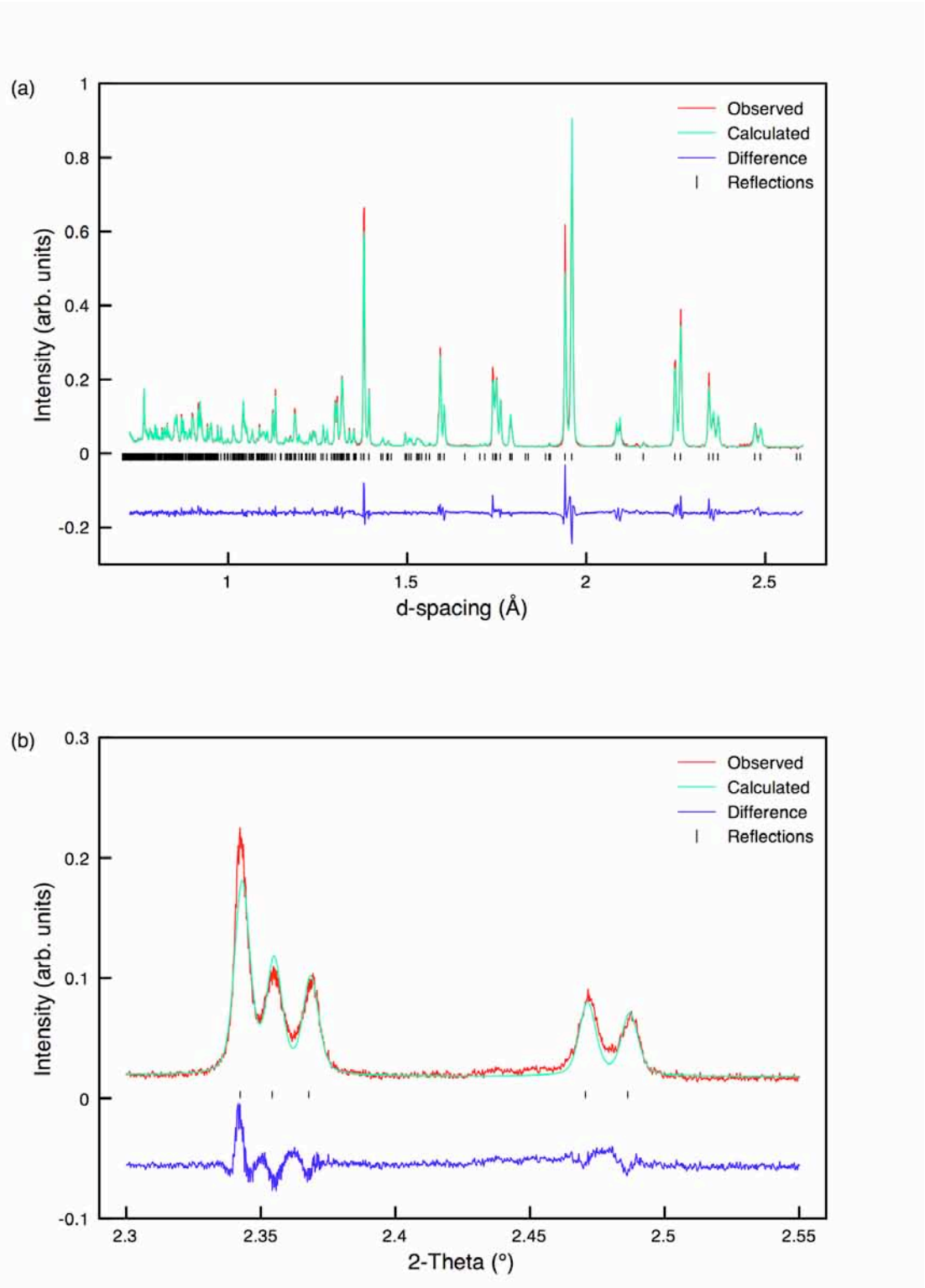

Figure 4.21: (a) Single phase Rietveld refinement of the NPD for $Li_{0.01}Na_{0.99}NbO_3$ using the $P2_1ma$ structural model and (b) an expansion of the superstructure region of the refinement, 2.3 Å – 2.55 Å, highlighting the considerably better level of fit obtained.

Table 4.9: Structural parameters for $Li_{0.01}Na_{0.99}NbO_3$ from NPD data, using isotropic thermal factors. Space group $P2_1ma$, a = 5.57134(6) Å, b = 7.76245(9) Å, c = 5.51288(7) Å and V = 238.417(7) Å^3. χ^2 = 10.9, wR_p = 8.1% and R_p = 7.8%.

Atom	Site	x	y	z	U(iso) × 100 / Å^2
Na1*	2a	0.2643(9)	0	0.7443(8)	1.22(12)
Na2	2b	0.2848(10)	0.5	0.7366(7)	1.69(13)
Nb1	4c	0.2677(4)	0.2497(3)	0.2463(3)	0.12(3)
O1	2a	0.2433(5)	0	0.3126(10)	0.68(10)
O2	2b	0.2283(5)	0.5	0.1923(10)	0.33(9)
O3	4c	0.0205(3)	0.2803(4)	0.5306(5)	1.47(6)
O4	4c	−0.0453(3)	0.2202(4)	0.0371(5)	0.56(5)
*Na 0.99, Li 0.01					

with wR_p = 17.9% and χ^2 = 53.1. Full refinement details for this single phase refinement are given in Appendix III. Most notably the superstructure peaks at ~2.47 Å and ~2.49 Å were not indexed correctly or allocated sufficient intensity using this model. This therefore suggested a different phase of $NaNbO_3$ to be present. It must be noted that $LiNbO_3$[286] possesses a different structure when compared with the orthorhombic phases of $NaNbO_3$. Interestingly, $LiNbO_3$ and the Ilmenite[225] polymorph of $NaNbO_3$ are very similar. The only major difference between the two structures is the presence of cation ordering in $LiNbO_3$. The additional peaks identified in the diffraction pattern did not appear to correlate with this particular phase. This therefore confirmed that the $LiNbO_3$ structure was not adopted at very low percentage doping in the LNN series. The peaks identified did, however, appear to correlate with those highlighted earlier in the KNN series as belonging to the $P2_1ma$ phase of $NaNbO_3$. Therefore, it appeared the $P2_1ma$ polymorph of $NaNbO_3$ was formed upon the addition of very small quantities of Li into the structure. Unlike the $K_{0.01}Na_{0.99}NbO_3$ sample, no additional peaks corresponding to unreacted metal oxides and/or carbonates appeared to be present in the diffraction pattern, suggesting the sample to be a single phase perovskite. Close inspection of the superstructure peaks in the diffraction pattern obtained

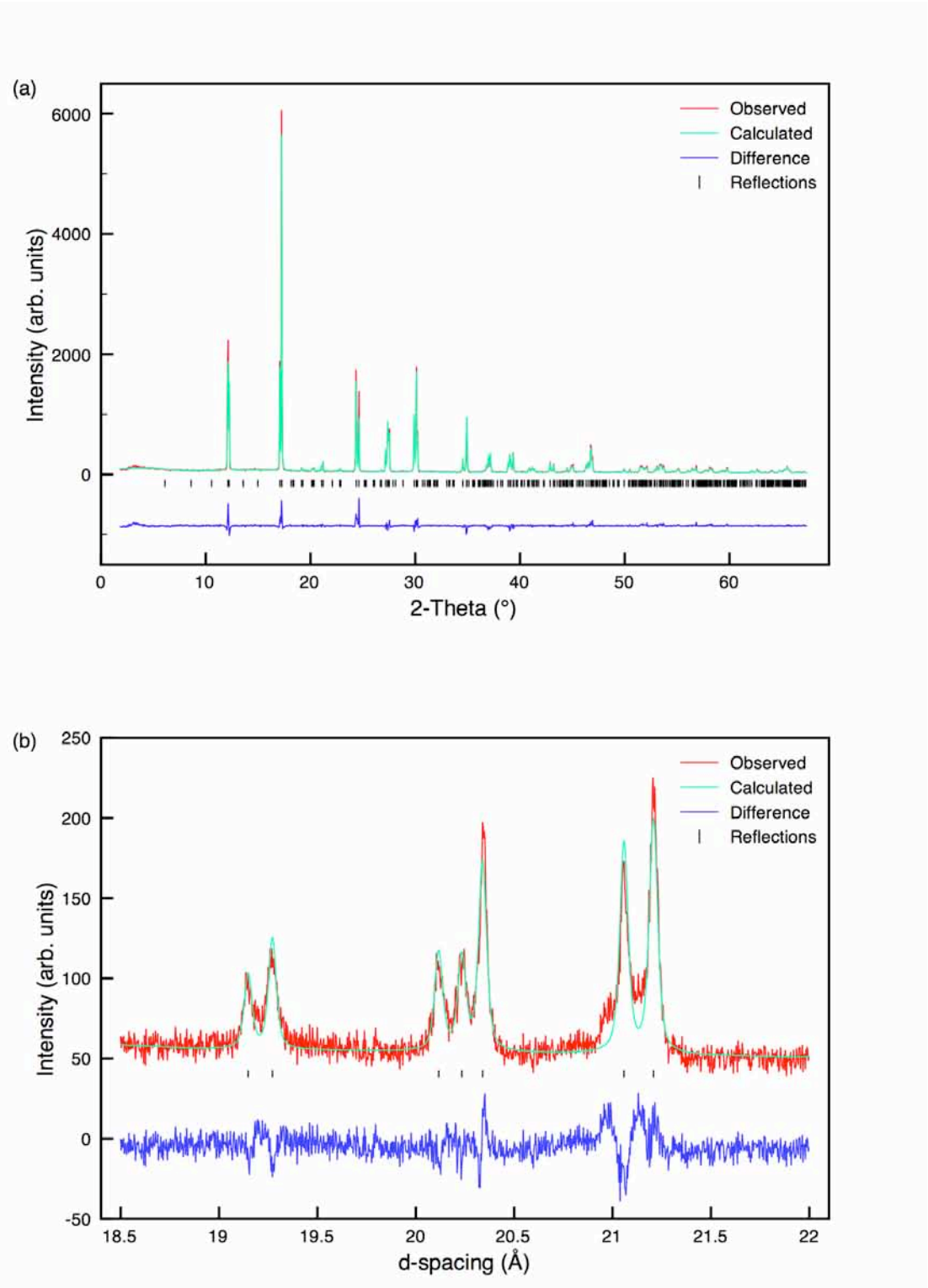

Figure 4.22: (a) Single phase Rietveld refinement of the s-PXRD for $Li_{0.01}Na_{0.99}NbO_3$ using the $P2_1ma$ structural model and (b) an expansion of the superstructure region of the refinement, 2.3 Å – 2.55 Å, highlighting a good level of fit.

Table 4.10: Structural parameters for $Li_{0.01}Na_{0.99}NbO_3$ from s-PXRD data, using isotropic thermal factors. Space group $P2_1ma$, a = 5.57112(3) Å, b = 7.76115(3) Å, c = 5.51243(3) Å and V = 238.348(2) Å^3. $\chi^2 = 3.3$, $wR_p = 13.6\%$ and $R_p = 10.7\%$.

Atom	Site	x	y	z	U(iso) × 100 / Å^2
Na1*	2a	0.2483(8)	0	0.7420(10)	1.10(4)
Na2	2b	0.2618(15)	0.5	0.7438(10)	1.40(4)
Nb1	4c	0.2698	0.2500(6)	0.2455(2)	0.97(1)
O1	2a	0.2550(19)	0	0.312(2)	1.57(4)
O2	2b	0.2309(12)	0.5	0.191(2)	1.57(4)
O3	4c	0.0542(14)	0.2764(11)	0.5225(12)	1.57(4)
O4	4c	−0.0175(13)	0.2136(11)	0.0522(12)	1.57(4)
*Na 0.99, Li 0.01					

for the $Li_{0.01}Na_{0.99}NbO_3$ sample revealed the presence of solely the $P2_1ma$ polymorph, as shown in Figure 4.20(b). This was in contrast to the $K_{0.01}Na_{0.99}NbO_3$ sample in the KNN series where small quantities of the Pbcm phase were found. A Rietveld refinement was therefore completed for the NPD data using solely the $P2_1ma$ structural model.[228] This produced a considerably better quality of fit, with $wR_p = 8.1\%$ and $\chi^2 = 10.9$, as shown in Figure 4.21(a). Using the $P2_1ma$ model the peaks previously identified at ~2.47 Å and ~2.49 Å as being incorrectly modelled using the Pbcm phase were subsequently fitted. This is shown in the expansion of the region 2.3 Å – 2.55 Å shown in Figure 4.21(b). Full refinement details can be found in Table 4.9. Corresponding bond distances are given in Appendix III.

The superstructure peaks present in diffraction patterns are well known to be magnified by neutrons, and so the interpretation of even the subtlest of changes in this region is considerably easier when using NPD data. Such distinctions are, however, considerably harder to make using s-PXRD data as the superstructure peaks are, typically, of much lower intensity, making it extremely challenging to detect subtle changes to the superstructure. In many cases it is often very difficult to successfully distinguish these peaks from the background, owing to their very low

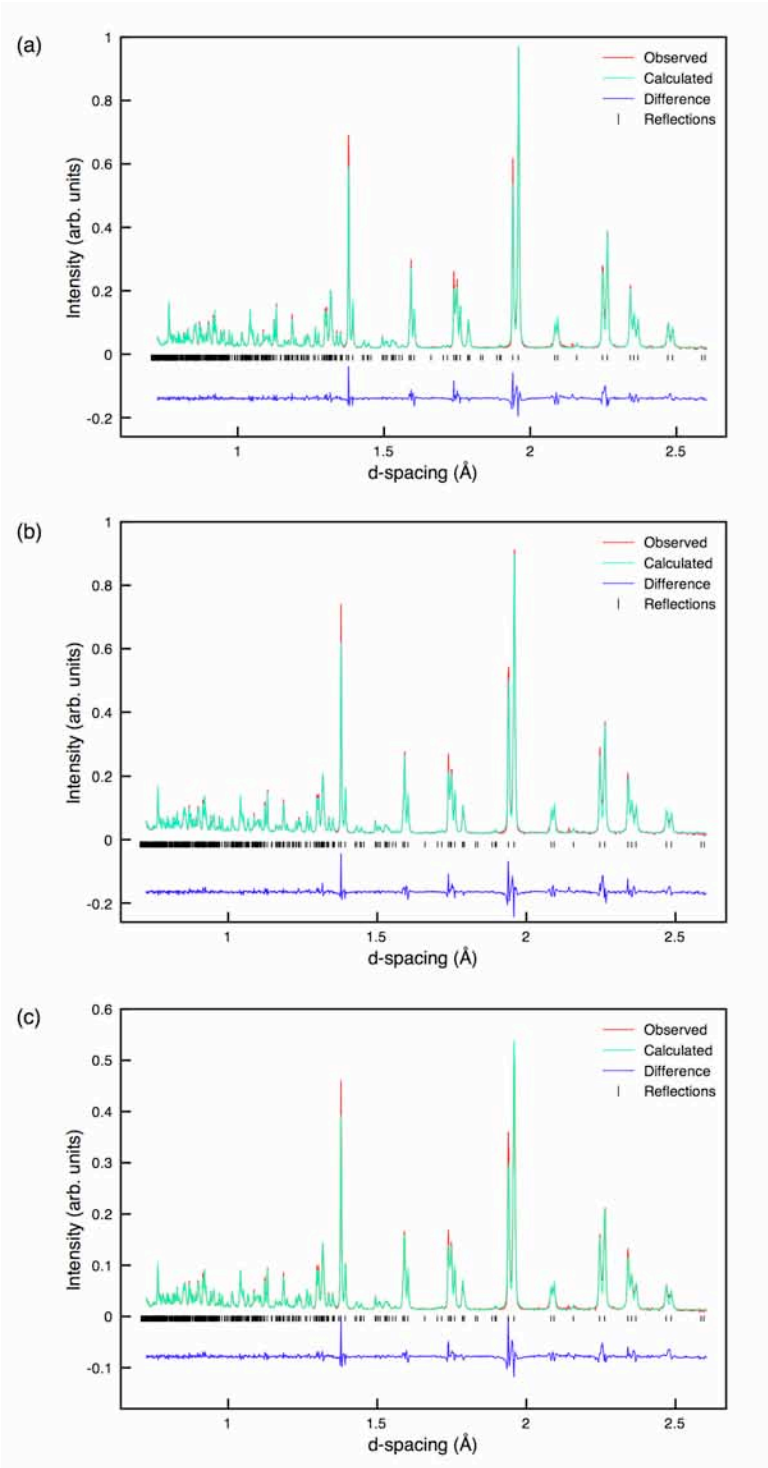

Figure 4.23: (a) Single phase Rietveld refinements completed using the NPD and $P2_1ma$ structural model for (a) $Li_{0.02}Na_{0.98}NbO_3$, (b) $Li_{0.03}Na_{0.97}NbO_3$ and (c) $Li_{0.04}Na_{0.96}NbO_3$.

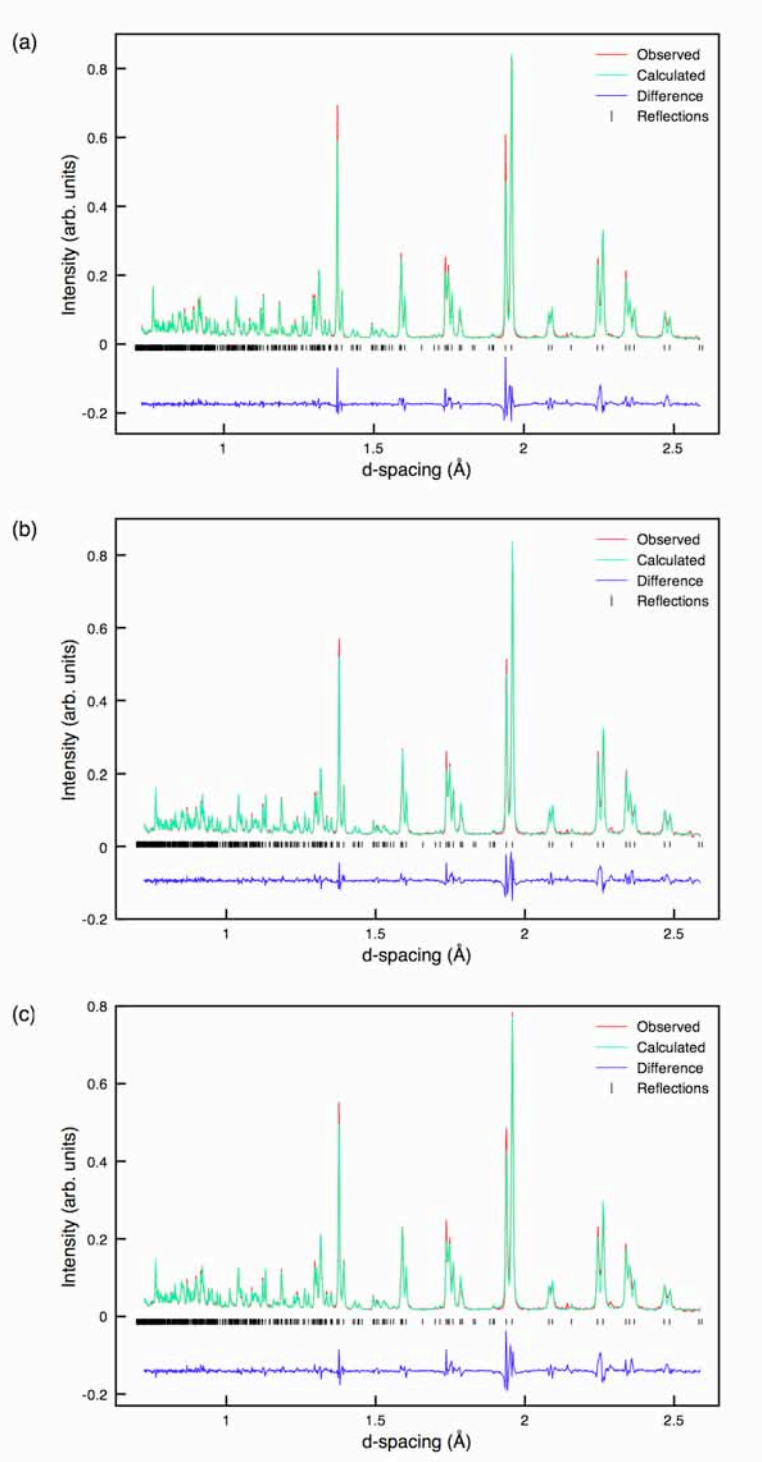

Figure 4.24: (a) Single phase Rietveld refinements completed using the NPD and $P2_1ma$ structural model for (a) $Li_{0.05}Na_{0.95}NbO_3$, (b) $Li_{0.06}Na_{0.94}NbO_3$ and (c) $Li_{0.07}Na_{0.93}NbO_3$.

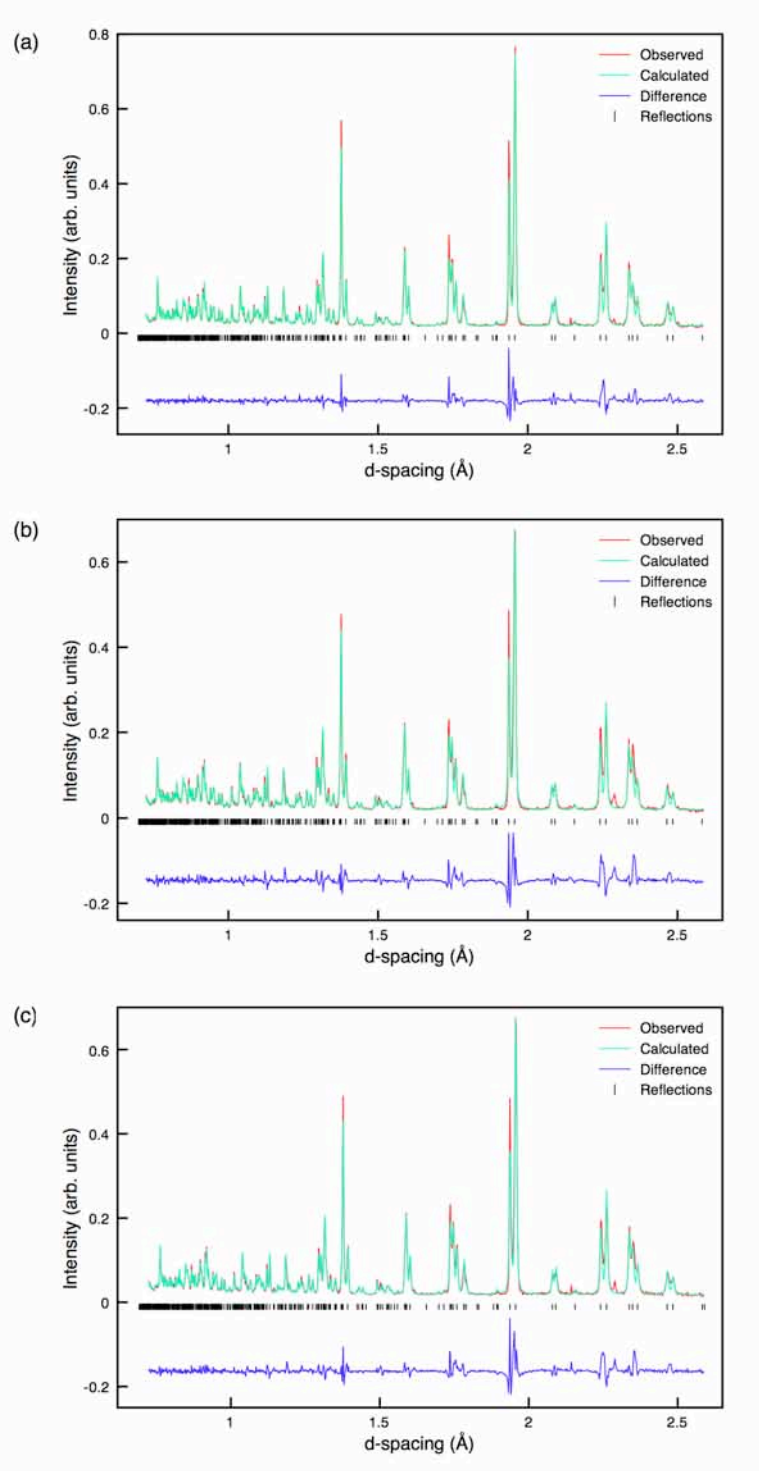

Figure 4.25: (a) Single phase Rietveld refinements completed using the NPD and $P2_1ma$ structural model for (a) $Li_{0.08}Na_{0.92}NbO_3$, (b) $Li_{0.09}Na_{0.91}NbO_3$ and (c) $Li_{0.10}Na_{0.90}NbO_3$.

Table 4.11: Structural parameters for $Li_{0.02}Na_{0.98}NbO_3$ from NPD data, using isotropic thermal factors. Space group $P2_1ma$, a = 5.57198(6) Å, b = 7.76086(8) Å, c = 5.51281(6) Å and V = 238.392(7) Å^3. $\chi^2 = 14.9$, $wR_p = 7.5\%$ and $R_p = 7.1\%$.

Atom	Site	x	y	z	U(iso) × 100 / Å^2
Na1*	2a	0.2606(8)	0	0.7432(7)	1.21(12)
Na2	2b	0.2841(9)	0.5	0.7357(7)	1.54(11)
Nb1	4c	0.2682	0.2497(3)	0.2455(3)	0.06(2)
O1	2a	0.2408(3)	0	0.3126(9)	0.66(9)
O2	2b	0.2249(3)	0.5	0.1929(9)	0.40(8)
O3	4c	0.0226(4)	0.2809(4)	0.5353(4)	1.04(5)
O4	4c	−0.0465(4)	0.2209(3)	0.0363(4)	0.58(5)

*Na 0.98, Li 0.02

Table 4.12: Structural parameters for $Li_{0.06}Na_{0.94}NbO_3$ from NPD data, using isotropic thermal factors. Space group $P2_1ma$, a = 5.57196(7) Å, b = 7.75106(10) Å, c = 5.50466(7) Å and V = 237.738(8) Å^3. $\chi^2 = 15.4$, $wR_p = 6.8\%$ and $R_p = 6.6\%$.

Atom	Site	x	y	z	U(iso) × 100 / Å^2
Na1*	2a	0.2552(9)	0	0.7536(9)	0.82(13)
Na2	2b	0.2869(10)	0.5	0.7322(9)	1.95(13)
Nb1	4c	0.2679	0.2501(3)	0.2441(3)	0.06(3)
O1	2a	0.2385(4)	0	0.3161(9)	0.63(10)
O2	2b	0.2225(4)	0.5	0.1886(9)	0.48(9)
O3	4c	0.0221(5)	0.2831(4)	0.5377(4)	0.85(5)
O4	4c	−0.0471(4)	0.2202(4)	0.0347(5)	0.95(5)

*Na 0.94, Li 0.06

Table 4.13: Structural parameters for $Li_{0.08}Na_{0.92}NbO_3$ from NPD data, using isotropic thermal factors. Space group $P2_1ma$, a = 5.56963(9) Å, b = 7.74910(12) Å, c = 5.49995(9) Å and V = 237.376(10) Å^3. χ^2 = 21.4, wR_p = 8.9% and R_p = 8.6%.

Atom	Site	x	y	z	U(iso) × 100 / Å^2
Na1	2a	0.2557(10)	0	0.7522(11)	0.88(15)
Na2	2b	0.2829(12)	0.5	0.7322(10)	2.18(16)
Nb1	4c	0.2680	0.2500(3)	0.2441(4)	0.08(3)
O1	2a	0.2387(4)	0	0.3171(10)	0.71(11)
O2	2b	0.2228(4)	0.5	0.1873(10)	0.50(9)
O3	4c	0.0230(5)	0.2838(4)	0.5378(5)	0.97(6)
O4	4c	−0.0468(5)	0.2198(4)	0.0349(5)	0.94(6)
*Na 0.92, Li 0.08					

intensity. The accurate assignment of the superstructure peaks in the NPD data therefore enabled an accurate single phase Rietveld refinement to be completed for the x = 0.01 sample using the s-PXRD data. The quality of refinement obtained was relatively good, with wR_p = 13.6% and χ^2 = 3.3. The full Rietveld refinement is shown in Figure 4.22(a), with a corresponding expansion of the superstructure peaks, 18.5° - 22°, also shown in Figure 4.22(b). The two peaks previously identified as belonging to the $P2_1ma$ phase in the s-PXRD data, 19.2° and 19.3°, were well fitted and in good agreement with the NPD findings. Full refinement details can be found in Table 4.10. All associated bond distances obtained from this refinement can be found in Appendix III.

Given the obvious presence of the $P2_1ma$ phase in the x = 0.01 sample similar single phase Rietveld refinements were completed using the $P2_1ma$ model[228] for all remaining samples in the LNN series. Each sample displayed good agreement with the presence of the polar $P2_1ma$ phase. All Rietveld refinements completed using the NPD data for all compositions can be found in Figures 4.23, 4.24 and 4.25 respectively. Full refinement details for x = 0.02, 0.06 and 0.08 can be found in Tables 4.11 - 4.13, with all corresponding wR_p and χ^2 values. All Rietveld refinement details for all remaining samples in this LNN series can be found in

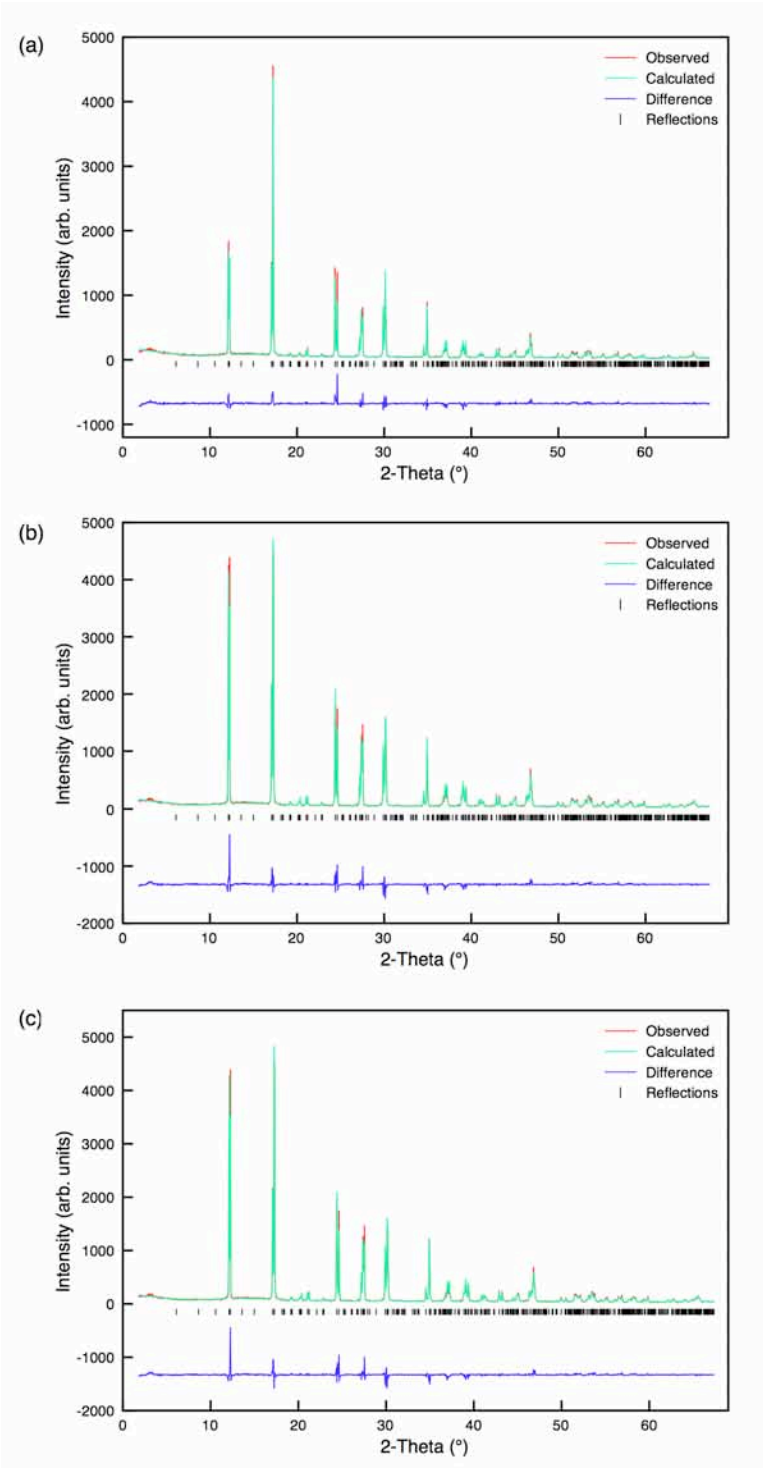

Figure 4.26: (a) Single phase Rietveld refinements completed using the s-PXRD and $P2_1ma$ structural model for (a) $Li_{0.02}Na_{0.98}NbO_3$, (b) $Li_{0.03}Na_{0.97}NbO_3$ and (c) $Li_{0.04}Na_{0.96}NbO_3$.

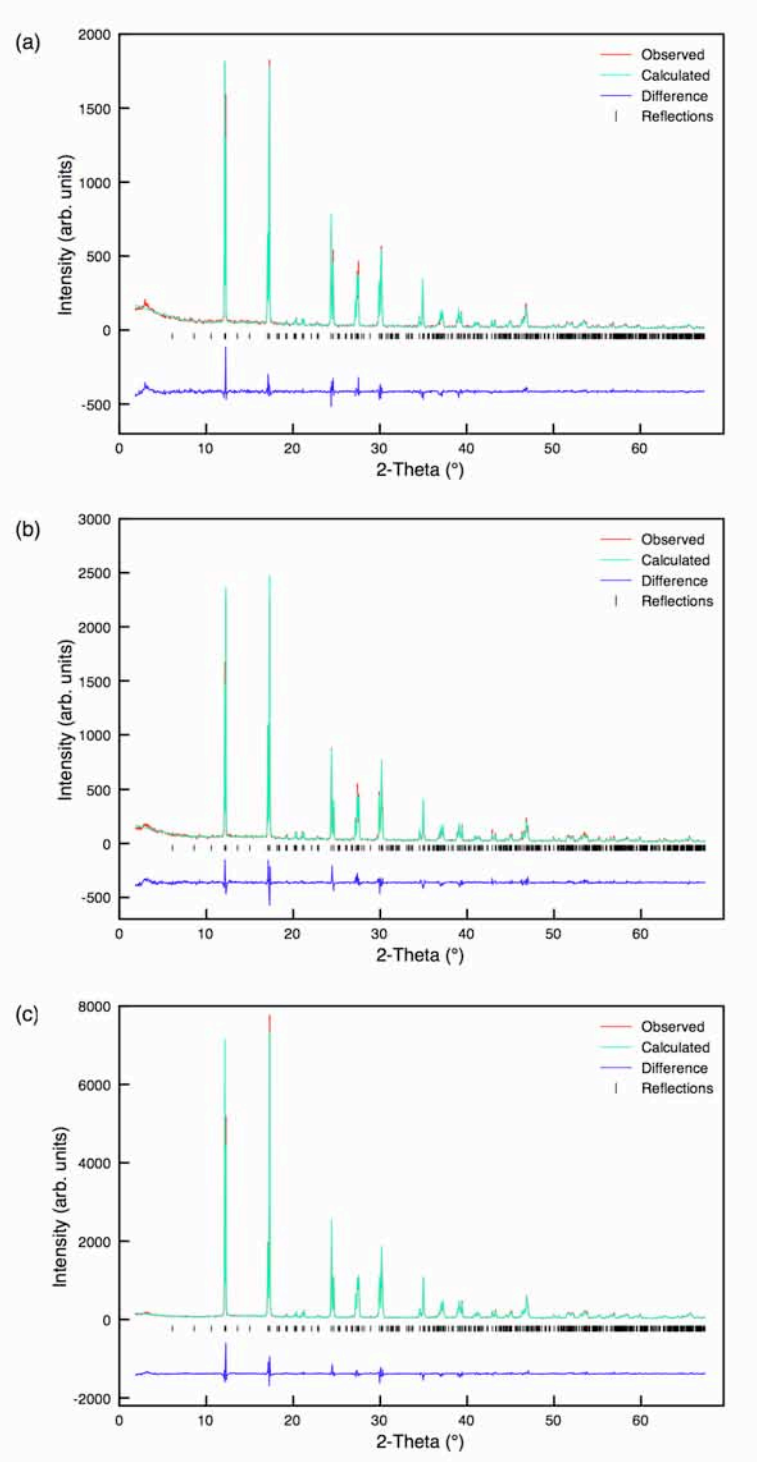

Figure 4.27: (a) Single phase Rietveld refinements completed using the s-PXRD and $P2_1ma$ structural model for (a) $Li_{0.05}Na_{0.95}NbO_3$, (b) $Li_{0.06}Na_{0.94}NbO_3$ and (c) $Li_{0.07}Na_{0.93}NbO_3$.

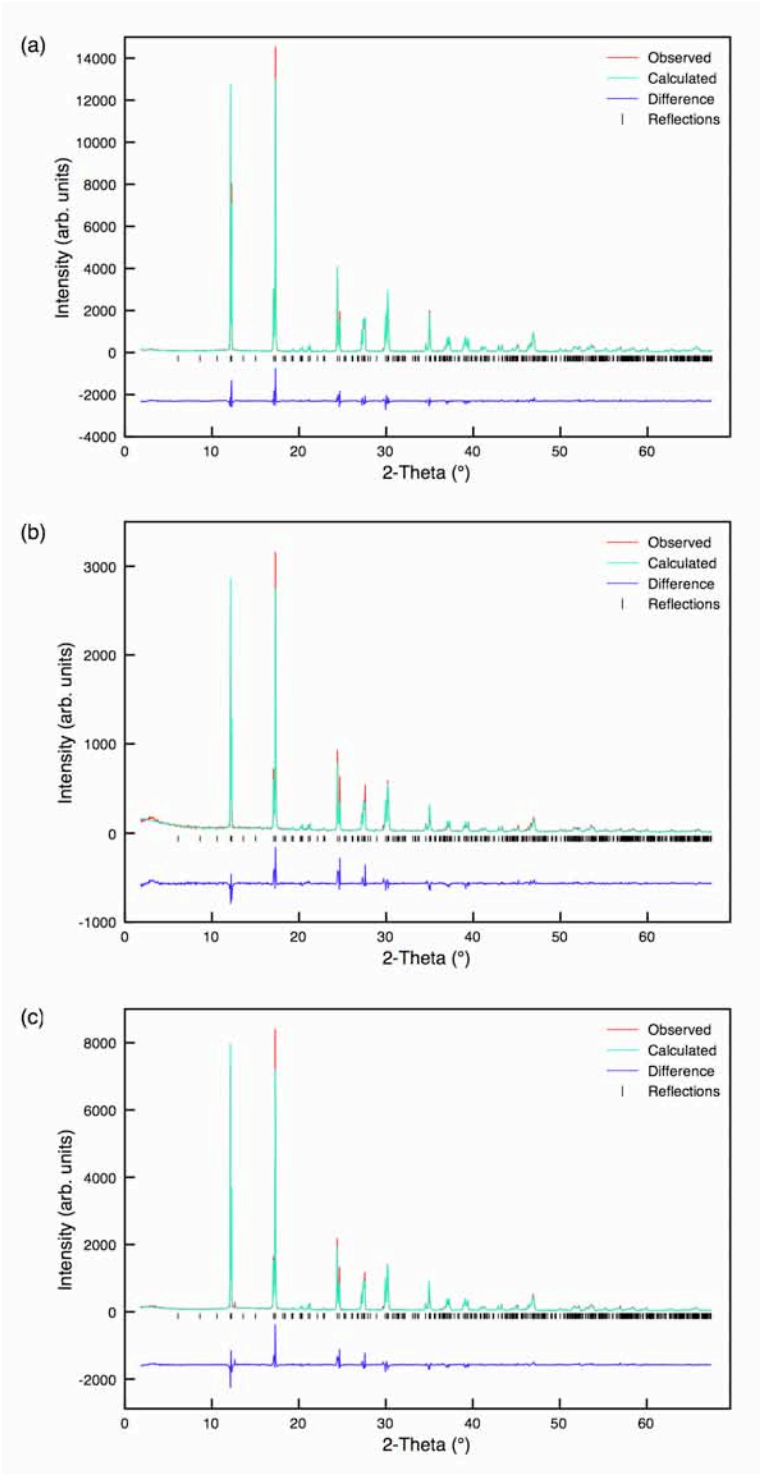

Figure 4.28: (a) Single phase Rietveld refinements completed using the s-PXRD and $P2_1ma$ structural model for (a) $Li_{0.08}Na_{0.92}NbO_3$, (b) $Li_{0.09}Na_{0.91}NbO_3$ and (c) $Li_{0.10}Na_{0.90}NbO_3$.

Table 4.14: Structural parameters for $Li_{0.02}Na_{0.98}NbO_3$ from s-PXRD data, using isotropic thermal factors. Space group $P2_1ma$, a = 5.57141(3) Å, b = 7.75924(4) Å, c = 5.51211(3) Å and V = 238.288(3) Å^3. $\chi^2 = 2.9$, $wR_p = 12.9\%$ and $R_p = 9.9\%$.

Atom	Site	x	y	z	U(iso) × 100 / Å^2
Na1*	2a	0.266(2)	0	0.7420(11)	1.72(5)
Na2	2b	0.2915(12)	0.5	0.7433(11)	1.19(9)
Nb1	4c	0.2719	0.2496(2)	0.2454(2)	1.02(1)
O1	2a	0.2463(19)	0	0.3119(18)	1.70(5)
O2	2b	0.2243(13)	0.5	0.191(3)	1.70(5)
O3	4c	0.0433(15)	0.2822(16)	0.5492(12)	1.70(5)
O4	4c	−0.0252(11)	0.2207(16)	0.0248(15)	1.70(5)

*Na 0.98, Li 0.02

Table 4.15: Structural parameters for $Li_{0.06}Na_{0.94}NbO_3$ from s-PXRD data, using isotropic thermal factors. Space group $P2_1ma$, a = 5.57290(3) Å, b = 7.74826(4) Å, c = 5.50523(4) Å and V = 237.717(3) Å^3. $\chi^2 = 2.7$, $wR_p = 14.9\%$ and $R_p = 11.2\%$.

Atom	Site	x	y	z	U(iso) × 100 / Å^2
Na1*	2a	0.268(3)	0	0.7531(13)	2.30(4)
Na2	2b	0.2947(11)	0.5	0.7355(10)	1.1(3)
Nb1	4c	0.2721	0.2503(4)	0.2437(2)	1.28(9)
O1	2a	0.262(3)	0	0.318(2)	2.11(6)
O2	2b	0.251(2)	0.5	0.186(2)	2.11(6)
O3	4c	0.0195(14)	0.2760(8)	0.5359(12)	2.11(6)
O4	4c	−0.0424(8)	0.2005(8)	0.0342(15)	2.11(6)

*Na 0.94, Li 0.06

Table 4.16: Structural parameters for $Li_{0.08}Na_{0.92}NbO_3$ from s-PXRD data, using isotropic thermal factors. Space group $P2_1ma$, a = 5.56853(3) Å, b = 7.74747(4) Å, c = 5.49902(4) Å and V = 237.239(1) Å^3. $\chi^2 = 4.4$, $wR_p = 13.5\%$ and $R_p = 10.3\%$.

Atom	Site	x	y	z	U(iso) × 100 / Å^2
Na1*	2a	0.2772(14)	0	0.7495(8)	0.9(2)
Na2	2b	0.2994(10)	0.5	0.7383(8)	1.7(2)
Nb1	4c	0.2704	0.2501	0.2434(1)	0.54(1)
O1	2a	0.2523(17)	0	0.3196(11)	2.06(7)
O2	2b	0.2399(14)	0.5	0.1891(12)	2.06(7)
O3	4c	0.0256(11)	0.2788(8)	0.5440(9)	2.06(7)
O4	4c	−0.0399(7)	0.2095(7)	0.0016(12)	2.06(7)

*Na 0.92, Li 0.08

Appendix III. Similarly, all associated bond lengths obtained from each refinement are also given in Appendix III. Single phase Rietveld refinements (using the $P2_1ma$ model[228]) were also completed using s-PXRD data for all samples in the range $0.02 \leq x \leq 0.1$ and, as observed for NPD, a good level of fit was obtained in each case. All Rietveld refinements completed using s-PXRD data are shown in Figures 4.26, 4.27 and 4.28. Structural parameters obtained for compositions x = 0.02, 0.06 and 0.08 can be found in Tables 4.14 – 4.16 respectively. Full refinement details obtained for all remaining samples in this series and corresponding structural parameters, such as bond distances, can be found in Appendix III. It must be noted that as x was increased an increase in peak broadening was observed in both the NPD and s-PXRD data. The peak broadening indicates the gradual introduction of disorder to the LNN system, as expected. Cation ordering across the A site is considerably harder to achieve when compared with B-site cation ordering. It is commonly only observed in anion deficient or double perovskites and therefore the likelihood of achieving A-site cation ordering in the $Li_xNa_{1-x}NbO_3$ solid-solution is extremely low as it does not meet the strict requirements previously detailed in Chapter 1. It is, therefore, of little surprise that the substitution of Li into the $NaNbO_3$ structure produces a

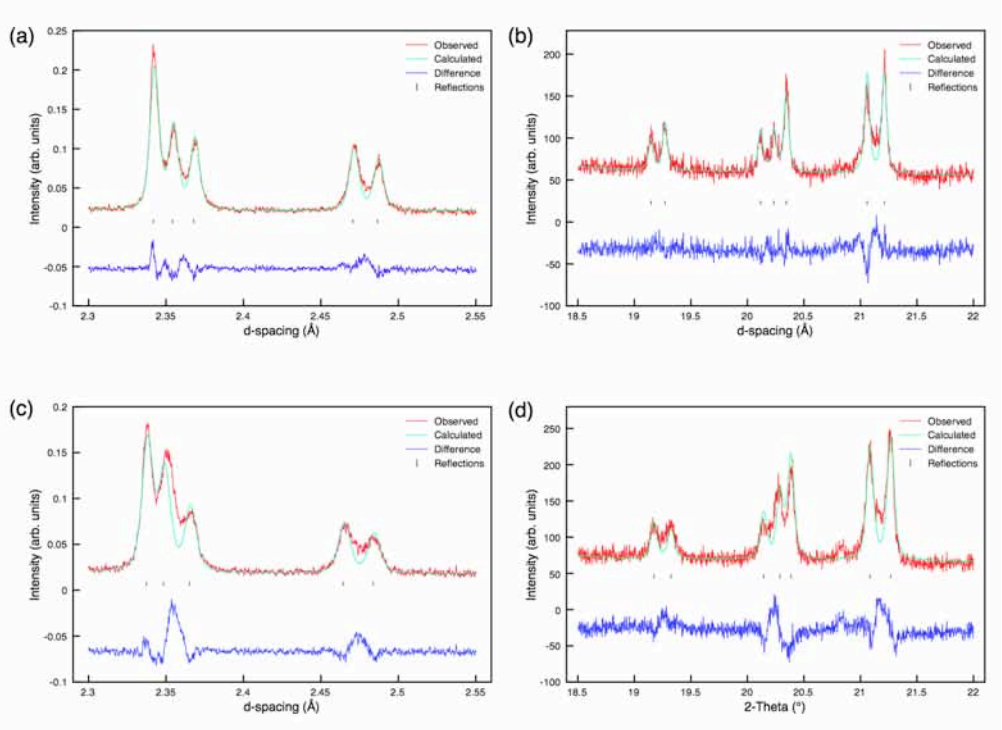

Figure 4.29: Expansions of the superstructure peaks obtained from Rietveld refinement of NPD and s-PXRD data for (a,b) $Li_{0.02}Na_{0.98}NbO_3$ and (c,d) $Li_{0.10}Na_{0.90}NbO_3$ highlighting the extent of peak broadening exhibited with increasing Li content in the LNN solid-solution.

series of disordered compounds. To highlight the extent of peak broadening exhibited in both the NPD and s-PXRD data an expansion of the superstructure peaks in the x = 0.02 and x = 0.1 samples are shown and compared in Figure 4.29(a-d) for both the NPD and s-PXRD datasets obtained. The significant loss in resolution of the observed peaks is clear. This highlights the effect disorder can produce on even the highest resolution diffraction data.

As expected, the substitution of Li into $NaNbO_3$ produced an associated change in both the lattice parameters and unit cell volume. As x was increased a decrease in the lattice parameters a, b and c was observed and, as a direct result, a corresponding decrease in the unit cell volume was also observed. Identical behaviour was exhibited in both the NPD and s-PXRD data and the variation of each parameter with x for each dataset is shown in Figures 4.30, 4.31, 4.32 and 4.33, respectively. As Li^+

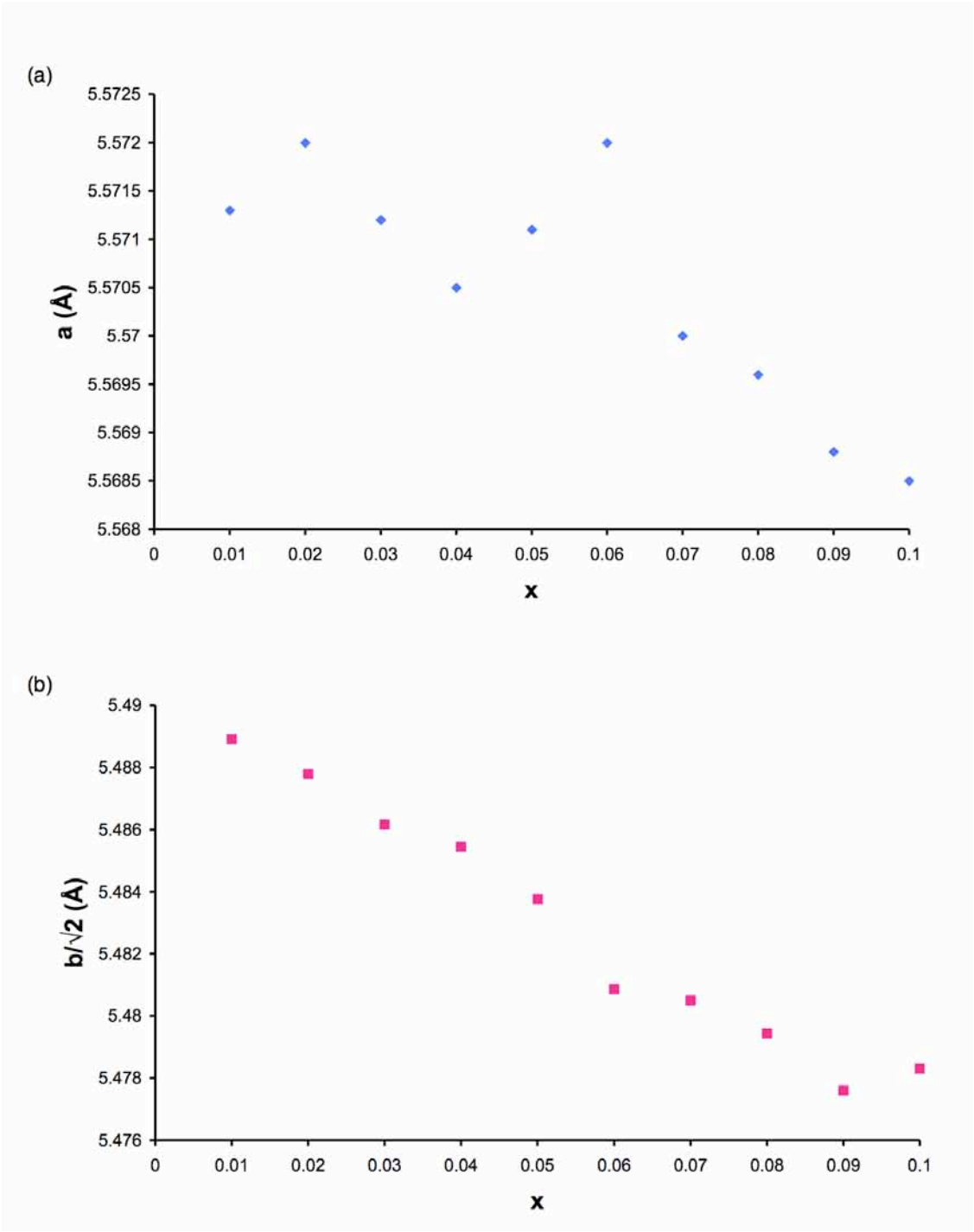

Figure 4.30: Variation observed in the unit cell parameters (a) a and (b) b with increasing x for $Li_xNa_{1-x}NbO_3$ using the NPD data. Note that for ease of comparison with unit cell parameters a and c, the b parameter has been divided by √2. The estimated error bars are smaller than the symbols used and are therefore not shown.

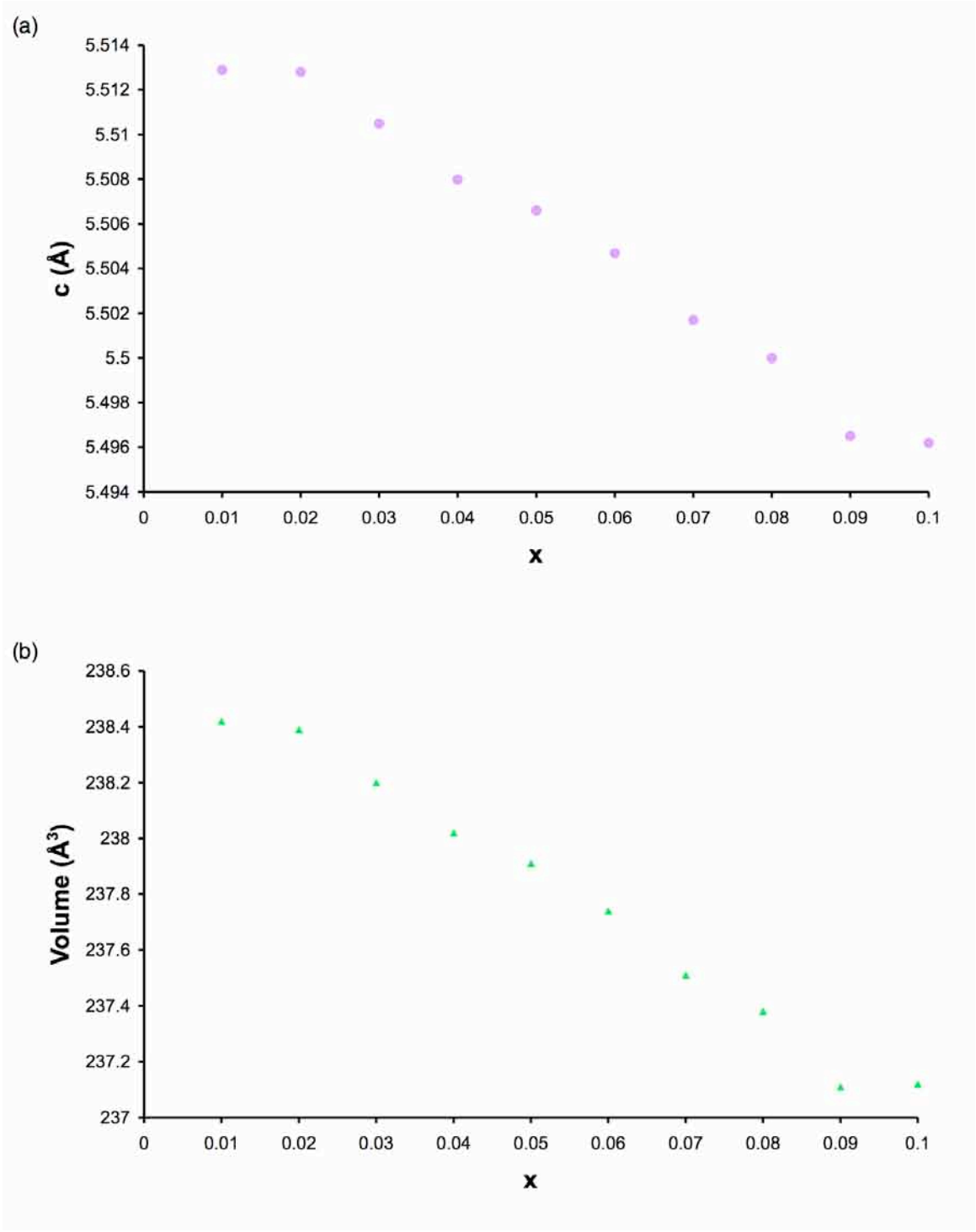

Figure 4.31: Variation observed in (a) the unit cell parameter c and (b) the unit cell volume with increasing x for $Li_xNa_{1-x}NbO_3$ using the NPD data. The estimated error bars are smaller then the symbols used and are therefore not shown.

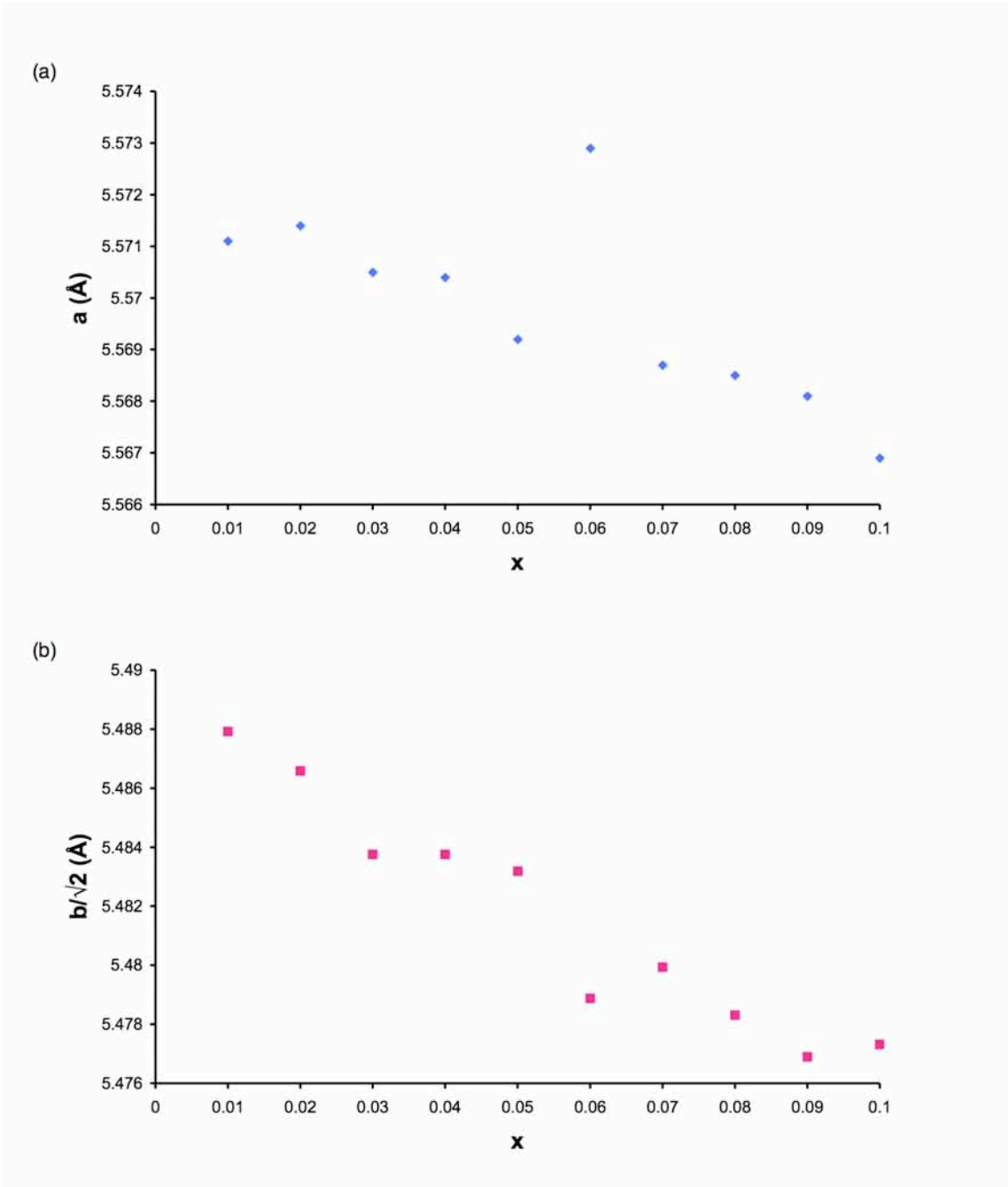

Figure 4.32: Variation observed in the unit cell parameters (a) a and (b) b with increasing x for $Li_xNa_{1-x}NbO_3$ using the s-PXRD data. Note that for ease of comparison with unit cell parameters a and c, the b parameter has been divided by √2. The estimated error bars are smaller than the symbols used and are therefore not shown.

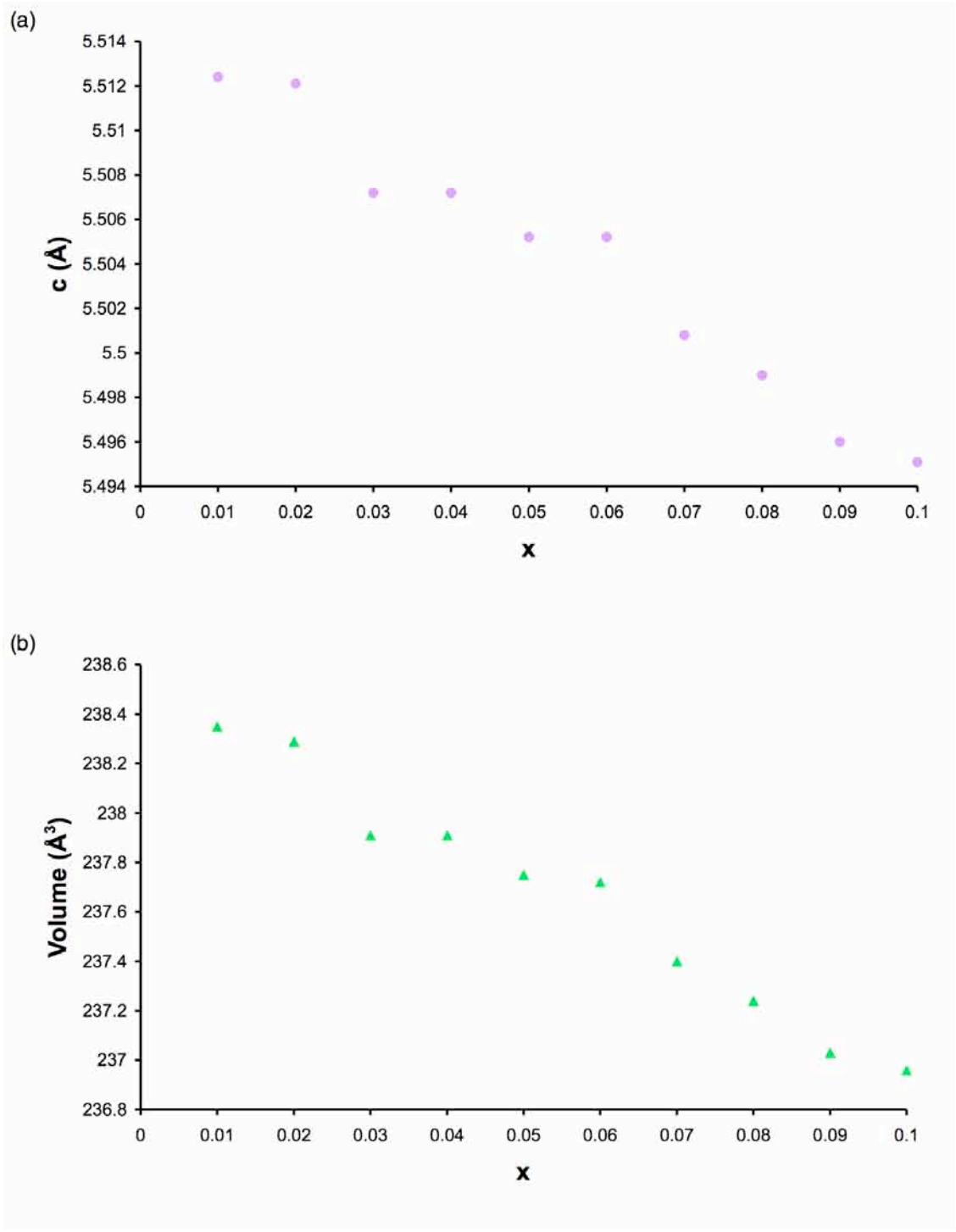

Figure 4.33: Variation observed in (a) the unit cell parameter c and (b) the unit cell volume with increasing x for $Li_xNa_{1-x}NbO_3$ using the s-PXRD data. The estimated error bars are smaller than the symbols used and are therefore not shown.

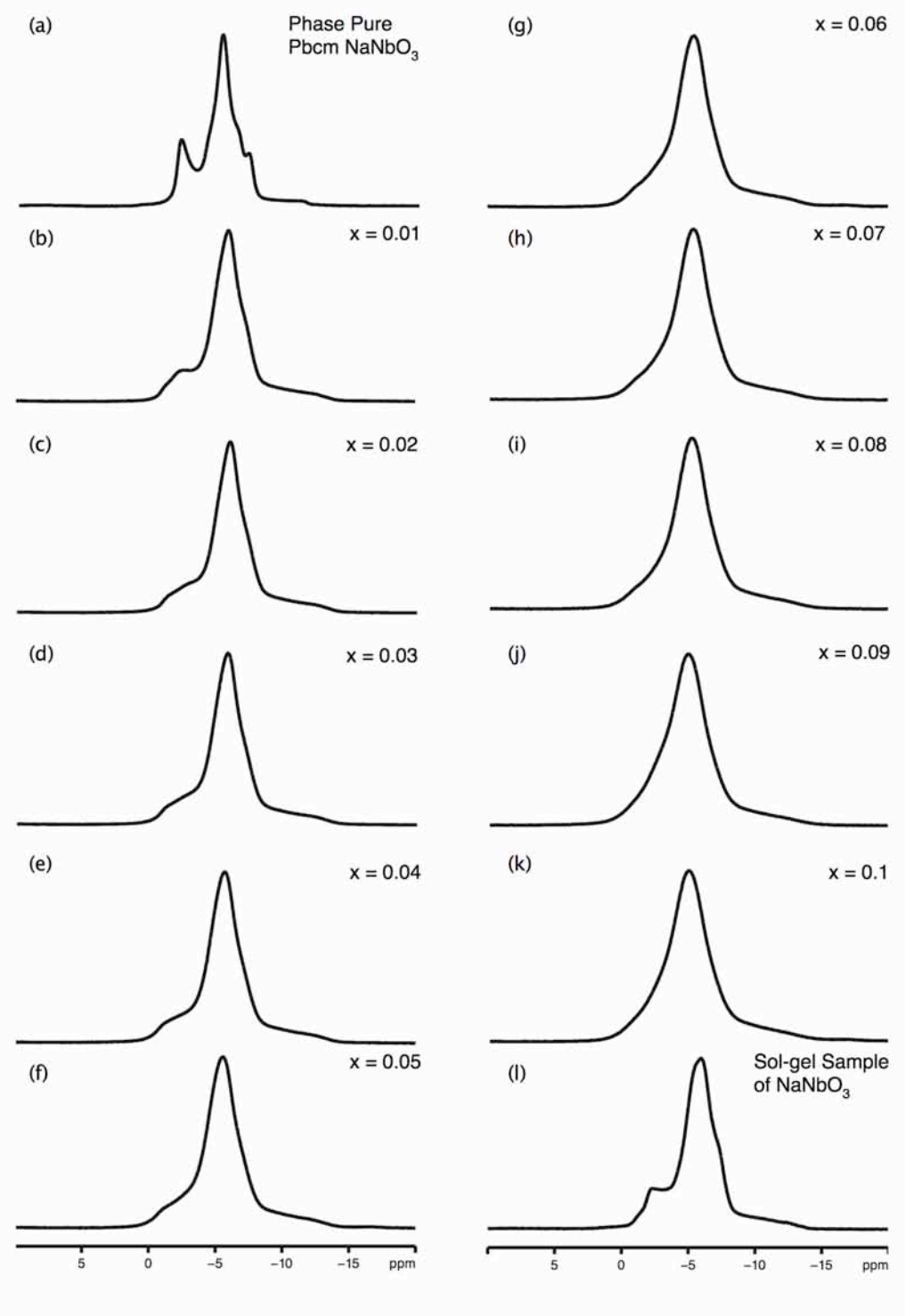

Figure 4.34: Comparison of ^{23}Na (14.1 T) MAS NMR spectra obtained for the LNN series. Also shown in (a) and (l) for comparison are phase pure Pbcm $NaNbO_3$ (synthesised using molten salt techniques) and the sol-gel sample of $NaNbO_3$ composed of ~90% of the $P2_1ma$ and ~10% of the Pbcm polymorphs of $NaNbO_3$.

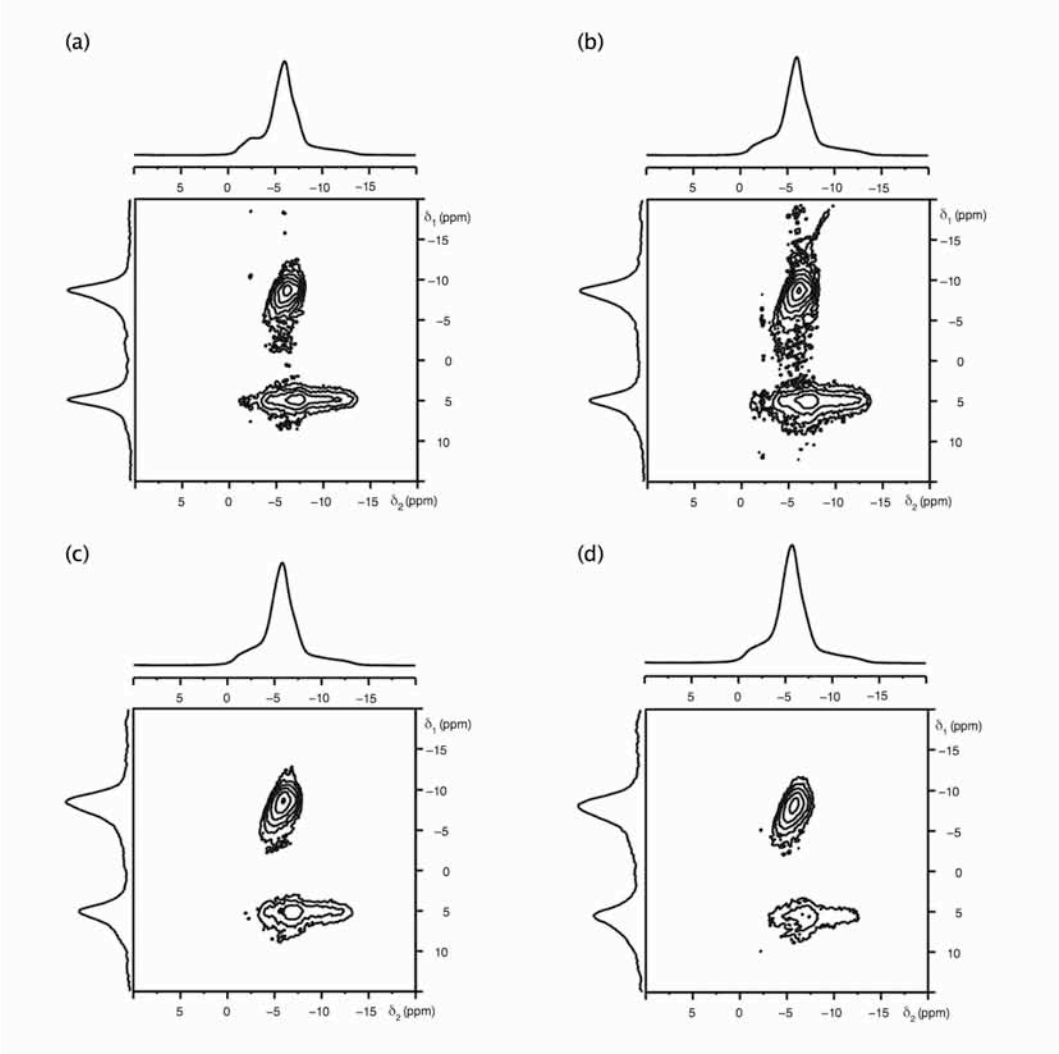

Figure 4.35: ^{23}Na MAS NMR spectra, triple-quantum MAS NMR spectra (14.1 T), and corresponding isotropic projections for (a) $Li_{0.01}Na_{0.99}NbO_3$, (b) $Li_{0.02}Na_{0.98}NbO_3$, (c) $Li_{0.03}Na_{0.97}NbO_3$ and (d) $Li_{0.04}Na_{0.96}NbO_3$. The extent of spectral broadening increases with increasing x, indicating the presence of disorder.

(0.76 Å) is substituted into the structure it would be expected to cause the unit cell to contract, in good agreement with the findings presented.

A ^{23}Na MAS NMR spectrum was recorded for each composition in the LNN series and, as observed for the KNN series, each appeared subtly different. These differences are highlighted in Figures 4.34(b-k) where all MAS spectra recorded in this series are compared. Each lineshape appears broadened relative to phase pure Pbcm (Figure 4.34(a)), with many of the distinct features lost owing to line broadening. Again, the broadening exhibited is characteristic of both inefficient removal of the

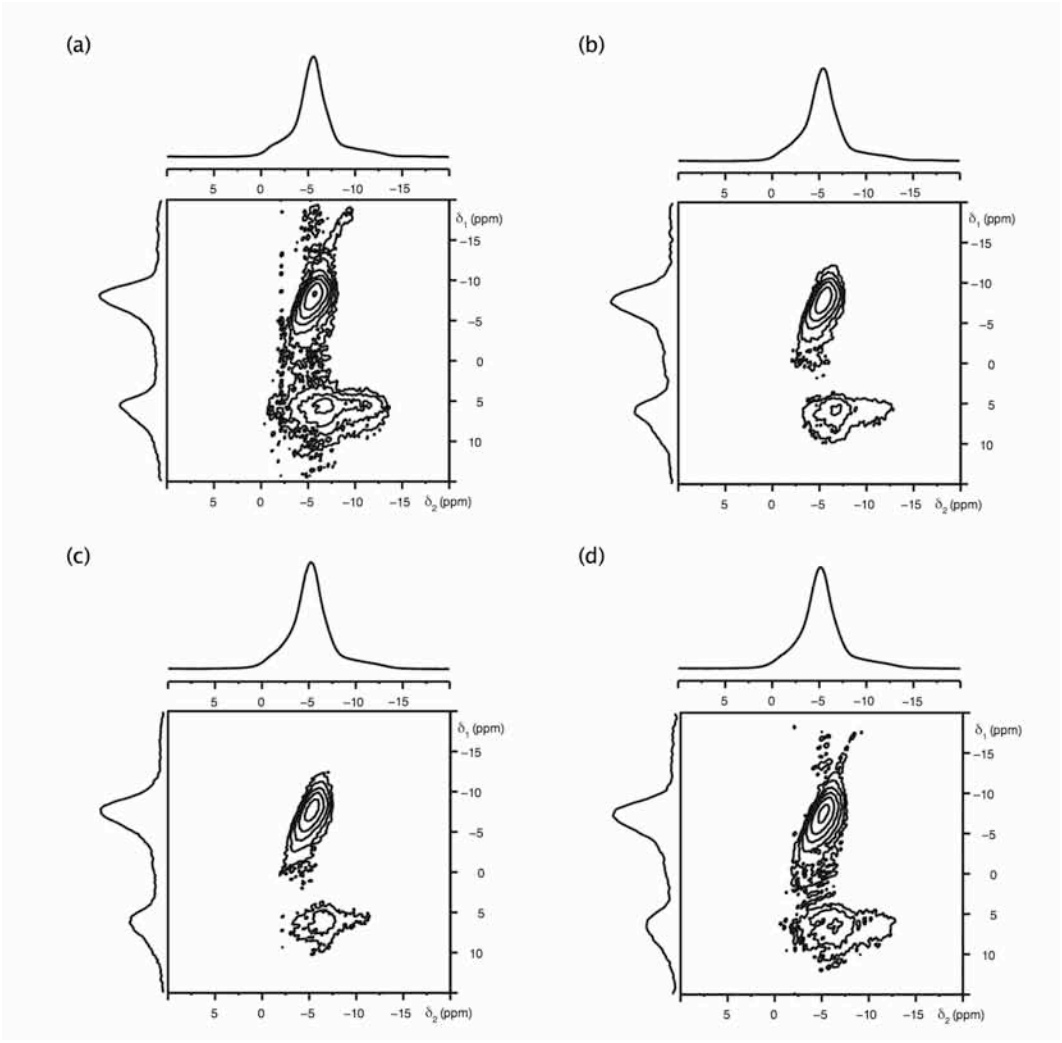

Figure 4.36: ^{23}Na MAS NMR spectra, triple-quantum MAS NMR spectra (14.1 T), and corresponding isotropic projections for (a) $Li_{0.05}Na_{0.95}NbO_3$, (b) $Li_{0.06}Na_{0.94}NbO_3$, (c) $Li_{0.07}Na_{0.93}NbO_3$ and (d) $Li_{0.08}Na_{0.92}NbO_3$. The extent of spectral broadening increases with increasing x, indicating the presence of disorder.

quadrupolar interaction and the gradual introduction of disorder to the system. The ^{23}Na MQMAS NMR spectra recorded for each composition are shown in Figures 4.35, 4.36 and 4.37 respectively. Each composition displays two relatively broadened Na sites. The ridge broadening exhibited by each site appears to be predominantly along +2.125, suggesting it is owing to a distribution of chemical shifts. This appears to be in agreement with the findings previously observed for the KNN series. These findings are also in good agreement with the peak broadening exhibited earlier in both the NPD and s-PXRD data. The two sites

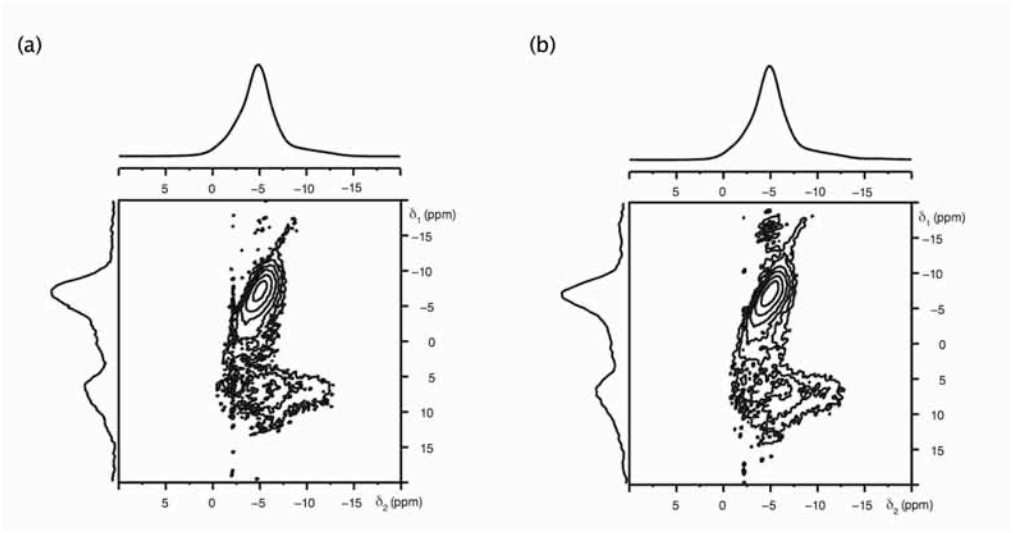

Figure 4.37: ^{23}Na MAS NMR spectra, triple-quantum MAS NMR spectra (14.1 T), and corresponding isotropic projections for (a) $Li_{0.09}Na_{0.91}NbO_3$ and (b) $Li_{0.10}Na_{0.90}NbO_3$. The extent of spectral broadening increases with increasing x, indicating the presence of disorder.

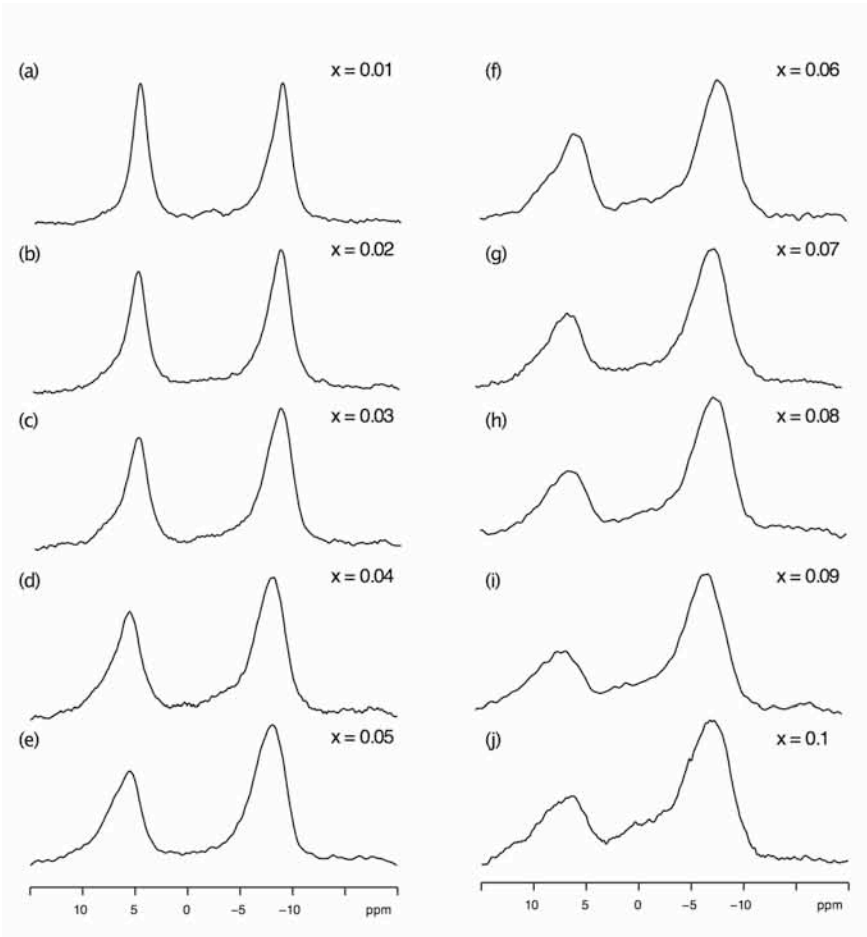

Figure 4.38: Comparison of the isotropic projections obtained from all two-dimensional ^{23}Na MQMAS NMR spectra recorded in the LNN series.

Table 4.17: ^{23}Na (14.1 T) MAS NMR parameters obtained for the $Li_{1-x}Na_xNbO_3$, where $0.01 \leq x \leq 0.1$. All parameters were obtained from the position of the centre of gravity.

x	$\langle\delta_1\rangle$ (ppm)	$\langle\delta_{iso}\rangle$ (ppm)	$\langle P_Q\rangle$ / MHz
0.01	−8.3	−4.7(5)	1.2(2)
	5.0	−1.2(5)	2.4(2)
0.02	−8.2	−4.7(5)	1.2(2)
	5.4	−1.0(5)	2.5(2)
0.03	−7.9	−4.5(5)	1.2(2)
	5.7	−0.9(5)	2.5(2)
0.04	−7.7	−4.5(5)	1.2(2)
	5.7	−1.0(5)	2.5(2)
0.05	−7.7	−4.4(5)	1.1(2)
	6.3	−0.6(5)	2.5(2)
0.06	−7.7	−4.4(5)	1.1(2)
	6.0	−0.8(5)	2.5(2)
0.07	−7.2	−4.1(5)	1.1(2)
	6.3	−0.5(5)	2.4(2)
0.08	−7.1	−4.1(5)	1.1(2)
	6.6	−0.4(5)	2.5(2)
0.09	−6.8	−4.0(5)	1.1(2)
	6.6	−0.4(5)	2.5(2)
0.10	−6.8	−3.9(5)	1.1(2)
	7.1	0.0(5)	2.4(2)

displayed in each spectrum appear to correlate with the two known Na sites identified earlier in the $P2_1ma$ polymorph of $NaNbO_3$. This broadening is mirrored in the isotropic projection of each site onto the δ_1 axis in each spectrum. To highlight the extent of broadening exhibited a comparison of all isotropic projections obtained from each spectrum recorded in the LNN series are shown in Figure 4.38. Considerable spectral broadening was exhibited by many of the samples in this series, particularly for the latter members. To highlight the variation observed in peak broadening with increasing x the linewidth ($\Delta\upsilon_{1/2}$) for each peak in the isotropic projection has been plotted against x. The variation of each peak with increasing x is shown in Figures 4.39(a) and (b). The broadening exhibited appears to increase linearly with increasing Li content. Owing to the presence of disorder $\langle P_Q \rangle$ values have been obtained for each site and are given in Table 4.17.

Both the high-resolution diffraction and ^{23}Na MAS NMR data presented are in good agreement. Each suggests doping the $NaNbO_3$ structure with Li in the range $0.01 \leq x \leq 0.1$ produces the polar $P2_1ma$ polymorph of $NaNbO_3$. The system does, however, become increasingly disordered with increasing Li content. The findings presented are in good agreement with recent work by Yuzyuk *et al.*,[283] in which a phase transition from the orthorhombic Pbma phase (alternative setting Pbcm) to a polar orthorhombic $P2_1ma$ phase was observed when small quantities of Li were added to the system (~2-3%). Hence, both investigations suggest the addition of Li into the $NaNbO_3$ structure consistently produces the $P2_1ma$ polymorph of $NaNbO_3$. Our findings also suggest that doping with quantities as low as 1% can produce the same polar phase. However, it must be noted that it becomes increasingly challenging to investigate materials such as the LNN series as the presence of disorder can often hinder the extraction of important structural information. There are, at present, several different techniques and methods being developed within NMR to aid in both the investigation and understanding of complex disordered materials.

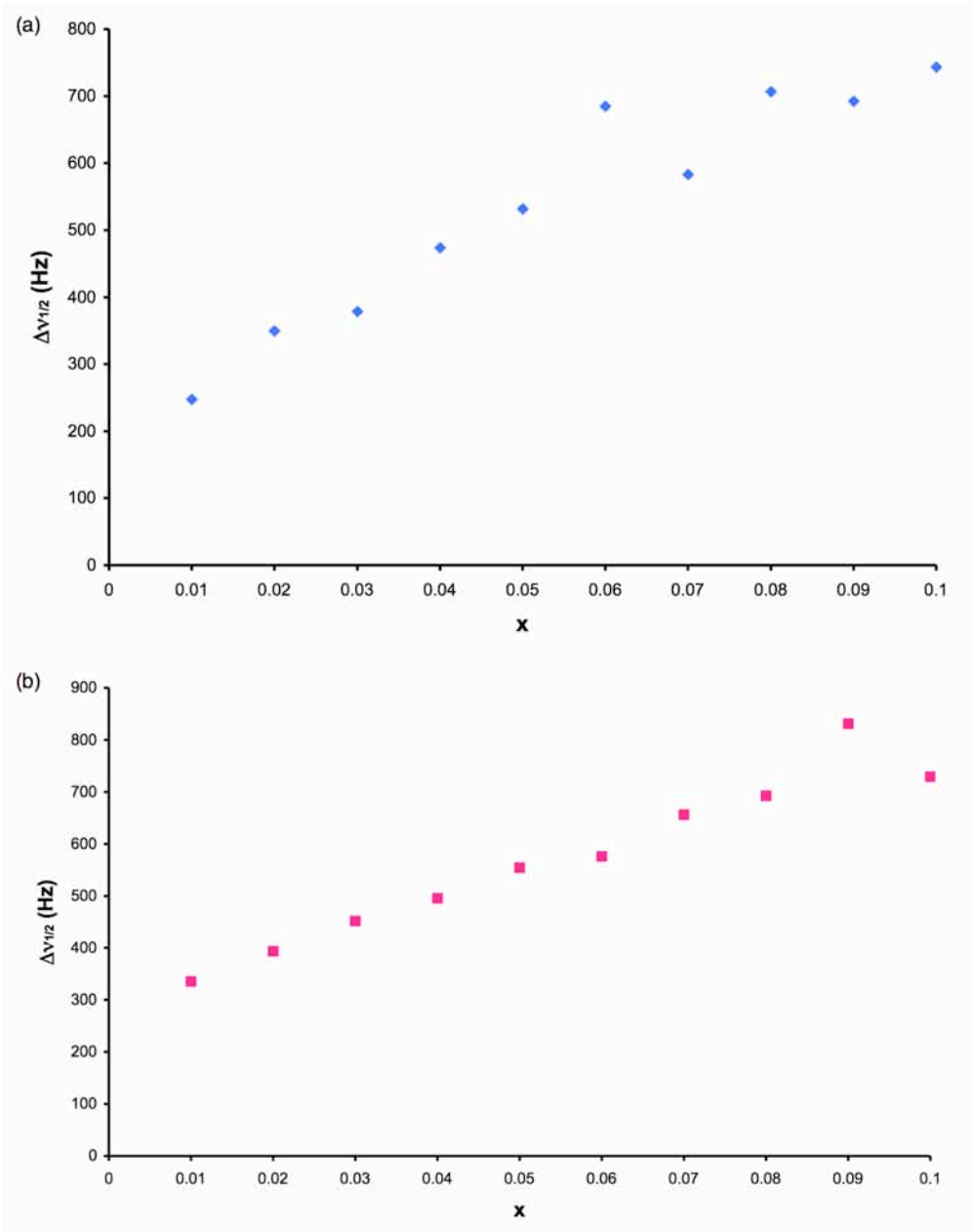

Figure 4.39: Variation in δ_1 linewidth of the resonances corresponding to the two Na sites (a) $\langle\delta_1\rangle \approx 5.0$ ppm and (b) $\langle\delta_1\rangle \approx -8.3$ ppm extracted from the spectra of $Li_xNa_{1-x}NbO_3$, with increasing x in Figures 4.35, 4.36 and 4.37, respectively.

4.3.3 The $Na_{1-x}Sr_{x/2}\square_{x/2}NbO_3$ Solid-Solution

Unlike the KNN and LNN series relatively large quantities of Sr (~10-40%) were doped into the $NaNbO_3$ structure, producing the solid-solution $Na_{1-x}Sr_{x/2}\square_{x/2}NbO_3$. In this particular system an A site vacancy is produced each time a strontium atom is introduced to the structure. This

is owing to an aliovalent substitution on the A site. The phase purity of each sample in the series was initially verified using l-PXRD and in each there appeared to be the presence of an unknown impurity phase, believed to be either a non-stoichiometric mix of reagents or unreacted metal oxides and/or carbonates. However, recent work by Torres-Pardo *et al.*,[287] suggests that for compositions greater than x = 0.4 a tetragonal tungsten bronze (TTB) phase is present as an impurity phase. Therefore, it is possible the unknown phase is a TTB composition. The quantity of this unknown phase appeared to vary from as little as a few percent up to ~10-15% depending on composition. This made it difficult to establish adequate reaction conditions to remove it completely from each composition. Samples containing the smallest quantities of the unknown phase were subsequently investigated using high-resolution s-PXRD. Peaks belonging to the unknown phase were clearly visible in each diffraction pattern recorded. Torres-Pardo *et al.*,[285] recently investigated the $Na_{1-x}Sr_{x/2}\square_{x/2}NbO_3$ series, concentrating on the compositional region $0 < x \leq 0.2$. Their work suggests the introduction of Sr into the $NaNbO_3$ structure produced a polar orthorhombic phase in space group $P2_1ma$. Interestingly, however, their x = 0.1 sample appeared to display a region of phase coexistence between two very similar orthorhombic phases, Pbma (alternative setting Pbcm) and $P2_1ma$. It was, therefore, of particular interest to determine whether a similar region of phase coexistence was exhibited in our x = 0.1 sample. Interestingly, the two phase region identified by Torres-Pardo and co-workers was found using TEM rather than the more conventional technique of powder diffraction. The room temperature study completed earlier for $NaNbO_3$ highlighted that the two orthorhombic phases of $NaNbO_3$ possessed virtually identical X-ray diffraction patterns and a considerable amount of work was required to accurately distinguish between the two. The superstructure peaks identified in both the NPD and s-PXRD data have thus far proved vital in separating the two phases. Therefore, to accurately determine precisely which phase(s) were present in the solid-solution $Na_{1-x}Sr_{x/2}\square_{x/2}NbO_3$ the region $2\theta = 18.5 – 22°$ was closely examined in each diffraction pattern.